1-1-2012

Insight into the Reactivity of Metastasis Inhibitor, Imidazolium trans-[tetrachloro (dimethyl sulfoxide)(imidazole)ruthenate(III)], with Biologically-active Thiols

Risikat Ajibola Adigun
Portland State University

Insight into the Reactivity of Metastasis Inhibitor, Imidazolium trans-[tetrachloro

(dimethyl sulfoxide)(imidazole)ruthenate(III)], with Biologically-active Thiols

by

Risikat Ajibola Adigun

A dissertation submitted in partial fulfillment of the
requirements for the degree of

Doctor of Philosophy
in
Chemistry

Dissertation Committee:
Reuben H. Simoyi, Chair
Albert S. Benight
Dean B. Atkinson
John G. Rueter
Radu Popa

Portland State University
© 2012

ABSTRACT

Imidazolium trans-[tetrachloro (dimethyl sulfoxide)(imidazole)ruthenate(III)], NAMI-A, is an experimental metastasis inhibitor whose specific mechanism of activation and action remains to be elucidated. In the nucleophilic and reducing physiological environment; it is anticipated that the most relevant and available reductants upon introduction of NAMI-A as a therapeutic agent will be the biologically-relevant free thiols. The kinetics and mechanisms of interaction of NAMI-A with biologically-active thiols cysteamine, glutathione, cysteine and a popular chemoprotectant, 2-mercaptoethane sulfonate (MESNA) have been studied spectrophotometrically under physiologically-relevant conditions.

The reactions are characterized by initial reduction of NAMI-A with simultaneous formation of dimeric thiol and subsequent ligand exchange with water to various degrees as evidenced by Electospray Ionization Mass Spectrometry. Stoichiometry of reactions shows that one molecule of NAMI-A reacted with one mole of thiol to form corresponding disulfide cystamine, dimeric MESNA, oxidized glutathione and cystine. Observed rate constants, k_o, for the reaction of NAMI-A with cysteamine, MESNA, GSH and cysteine were deduced to be $6.85 \pm 0.3 \times 10^{-1}$, $9.4 \pm 0.5 \times 10^{-2}$, $7.42 \pm 0.4 \times 10^{-3}$ and $3.63 \pm 0.3 \times 10^{-2}$ s^{-1} respectively.

Activation parameters determined from Arrhenius plots are indicative of formation of associative intermediates prior to formation of products. A negative correlation was obtained from the Brønsted plot derived from observed rate constants

and the pKa of the different thiols demonstrating significant contribution of thiolate species towards the rate. In conclusion, interactions of NAMI-A with biologically-active thiols are kinetically and thermodynamically favored and should play significant roles in *in vivo* metabolism of NAMI-A.

DEDICATION

To Almighty Allah,

to my husband, Adeniran, who was there for late nights and weekends in the lab and my daughter, Amal who has not seen much of me yet.

ACKNOWLEDGEMENTS

TABLE OF CONTENTS

CHAPTER ONE: Introduction

CHAPTER TWO: Instrumentation, Materials and Methods

CHAPTER FIVE: Kinetics and Mechanism of Interaction of NAMI-A with Glutathione

CHAPTER SIX: Kinetics and Mechanism of Interaction of NAMI-A with Cysteine

LIST OF TABLES

LIST OF FIGURES

LIST OF SCHEMES

LIST OF ABBREVIATIONS

NAMI: New Antitumor Metastasis Inhibitor (Sodium trans-[tetrachloro (dimethyl sulfoxide)(imidazole) ruthenate(III)])

NAMI-A: New Antitumor Metastasis Inhibitor-A (Imidazolium trans-[tetrachloro (dimethyl sulfoxide)(imidazole) ruthenate(III)])

GSH   Glutathione

GSSG   Oxidized glutathione

Cisplatin   Cis-diamminedichloroplatinum(II),

MESNA   Sodium mercaptoethane sulfonate

ESI-MS   Electrospray ionization mass spectrometry

EPR   Electron paramagnetic resonance spectroscopy

UV-Vis   Ultraviolet visible spectroscopy

FTIR   Fourier transform infrared spectroscopy

DMSO   Dimethyl sulfoxide

S-DMSO   Dimethyl sulfoxide coordinated through sulfur

r.m.s   Root mean square

Carboplatin   cis-Diammine(1,1-cyclobutanedicarboxylato)platinum(II)

Nedaplatin   cis-Diammine(glycolato)platinum(II)

ICR   Imidazolium trans-bis(imidazole)tetrachlororuthenate(III)

IndICR   Indazolium trans-bis(indazole)tetrachlororuthenate(III)

$\Delta H^{\neq}$ Activation enthalpy

$\Delta S^{\neq}$ Activation entropy

$\Delta G^{\neq}$	Free energy of activation
DMPO	5,5-Dimethyl-1-pyrroline N-oxide
EDTA	Ethylenediaminetetraacetic Acid
BNP7787	Disodium 2,2′-dithio-bis-ethanesulfonate
pKa	Acid dissociation constant
DNA	Deoxyribonucleic acid
HSA	Human serum albumin
p53	Tumor suppressor protein
NSCLC	Non-small cell lung cancer
FDA	US Food and drug administration

CHAPTER ONE

1.0 Introduction

1.1 Metals in nature

The existence and importance of metal ions in the physiological system is well established.[1-3] Nature utilizes metal ions for functions such as oxygen transport, synthesis of vitamin A, fatty acids and cholesterol; formation of urea, detoxification, bone development, and normal functioning of the nervous system.[4-8] Transition metal ions are of particular interest because, even though they occur in trace amounts, their excess or deficiency may result in deleterious conditions such as anemia,[2] liver and oxidative damage, among others.[3;9] Iron, for instance, supports fundamental biological functions involved in the handling and transport of oxygen, detoxification and synthesis of DNA,[10] but is potentially toxic to cells.[11-13] It has been implicated in events that lead to liver and heart diseases,[14] neurodegenerative disorders,[15] diabetes,[2] cancer[16] and catalytic production of free radicals.[9] Transition metals are mostly found complexed in the active sites of metalloenzymes such as nickel in urease[17] or iron in tyrosine hydroxylase, carbonic anhydrase dioxygenases, and isopenicillin N-synthase.[18]

Today there is increased understanding of the activities of transition metal ions and complexes in biological systems.[19] Enlightenment in areas such as metalloprotein functions, models of metal ion active sites, how metal ions are delivered to the active sites,[20;21] and involvement of transition metals in some disease states[22,23] have stimulated the use of metal ions and complexes for therapeutic strategies. One area of global application of metal-based therapeutics is in the treatment of cancer.[24]

1.2   Cancer and cancer statistics

According to the American Cancer Society, cancer is a group of diseases characterized by uncontrolled growth and spread of abnormal cells that result from sequential acquisition of mutations in genes that control cell growth, differentiation, and death.[25] A recent report from Centers for Disease Control and Prevention's National Center for Health Statistics names cancer as the second leading cause of death in the United States, solely accounting for 559,888 (23%) of the 2.42 million total registered deaths in 2006.[26] It is second only to heart disease which accounts for twenty six percent of registered deaths.[26;27] Although overall cancer incidence rates have been on the decline, 1,638,910 new cases and 577,190 cancer deaths are predicted to occur in 2012.[28;29] Considerable treatment success has been achieved with the use of transition metal complexes, especially in the case of testicular cancer with the use of cis-diamminedichloroplatinum(II) (Cisplatin).[30] The structure is shown in Figure 1. Cisplatin is able to damage DNA by binding to N-7 of adjacent guanosine residues which effects distortions that make DNA function and repair impossible.[31] Cisplatin has up to a 90% cure rate for testicular cancer and, in combination with other drugs, has a very high activity against ovarian, cervical and bladder carcinomas.[32-35]
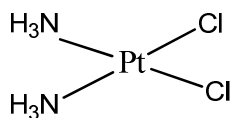
Figure 1-1: *cis-diamminedichloroplatinum(II), (Cisplatin)*

This success is, however, marred by neurotoxicity, nephrotoxicity, alopecia and a lack of selectivity towards cancer cells.[36;37] Drug resistance, metastasis and activity over a small range of cancer types are other limiting factors. Analogues of cisplatin, two of which are shown in Figures 1.2a-b, have been synthesized, in an effort to circumvent the aforementioned problems. These complexes are also in clinical use[38] and have demonstrated similar mechanism of action to that of Cisplatin.[39]

(a)   (b)
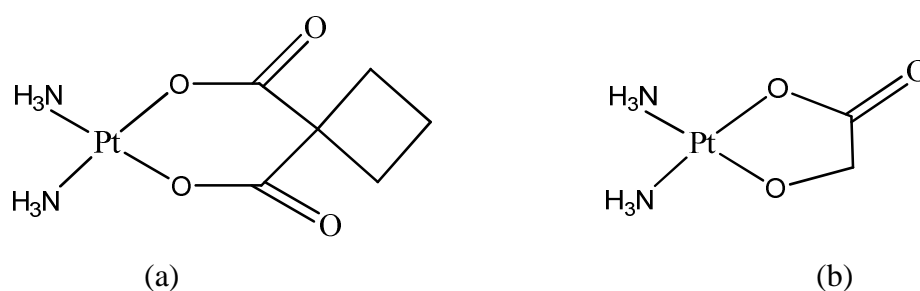
Figure 1-2: *(a) cis-Diammine(1,1-cyclobutanedicarboxylato)platinum(II),*

(Carboplatin)

(b) cis-Diammine(glycolato)platinum(II), (Nedaplatin)

Carboplatin and Nedaplatin are less toxic. Cisplatin and its analogues, however, are almost inactive against several malignancies with high incidence rates such as colon and rectum, lung, breast and prostate carcinomas.[40-43] Also, a commonly occurring side effect of platinum anticancer drugs is ototoxicity.[44] Reports have indicated elevation of hearing threshold in greater than 50% of patients treated with cisplatin,[45] and 84% of children treated with both cisplatin and carboplatin experience hearing loss.[44] Otoxicity

3

has been labeled as a commonly occurring toxicity that may influence academic and social development.[44]

1.3   Metastasis

Metastasis describes the ability of cancer cells to penetrate into lymphatic and blood vessels, circulate through the bloodstream, and then invade normal tissues elsewhere in the body. Metastasis, rather than primary tumor, is the major cause of death for cancer patients with solid tumors.[46] This is reflected by 5-year-survival rates which are higher than 90% for patients in early stages, which drop to 65% for patients initially diagnosed with regional lymph node metastases and is further reduced to less than 10% in patients with distant metastases.[47-49] Metastasis involves a series of events through which cancer cells separate from the parent tumor and enter the circulatory system, float elsewhere, continue proliferation and form a secondary locus of tumor.[50] This process is grossly inefficient in that only few of millions of cells released into circulation are able to colonize a secondary site.[51;52] Alarming failure rate of the process might be due to hostility of normal healthy tissues.[53] Metastatic cells acquire characteristics making them adaptable to their new microenvironment: these characteristics differentiate them from the primary tumor and consequently present differing chemical sensitivity to cytotoxic agents.[54-57] Figure 1-3 highlights the selectivity of metastatic cells for their preferred site for colonization in comparison to primary tumor. Tumor cells can survive in their new microenvironment only if they meet certain cellular preconditions which explain organ-specific metastatic behavior.[50]

These cells flourish in new tissue habitats and ultimately cause organ dysfunction and death. No effective therapeutic option is currently available for metastasis,[58] neither is there an anticancer drug with activity over a wide range of cancer and metastasis. Hence, the intense research efforts towards finding therapeutics of a more desirable profile.
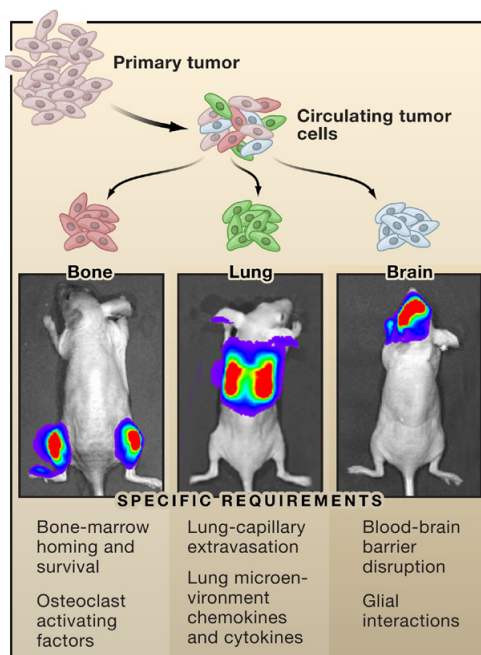
Figure 1-3: *Organ specific colonization demonstrated by metastatic cells. Secondary organs place certain demands on invading tumor cells.[50]*

1.4   Anticancer prodrugs

Prodrugs are chemicals with little or no pharmacological activity before undergoing biotransformation to a therapeutically active metabolite.[59] In drug research and development, several possible improvements on the pharmacological profile of a

drug may be achieved by exploring the prodrug concept. Several improvements have been achieved with this concept. Figure 1-4 summarizes the possible effects.
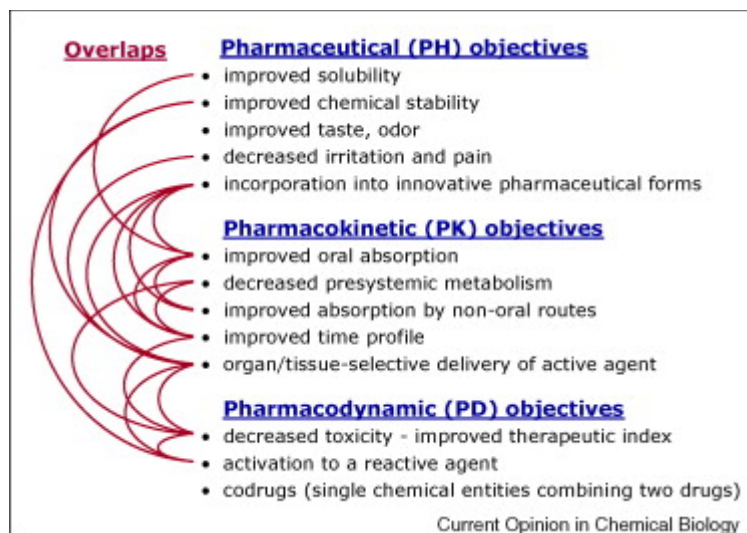
Figure 1-4:   *Classification of prodrug research objectives. [Adapted from Testa, B. 2009. [59]]*

Several non-platinum transition metal complexes have been synthesized for possible reduction or elimination of the undesired effects associated with platinum anticancer drugs presently in clinical use.[60-65] Of special interest are ruthenium complexes that have shown activity against platinum resistant cancer cell lines, colorectal cancer and metastasis Figure 1.5(a-d).[58] Indazolium trans-bis(indazole)-tetrachlororuthenate(III), IndICR, is active against colon carcinomas and a variety of primary explanted human tumors.[66;67] It is noteworthy that 83% of patients with solid tumors who were treated with IndICR present stable disease.[68] Sodium trans-[tetrachloro (dimethyl sulfoxide)(imidazole) ruthenate(III)], called by the acronym

6

NAMI (Figure 1-5c) also shows low host toxicity in active doses.[69;70] The observed reactivities of these complexes can be considered peculiar since ruthenium to date has no known biological function.

(a) NAMI-A

(b) ICR

(c) NAMI

(d) IndICR
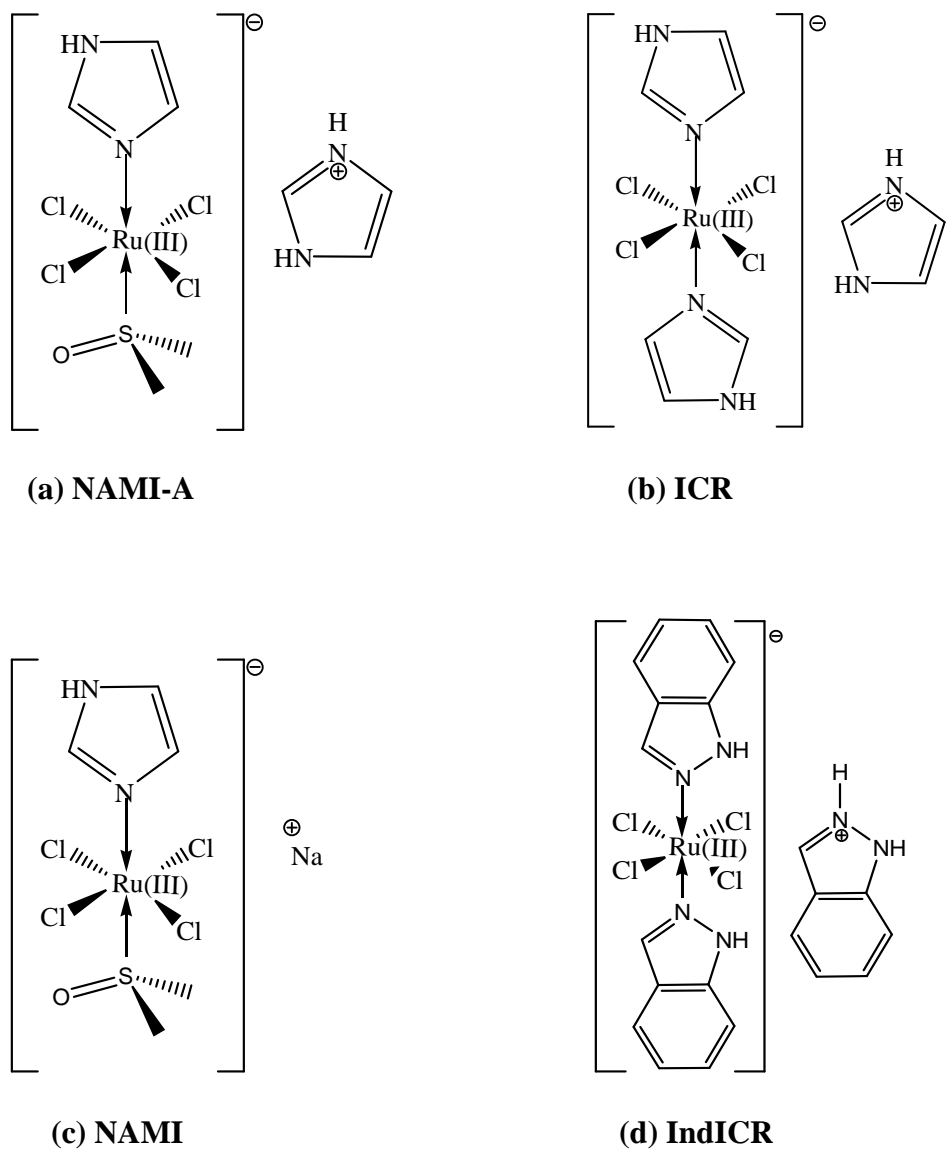
Figure 1-5: *Ruthenium anticancer prodrugs*

1.5   Antitumor Metastasis Inhibitor

Imidazolium trans-[tetrachloro (dimethyl sulfoxide)(imidazole)ruthenate(III)], NAMI-A (Figure 1-5 a), is a ruthenium complex that shows low host toxicity with marked efficacy against metastases.[70-72] It has successfully completed phase I of clinical trials and is currently undergoing phase II studies.[73] Results of Phase I and pharmacological study of this prodrug demonstrate no severe side effect (formal common toxicity criteria (CTC) grade 3) was developed from its use. Formation of painful blister was considered dose limiting.[73] NAMI-A has demonstrated up to 100 % metastasis reduction on preclinical models of solid metastasizing tumors such as Lewis lung carcinoma, TS/A mammary adenocarcinoma,[72] MCa mammary carcinoma,[74] B16 melanoma,[75] and up to 90 % on H460M2 human NSCLC xenograft.[74;76]

One of the initial stages in metastasis progression is reduction of cell adherence leading to detachment from a primary site,[50] NAMI-A has been found to increase cell adherence thereby interfering with other processes leading to full colonization.[76-78] NAMI-A has very high selectivity towards metastases while still having some effect on the primary tumor. Figure 1-6 illustrates the effect of NAMI-A.[79] NAMI-A has been shown to be effective, irrespective of the origin or the stage of growth of metastasis.[72] A critical observation of Figure 1-6 also reveals the inconsequential effect of NAMI-A on primary tumor.
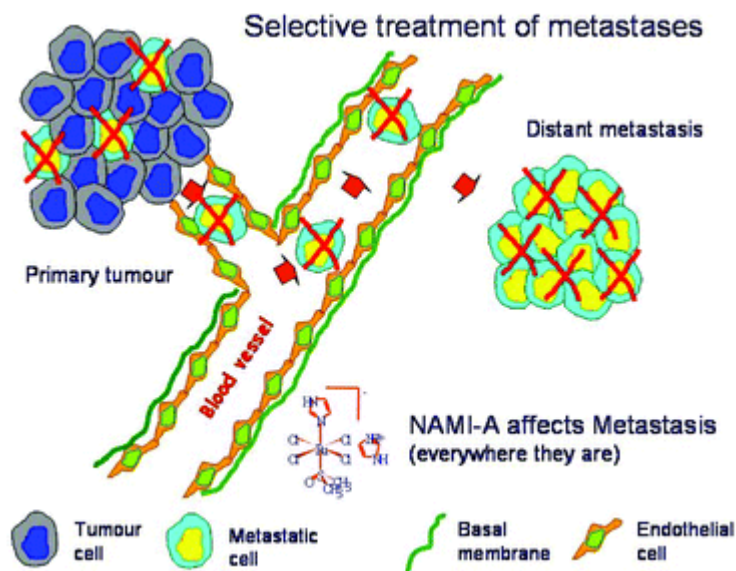
Figure 1-6: *Selective metastatic removal by NAMI-A. It shows weak reduction of primary tumor while removing close to 100% of metastatic cells.[79]*

Cancer cells are constantly proliferating and an important characteristic of tumor growth is the doubling time. Usually a tumor is undetected until it has doubled 30 times (10^9 cells). A tumor mass is sufficient to kill its host after 35 doublings which corresponds to 10^{12} cells.[80] Figure 1-7 illustrates the relationship between tumor cell count, number of doublings and tumor detection. This indicates that a significant portion of tumor growth is completed by the time of detection, although, methods such as ultrasonography and Magnetic Resonance Imaging offers detection of tumors less than 1 cm.[81] A chemotherapy regimen that focuses solely on elimination of metastasis will spare the primary tumor which continues its growth cycle normally. It is then rational to suggest that a regimen that will maximize NAMI-A to full potential should contain another anticancer drug that is effective towards primary tumor.
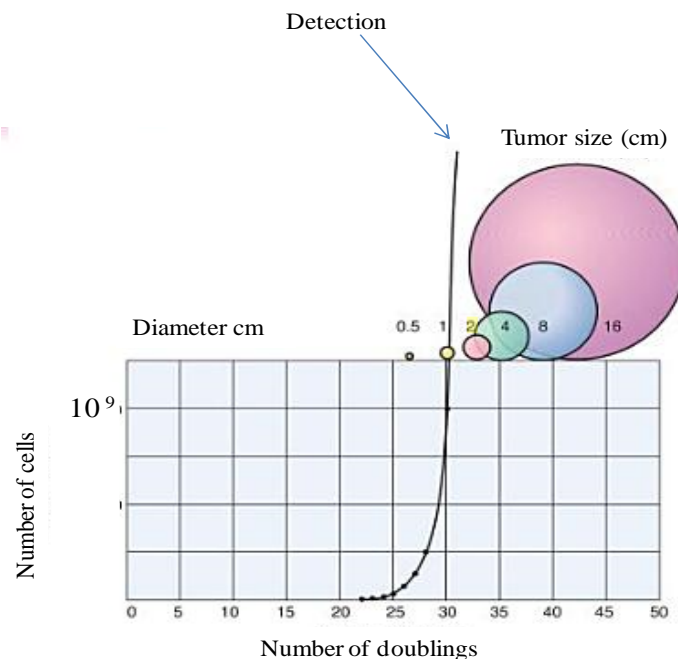
Figure 1-7: *Hypothetical tumor growth curve.*[80]

Research efforts directed at understanding the mechanism of action of NAMI-A are still in their infancy, with recent efforts focused on finding the effects of chemical stability, photostability, interaction with human serum albumi and comparison of treatment outcomes employing different routes of application, among others.[79;82-86]

1.6   Activation by reduction hypothesis

Transition metal complexes readily undergo ligand substitution and redox reactions. The roles of these reactions and the biological activity of a metal complex depend both on thermodynamics and kinetics. Activation by reduction has been proposed for this prodrug, NAMI-A, [33;82;87;88] which may be a factor in its preferential toxicity towards hypoxic tumor and metastatic cancer cells.[33] In support of this

10

"activation-by-reduction" hypothesis, ligand exchange and antimetastatic activity of NAMI-A is enhanced upon addition of biological reductants such as ascorbic acid, cysteine, or glutathione.[84;89]

The major difference between solid tumors and healthy tissues is the nutritional and metabolic environment. The vasculature of tumors is often inadequate to supply the nutritional needs of constantly growing tumor cells leading to oxygen deficiency (hypoxia). Tumor cells produce lactic acid due to their high dependence on aerobic glycolysis, resulting in low pH.[90] Low pH environment and low oxygen favor reduction and this contributes towards the specificity of reduction-activated prodrugs. Ruthenium is able to mimic iron by binding to certain biological molecules such as serum transferrin and albumin since ruthenium and iron are in the same group.[91] Transferrin and albumin are proteins used by mammals to solubilise and transport iron, thereby reducing its toxicity. Preferential selective delivery of the prodrug to tumor cells by transferrin transport has been suggested.[91] Rapidly dividing cancer cells have higher demand for iron and thus have an increased number of transferrin receptors compared to normal cells, resulting in selective deposition of the prodrug.[85;92] Figure 1-8 illustrates the low host toxicity of the ruthenium complex. Binding of NAMI-A to albumin and tranferrin were reported not to be particularly beneficial for antimetastatic activity although may extends biological half life.[93]

Ruthenium complexes in the +3 state are kinetically inert compared to the +2 complexes. This kinetic inertness offers an advantage in that the prodrug gets to its target before transformation or activity. Electrons needed for this reduction are

physiologically accessible and may be provided by biological reductants such as glutathione, ascorbic acid and cysteine residue of proteins.[94]

Ruthenium loaded transferrin

Transferrin receptor
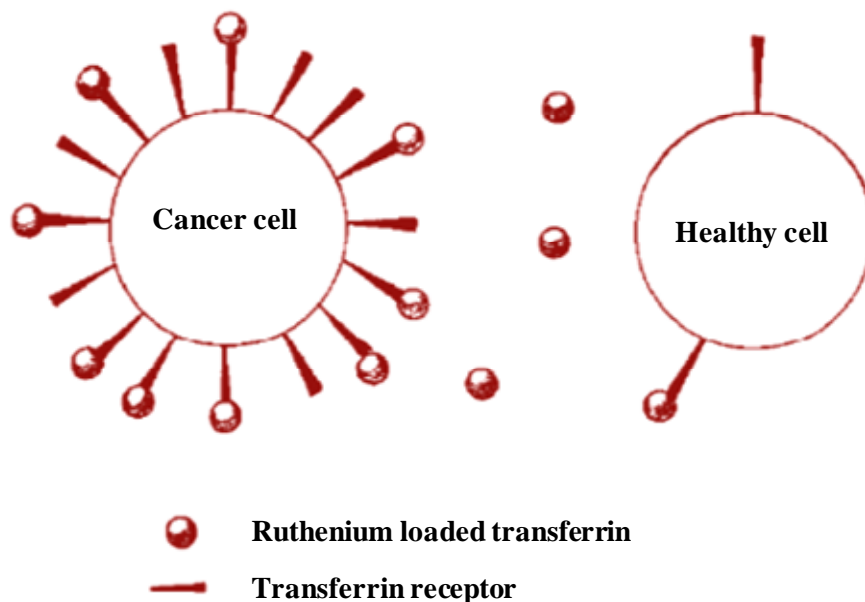
Figure 1-8: *Selective uptake of ruthenium loaded transferrin by cancer cells.[92]*

1.7 Thiols

Thiols are sulfhydryl compounds. The presence of thiol functionality in compounds makes them susceptible to various transformations due to wide range of accessible oxidation states of sulfur, -2 to +6. Endogenous thiols include glutathione (GSH), cysteine, cysteamine and homocysteine. GSH, a tripeptide, is the most abundant and occurs in virtually all mammalian cells.[95] Thiols are involved in many redox processes especially in maintaining the intracellular redox state through thiol-disulfide exchange.[96] Extracellular cysteine/cystine redox status has been implicated in cell

growth and apoptosis.[97] Also, inadequate sulfur amino acid intake results in oxidized thiol/disulfide redox status which is associated with oxidative stress and onset or progression of diseases.[98;99] An interesting illustration of the importance of redox status is that the reduction potential of a cell with 1.0 mM intracellular GSH concentration changes from -250 mV to -190 mV if 18 µM of the GSH is oxidized.[97] This change in reduction potential is adequate to change the functional state of the cell from proliferation (multiplication of epithelial cells) to differentiation (specialization or maturation).[97;100-103] Involvement of thiols in several important cell functions makes it impossible to exclude their interaction with most drugs in establishing a detailed mechanism of drug biotransformation and action.

There are biologically-active thiols that may be introduced as pharmaceuticals. For example, N-acetyl cysteine is used as an adjuvant in respiratory conditions with excessive mucus production and has been shown to prevent metastasis in animal models.[104] Sodium-2-mercaptoethanesulfonate, MESNA, prevents ischemia/reperfusion-induced renal damage, and is also used as a detoxifying agent to inhibit the hemorrhagic cystitis induced by chemotherapy drugs.[105-109] 2-mercaptopropionyl glycine, also known as thiopronin, prevents hepatotoxicity of Isoniazid used in tuberculosis treatment by inhibiting and scavenging free radicals.[110] It reduces cisplatin-induced nephrotoxicity[111] and is also used in treatment of rheumatoid arthritis and cystinuria.[112;113] Thiol protection may not necessarily be desirable in some cases since this may result in drug resistance as observed in reduced anticancer activity of cisplatin in the presence of homocysteine and N-acetyl cysteine.[114] It has been

13

reported that a possible pathway for regulation of human immunodeficiency virus 1(HIV-1) protease activity involves modification of the cysteine residue of HIV-1.[115]

The highly nucleophilic sulfur center is critical to the functioning of thiol-based drugs as radioprotective agents and in DNA repair. The chemistry involved in DNA repair by thiols is represented by R 1.1 – R 1.4.[116]

$$DNA^{\cdot +} + RSH \longrightarrow DNA + RS^{\cdot} + H^+ \qquad R1.1$$

$$DNA^{\cdot +} + RS^- \longrightarrow DNA + RS^{\cdot} \qquad R1.2$$

$$RS^{\cdot} + RSH \rightleftharpoons RSSR^{\cdot -} + H^+ \qquad R1.3$$

$$RSSR^{\cdot -} + DNA^{\cdot +} \longrightarrow DNA + RSSR \qquad R1.4$$
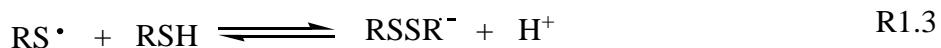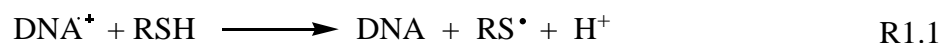
1.7.1 Thiol oxidation

Most biological processes involving the thiol moiety occur through oxidation, some of which were mentioned earlier.[97;117] Non-radical oxidants of potential relevance to oxidative stress include H_2O_2, HOCl and ONOOH,[118-120] and these can react with cysteine or methionine residues of proteins. Oxidation of thiols may proceed through a variety of pathways resulting in series of different metabolites and products.[121-125] Studies from our lab have demonstrated exotic dynamics in oxidation of low molecular weight organosulfur compounds involving some of these oxidants.[126-130] Scheme 1-1 shows possible oxidation pathways for a thiol ranging from a one electron oxidation to disulfide all the way to eight-electron oxidation to form sulfate.

14
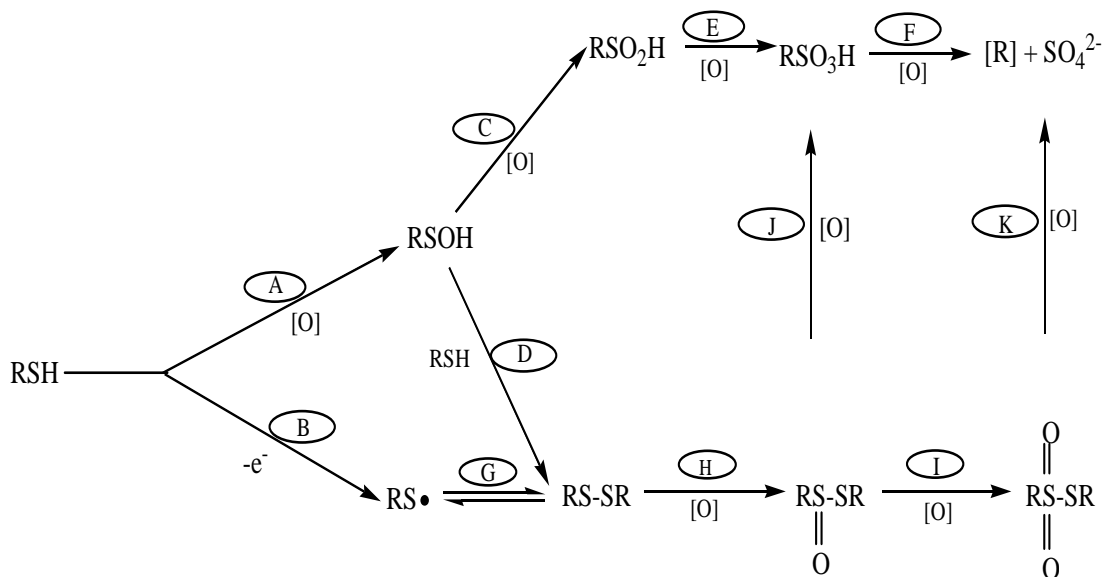
Scheme 1-1: *Possible oxidation pathways for a thiol*[127]

Enzymatic oxidation of thiols by peroxidase; mainly by horseradish peroxidase, lactoperoxidase, and myeloperoxidase, have been shown to yield thiyl radicals[131;132]. Thiols can also be oxidized to disulfide by metal ions or complexes. This oxidation generally proceeds through thiyl radical formation (R1.5 and 1.6). Once formed, the thiyl radical can undergo several other reactions depending on what species are immediately available. Two thiyl radical molecules can react to form the disulfide (R1.6), a thiyl radical can react with the parent thiol (R1.7) or thiolate anion (R1.8) to form disulfide radical anion.[133-135] Thiyl radicals have also been shown to form sulfenic acid and other oxygen containing products.[133;135;136]

$$RSH \quad + \quad M^n \longrightarrow \quad RS^{\bullet} \quad + \quad M^{n-1} \quad + \quad H^+ \qquad \qquad R1.5$$

$$RS^{\bullet} \quad + \quad RS^{\bullet} \longrightarrow \quad RSSR \qquad \qquad R1.6$$

$$RS^{\bullet} \quad + \quad RSH \longrightarrow \quad RSSR^{\bullet -} \quad + \quad H^+ \qquad \qquad R1.7$$

$$RS^{\bullet} \quad + \quad RS^- \longrightarrow \quad RSSR^{\bullet -} \qquad \qquad R1.8$$

$$RSSR^{\bullet -} \quad + \quad M^n \longrightarrow \quad RSSR \quad + \quad M^{n-1} \qquad \qquad R1.9$$

$$RS^{\bullet} \quad + \quad M^n \quad + \quad H_2O \longrightarrow \quad RSOH \quad + \quad M^{n-1} \quad + \quad H^+ \qquad R1.10$$
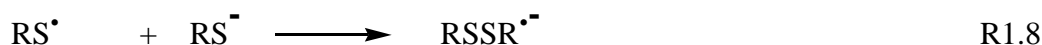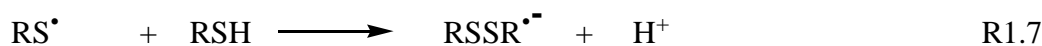
Scheme 1-2: *Reactions involved in thiol oxidation by a metal ion or complex.*[133-135]

1.7.2 Metal binding

Thiols can form complexes with metals ions or transition metal complexes where the sulfur atom of the SH group acts as the binding site.[137;138] For instance, D-penicillamine has been shown to form variable complexes; a purple paramagnetic complex and a yellow diamagnetic complex with copper; depending on the ratio of copper to penicillamine.[139] The ability of thiols to form complexes with metals is being utilized in medicine for treatment of diseases involving excess metals in the physiological environment such as Alzheimer's, Parkinson's and Huntington's diseases.[140] Thiols can effectively remove excess metal by competing for the metal ion with biological binding sites. This type of treatment requires selectivity of the thiol towards certain metals in order to avoid possible depletion of essential metals. D-penicillamine, a disubstituted cysteine, chelates excess copper and enhances copper excretion in Wilson's disease.[141;142] A process involving thiol-disulfide exchange in zinc fingers has been used to release complexed zinc. This process has been found to inhibit

both laboratory strains and clinical isolates of HIV-1.[143-145] Dimercaptosuccinic acid and dimercaptopropionic sulfonate have gained general acceptance in the management of many human metal intoxications which include lead, arsenic, and mercury compounds.[146-150] Metal binding properties of thiols have also been explored in modulating the functions of proteins containing the thiol moiety.[151]

In platinum cancer therapy, the metal binding characteristic of thiols may be beneficial[152] but more often is undesirable since this interaction leads to reduced availability and deactivation of the platinum complex.[153] Reports have shown this to play a significant role in drug resistance and inactivation[153-157] Scheme 1-3 describes interactions of cisplatin with L-cysteine that results in its unavailability for its desired function.[153;158]

It is interesting that interactions of NAMI-A with biological reductants such as thiols have been proposed to play a significant role in its activation as opposed to deactivation in the case of platinum drugs.[153;158] It has also been shown that NAMI-A is rapidly reduced under physiological conditions[94] with ambiguity as to whether its reduced form or hydrolytic derivative react with human serum albumin and ascorbic acid in acidic medium.[159] There have been several reports of hydrolysis pathways for the promising prodrug,[160;161] the mechanism of action and the nature of chemical species responsible for the pharmacological properties of this prodrug are yet to be unraveled and kinetics studies directed at elucidating the mechanism of its interaction with biologically-relevant thiols is simply nonexistent.
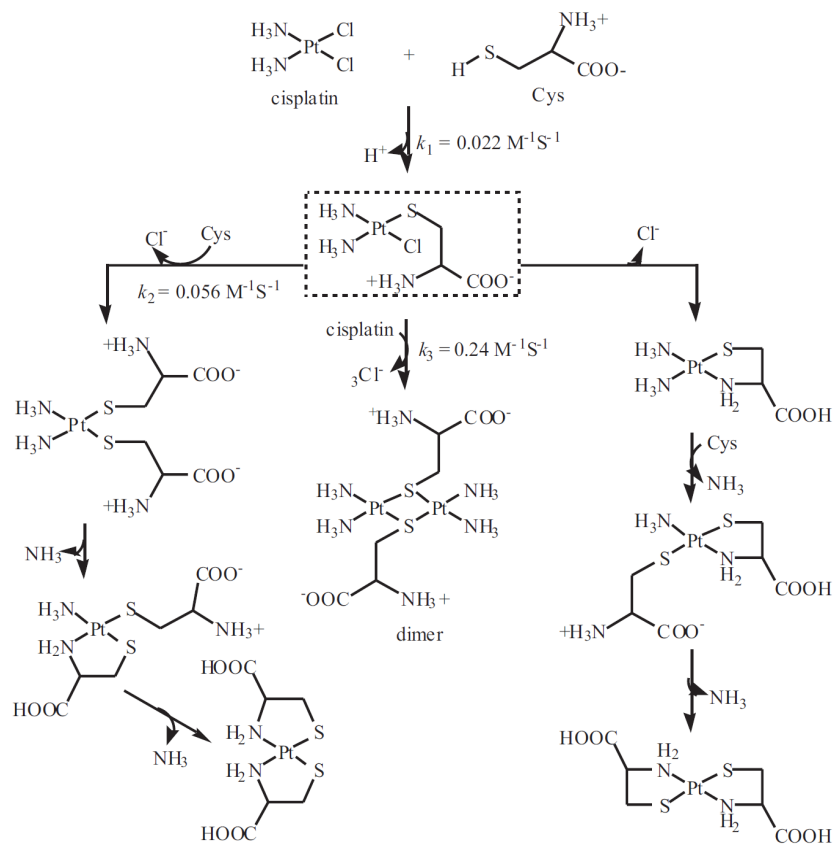
Scheme 1-3: *Reactions between cisplatin and L-cysteine at neutral pH*[153;158]

Legend: *Cys – Cysteine, Cl⁻ - Chloride ion*

1.8   This Study

Metastases, due to their inadequate responsiveness towards any clinically available cancer drug heighten the need for drugs that are effective against metastases. Development of NAMI-A, a compound that is 1,053 times less toxic than cisplatin, [162] is a step towards achieving the long desired activity against metastasis. Reports have excluded DNA binding as the major target for antimetastatic activity of NAMI-A[163-165] suggesting that its interaction with biomolecules other than nucleobases may represent

the molecular basis for its peculiar biological activity. An understanding of the chemical transformations of NAMI-A upon interaction with endogenous molecules and xenobiotics is of prime importance for its pharmaceutical and biomedical applications.

Absorption, distribution, metabolism, excretion and toxicity (ADMET) are important concepts in drug therapy and depend on kinetics and thermodynamics of interactions of the drug with biomolecules. Even after 40 years of clinical use of Cisplatin (world's most widely used anticancer drug), the mechanism of action of the drug is yet to be completely unraveled.[166] Recognizing this fact and understanding that interaction of NAMI-A with xenobiotics are of potential biological importance, the work reported in this dissertation therefore focused on:

(1)   Investigating molecular transformations involved in the interactions of NAMI-A with select thiols (GSH, cysteine, cysteamine and MESNA) and identification of observable species. The choice of these thiols examines reactions of NAMI-A with cellular thiols and clinical chemoprotectant, MESNA, while providing a model for NAMI-A interaction with proteins and enzymes with thiol residues.

(2)   Studying and determining the kinetics and thermodynamics of these interactions.

(3)   Deduction of plausible mechanism of interaction from experimental results. Plausible reaction mechanisms will be proposed for the studied reactions based on experimental results obtained.

This is information necessary for any xenobiotic, especially an experimental drug with a desirable pharmacological profile whose cellular target remains to be determined. An understanding of these interactions on a molecular level may give access to control of

19

drug activity, refinement of structures for more desirable effects and, most importantly,

ensure that treatment/drug metabolism proceeds in a predictable manner.

CHAPTER TWO

2.0   Instrumentation, Materials and Methods

2.1   Introduction

Kinetics deal with the study of reaction rates in an effort to understand the quantities that influence the rates, describe the series of elementary steps involved in reaction systems (the mechanism) and deduce rate parameters governing such reactions. Knowledge of reaction rates has many practical applications including, but not limited to, designing an industrial process, understanding complex dynamics of the atmosphere, optimizing synthetic processes, establishing the best administration mode for a drug, deducing metabolic pathways and improving specificity of therapeutics. Kinetics can also be employed in establishing indices responsible for drug resistance and elucidating pathways to such drug resistance. In order to achieve these applications, reaction dynamics require a series of information on the progress of reaction. The necessary information includes dynamical variables such as temperature, pressure, pH, reactant concentrations, solvent and ionic strength.

The reaction to be studied dictates the set of conditions required. Careful choice of analytical techniques and instrumentation, therefore, is required for reliable kinetic outcomes. The stoichiometry of reaction is the first step in establishing an overall equation for a reaction. Specialized analytical methods such as nuclear magnetic resonance spectroscopy, electron paramagnetic resonance spectroscopy, infrared and Raman spectroscopy, ultraviolet and visible spectrophotometry, mass spectrometry, stopped flow spectrophotometry, etc. are tools used for monitoring reaction progress via

21

determination of reactants or intermediate concentrations as well as product identification.

2.2   Instrumentation

2.2.1   Conventional UV/Vis Spectrophotometry

UV-visible spectroscopy measures absorption of the electromagnetic radiation caused by electronic transitions from the ground state to the excited state of bonding and non-bonding electrons of ions or molecules. For this study, a Perkin-Elmer Lambda 25 UV-VIS spectrophotometer featuring a double beam, all-reflecting system with a spectral range of 200 nm to 700 nm was used. For this instrument, the visible region uses a halogen lamp and the UV region uses a deuterium lamp.[167] The spectrophotometer is interfaced to a computer with Perkin-Elmer UV WinLab software[167] for data acquisition, storage and analyses. The instrument is attached to a thermostated water bath for maintenance of constant temperature. Spectral changes of reaction mixtures were recorded over the wavelength range to establish suitable wavelength for kinetics observations.

2.2.2   Stopped-flow Spectrophotometry

Stopped-flow spectrophotometry has the advantage of using small amounts of reactants, and providing rapid and efficient mixing that comes with an analytical response that has good time resolution. It allows for changes in optical properties of solutions (in this case absorbance) to be monitored using UV-VIS detection. It offers an

advantage in the study of fast reactions which might have been impossible with conventional UV/Vis spectrophotometric techniques. A Hi-Tech Scientific SF61-DX2 double mixing stopped-flow spectrophotometer was used for all kinetic studies. Amplification and digitization of detector signal from the spectrophotometer was done via an Omega Engineering DAS-50/1 16-bit A/D board interfaced to a computer for storage and data analysis. A dead time of 1.0 ms will ensure observation of the crucial initial parts of rapid and even complex reactions which otherwise might have been impossible. The light source is a 75W super quiet Xenon arc lamp. Figure 2.1 is a schematic diagram for the sample handling unit that separates compartments for up to three reactants allowing for different mixing sequences in optimizing experiment procedure.

The double mixing mode enables transient species formed by mixing reactants in A and B to be subsequently mixed with a third reactant, C, after a delay period if needed (refer to Figure 2-1). Reactant reservoir D can be reserved for the buffer and this pushes the premixed solutions A and B (from mixer 1) to a second mixer (mixer 2) where it reacts further with reactant C. The resultant mixture passes through a measurement flow cell and into a stopping syringe where the flow is stopped. Just prior to stopping, a steady state flow is achieved.
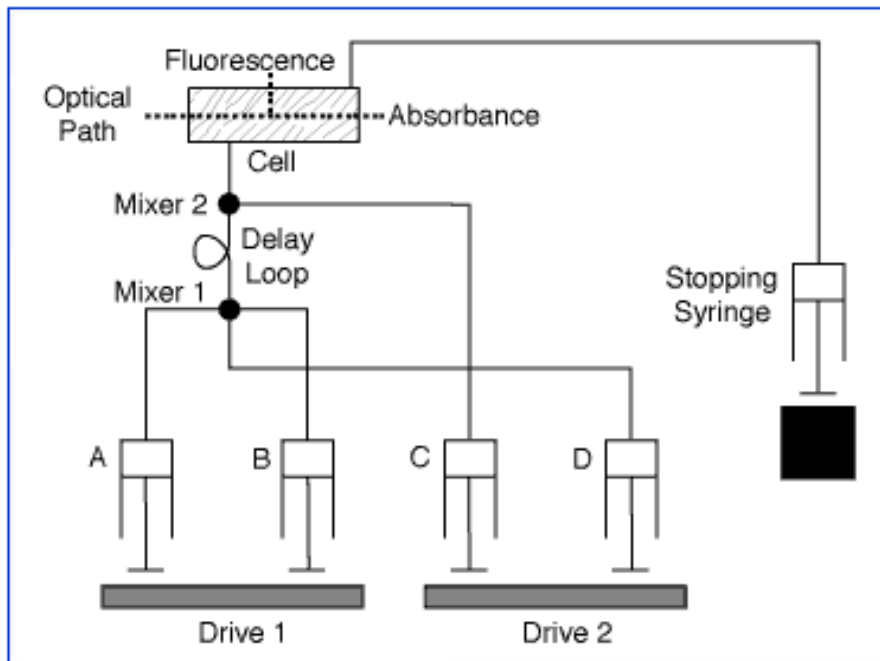
Figure 2-1: *Sample Handling Unit (SHU) flow circuit diagram for the SF-61DX2 Hi-Tech KinetAsyst stopped-flow spectrometer. [Courtesy of Hi-Tech Scientific operator's Manual]*

2.2.3 Electrospray-Ionization Mass Spectrometry (ESI-MS):

Mass spectrometry, MS, is an analytical technique that sorts and measures ionized molecules based on their mass-to-charge ratios. The possibility of observing the fragmentation pattern of a molecule makes MS an invaluable technique for structural elucidation. This spectrometric method works on the basic principle of separation of ions of a compound on the basis of their mass-to-charge ratio (m/z) and the number of ions representing each m/z unit when a compound is ionized. Ionization method is dictated by the nature of analyte. Electrospray ionization method which has the advantage possible molecular determination of intact analytes is a method of choice.

24

Figure 2-2 describes the mechanism of ion formation using ESI. An analyte, usually dissolved in a polar volatile solvent, is introduced and passes through the electrospray needle to which a high potential difference has been applied (typically 2.5 to 4 kV). This potential difference forces the spraying of droplets with a surface charge of the same polarity as the needle. Solvent evaporation occurs as the charged droplets are repelled towards the counter electrode (shown in blue). The rapid shrinking of the droplets by evaporation of solvent increased charge density on their surface, a critical point (Rayleigh Stability limit) is reached when the charge density of the droplet and the attraction of the positive ions to the counter electrode overcomes the surface tension holding the droplet together, leading to fission (coulombic explosion) with the release of smaller droplets containing charged analyte molecules.[168;169]
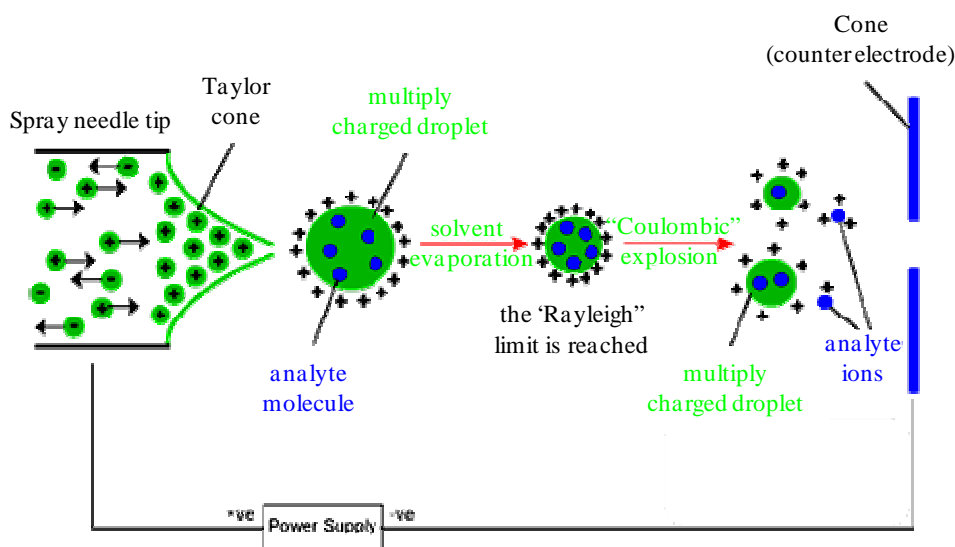
Figure 2-2: *Schematic for ion formation in ESI.[170]*

The mass spectral analysis for product identification in this study was performed using a Thermo LTQ Orbitrap Discovery hybrid mass spectrometer (San Jose, CA), equipped with an Ion Max ESI source. This combines a soft ionization technique, large mass range of (50 - 2000 m/z), mass accuracy of <2 ppm root mean square (r.m.s) and up to 30,000 resolving power with a detect time of 400 ms.[171;172] (LTQ Orbitrap Discovery Hardware Manual 1-5 ThermoFisher Scientific)

2.2.4   Nuclear Magnetic Resonance Spectroscopy (NMR)

Nuclear Magnetic Resonance spectroscopy is an essential analytical tool used in chemical analysis and fundamental research. Its versatility derives from the atomic nature of the information it provides. In principle, nuclei that contain odd mass numbers (such as ^{1}H, ^{13}C, ^{19}F, and ^{31}P) or odd atomic number (such as ^{14}N and ^{2}H) absorb electromagnetic radiation at a frequency characteristic of the nuclei in the presence of an external magnetic field.[173] The signal in NMR spectroscopy is due to the disparities in the energy absorbed by the nuclei as they are excited from the lower energy state to the higher energy state, and the energy emitted by the nuclei as they relax from the higher energy state to the lower energy state. The NMR technique was used in this study for confirming the structure of NAMI-A, where a comparison was made to literature.

2.2.5 Electron Paramagnetic Resonance Spectroscopy (EPR)

EPR is a technique for measuring absorption of electromagnetic radiation by an electron spin system.[173] EPR has evolved to be a nondestructive, noninvasive analytical technique for structural and dynamical information. It has very high sensitivity with a detection limit in the nanomolar range. EPR has been applied in the measurement of both *in vitro* and *in vivo* free radical intermediates from drugs and oxidative processes. Pharmacokinetic information of paramagnetic compounds in mice have been obtained in mice just by placing the tail of the animal directly in the EPR resonator.[174] EPR has proven useful in evaluation of oxidative stability of vegetable oils.[175]

Free radicals have been implicated in metabolism of sulfhydryl moieties especially in oxidative disease states.[176] Since reactions in this study involve electron transfer, the possibility therefore arises for involvement of free radical mechanisms. EPR measurements were carried out for detection and possible quantification of free radicals on a Bruker™ Biospin e-scan spectrometer designed to perform EPR measurements in the X-band-range. However, our reactions did not demonstrate involvement of free radicals as indicated by EPR silent reaction solutions in the presence of DMPO spin trap. This gave an indication that at least, non-metal centered radical (sulfur, oxygen or carbon) were not involved, since the 300G sweep width of our instrument is not sufficient for a most metal based radicals.

2.3   Materials

Glutathione, cysteamine, L-cysteine, 2-mercaptoethane sulfonate (MESNA), sodium hydroxide, sodium chloride, sodium perchlorate, perchloric acid, absolute ethanol, acetone, diethyl ether, hydrochloric acid, imidazole, dimethyl sulfoxide, deuterium chloride, deuterium oxide (all from Sigma-Aldrich), monosodium phosphate, monohydrate, disodium phosphate heptahydrate (from Fisher Scientific) and ruthenium chloride (from GFS chemicals) were of analytical grade and used as obtained. Aqueous solutions of reactants and buffers were prepared in distilled deionized water obtained from a Barnstead Sybron Corporation water purification unit that dispenses water with resistance of at least 18MΩ.

pH of the solutions was measured with a 720 A+, Thermo Orion pH meter. Phosphate or acetate buffer was used to adjust the pH of the experimental solutions. Reactions were carried out at $25.0 \pm 0.1°C$ (except for when isolating the effect of temperature) and at a constant ionic strength of 1.0 M using $NaClO_4$ or NaCl (except when isolating the effect of ionic strength).

2.4   Experimental Methods

2.4.1   Synthesis of hydrogen *trans*-bis(dimethyl sulfoxide)tetrachlororuthenate-(III)

NAMI-A precursor, Hydrogen *trans*-Bis(dimethyl sulfoxide) tetrachloro-ruthenate(III), was synthesized using published method.[177] Briefly, 1.0 g of $RuCl_3.3H_2O$ was dissolved in 30 mL of ethanol and refluxed for 3 hours. The filtered solution was

concentrated to about 3 mL and a mixture of 1 mL of 37 % HCl and 2 mL of DMSO was added. The resulting solution was kept at 80 ^{o}C for 15 minutes and a bright orange solution was obtained. The solution was cooled to room temperature and a 10 mL aliquot of acetone was added and then four drops of ethyl ether. Crystals were filtered, washed with cold acetone and ethyl ether and dried in a desiccator. The obtained crystals were characterized using X-ray crystallography using a Siemens P4 diffractometer equipped with a graphite monochromator, a monocap collimator, a Mo Kα radiation source (λ = 0.71073 Å), and a SMART CCD detector.

2.4.2 Synthesis of NAMI-A: NAMI-A was synthesized from this precursor.[8] 0.49 g of imidazole was added to 1.0 g of precursor suspended in 20 mL of acetone at room temperature. This mixture was stirred for 4 hours. The precipitate obtained in this manner was washed with cold acetone and ethyl ether. Characterization of this complex was done using FTIR, UV/VIS, NMR and electrospray ionization mass spectrometry (ESI-MS). Spectral data are in good agreement with those reported in the literature.[178]

Stock solution of NAMI-A was freshly prepared for each experiment. Proctection from light was not necessary due to reported evidence of photostability of NAMI-A solutions[179]and more importantly, it maintained pharmacological efficacy even after aging up to 8 hours.[84]

2.4.3 Stoichiometric Determinations: Different ratios of NAMI-A to thiol concentrations were prepared from freshly prepared stock solutions vis: 0.25 to 4.

Residual absorbance at 390 nm of the solutions were measured and plotted against corresponding oxidant to reductant ratio. The stoichiometry was obtained as the ratio beyond which no more NAMI-A was consumed.

2.4.4   Product Identification: Possible detection and identification of intermediates and product would be performed utilizing UV/VIS, NMR, ESI-MS or EPR techniques as the reactions require. For ESI-MS, aqueous reactant solutions were prepared in distilled deionized water with resistance of at least 18MΩ.

2.4.5   Reaction Dynamics: Kinetics measurements were performed on the Hi-Tech Scientific single mixing (SF-61SX2) and double mixing (SF-61DX2) models stopped-flow spectrophotometers. Stock solutions of thiols and metal complexes were freshly prepared for each set of experiments. The biologically-active thiols used in this work lack distinct absorption in the 200 – 700 nm region. This necessitated monitoring of reaction progress at the absorption wavelength of NAMI-A which has a distinct absorption in the visible region, λ_{max} 390 nm. All kinetics experiments were carried out at 25.0 ± 0.1 °C except when the effect of temperature was monitored, in which case temperature range was 10 °C - 37 °C. A constant ionic strength of 1.0 M was maintained using sodium chloride or sodium perchlorate except when the effect of ionic strength was explored. For evaluation of reaction dependence on ionic strength, kinetics of reactions were examined using varying amounts of $NaClO_4$. Contributions from all charged species (buffer, NAMI-A and sometimes the thiol) present in solution were

taken into consideration for these measurements using the standard calculation for ionic strength.

To evaluate effect of oxygen, argon was bubbled into freshly prepared solutions, and since reaction rate and profile did not change significantly from reactions run in ambient air. Similar results have been reported for the reaction of Indazolium trans-bis(indazole)tetrachlororuthenate(III) with glutathione.[180] All reactions were as such run in ambient air. In an attempt to simulate the physiological environment, experiments were carried out using bicarbornate buffer. The results, however, demonstrated that the pH was not adequately maintained. Phosphate buffer was therefore used to maintain a pH of 7.4. For reactions of NAMI-A with MESNA, reaction profile was monitored at four other pHs: 3, 4, 5, 6. Phase I clinical trials reported that NAMI-A can be safely administered at 300 mg/m^2/day for 5 days every 3 weeks,[181] corresponding to 6.55 x 10^{-4} mol/m^2/day, therefore, < 1.50 x 10^{-4} M of NAMI-A was used. Pseudo-first-order condition of excess thiol was adhered to.

Chloride is found in most body fluids, including blood, plasma, serum, urine and saliva. Plasma chloride concentrations approximate to 100 mM in normal human blood. Kinetics experiments with this chloride concentration were considered initially, however, kinetics traces containing 0.1 and 1.0 M NaCl were indistinguishable. Therefore, chloride concentrations greater than 0.5 M were used. This is particularly advantageous for ensured stability of NAMI-A, since inhibition of chloride and DMSO hydrolysis of NAMI-A at high chloride concentrations have been reported.[160]

CHAPTER THREE

3.0   Kinetics and Mechanism of Interaction of NAMI-A with Cysteamine

3.1   Introduction

One of the most devastating facts about cancer treatment is lack of specificity for cancerous cells such that an effective drug candidate has equal potential of harming (normal) healthy cells. According to the National Cancer Institute, cancer treatment options include surgery, chemotherapy, radiation therapy, biological and targeted therapies, all with an endless list of side effects that are sometimes lethal.[182] Up to 30% of patients undergoing radiation-therapy for lung cancer, breast cancer, lymphoma, or thymoma present radiation-related symptoms.[183;184] Incidences of acute adverse effects of chemotherapy such as bone marrow suppression, renal failure, cardiotoxicity, mutagenicity and emesis are well documented.[185-188]

Cancer treatment options attempt to strike a balance between beneficial and adverse effects, necessitating the use of agents that protect healthy cells from toxic effects of these treatment types.[189-191] Aminothiols have been successful as chemo and radio protectants.[192;193] Prevention of immediate and delayed effects of therapy is expected of an ideal protectant. A Phase III clinical trials report has proven Amifostine, an FDA approved aminothiol, as the only effective cytoprotectant against cisplatin-induced cumulative renal toxicity.[194;195] Amifostine was originally selected as a radioprotective agent by the Antiradiation Drug Development Program of the U.S. Army Medical Research and Development Command after synthesis and testing of 4,400 compounds.[196] The range of applications of Amifostine is on the increase (see

Table 3.1). Studies have demonstrated selective chemo and radio protection of normal cells by Amifostine.[197]

Agent	Adverse Effect
Cisplatin	Nephrotoxicity Neurotoxicity Renal toxicity Peripheral nerve damage
Cyclophosphamide	Pulmonary toxicity
Fotemustine	Mutagenicity
Doxorubicin	Cardiotoxicity
Mitomycin C	Hematological toxicity
Radiation therapy	Hematological toxicity Mutagenicity Carcinogenicity Mucosa, skin and salivary gland damage

Table 3.1: *Summary of selected anticancer agents and corresponding effects against which Amifostine offers protection.[195;198-201]*

In vivo, Aminofostine is dephosphorylated by alkaline phosphatase enzyme to the free thiol, WR-1065, which is the active metabolite (see Scheme 3-1). Alkaline

phosphatase is expressed more in normal cells compared to cancerous cells leading to higher contents of WR-1065 in normal cells.[202-204] WR-1065 is structurally related to cysteamine, a cellular thiol (Figure 3-1).
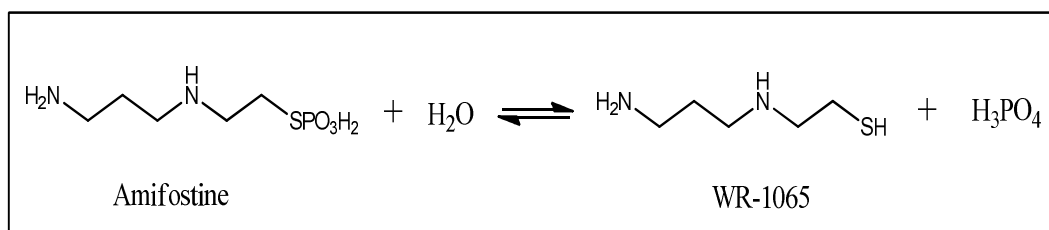
Scheme 3-1: *Hydrolysis of amifostine to form its active metabolite, WR-1065*
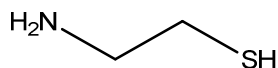
Figure 3-1: *2-aminoethanethiol also called cysteamine. Structurally related to the active metabolite of amifostine, WR-1065.*

Cysteamine modulates cellular levels of glutathione[205] and is an important intermediate in the alternative pathway of taurine biosynthesis (i.e coenzyme A degradation).[206] The discovery of cysteamine dioxygenase emphasizes biological importance of this simple thiol. Cysteamine dioxygenase adds two atoms of oxygen to free cysteamine to form hypotaurine which is further oxidized to taurine.[207-209] Cysteamine has been approved by the FDA for treating nephropathic cystinosis, a rare lysosomal storage disease that might result in kidney failure or death if unattended.[210-212] Applications of cysteamine are on the increase with recent studies demonstrating its specific activity against

Plasmodium malaria parasite[213] and potentiation of antimalaria activity of artemisinin.[214;215]

Reports on effectiveness of cysteamine in radioprotection and chemoprotection are extensive.[216-220] Documented effectiveness of cysteamine in cystinosis treatment, radio and chemo protection and its structural similarity to amifostine makes its interaction with NAMI-A a possibility in a combination-regimen involving NAMI-A and any cancer treatment against which protection is necessary. In this chapter, results are presented for such an interaction.

3.2 Results

3.2.1 Stoichiometry and Product Identification: Stoichiometric determinations employing measurement of residual absorbance at 390 nm of solutions containing varying ratios of NAMI-A and cysteamine are shown in Figure 3-2. Absorbances were recorded within 2 minutes of solution preparation.
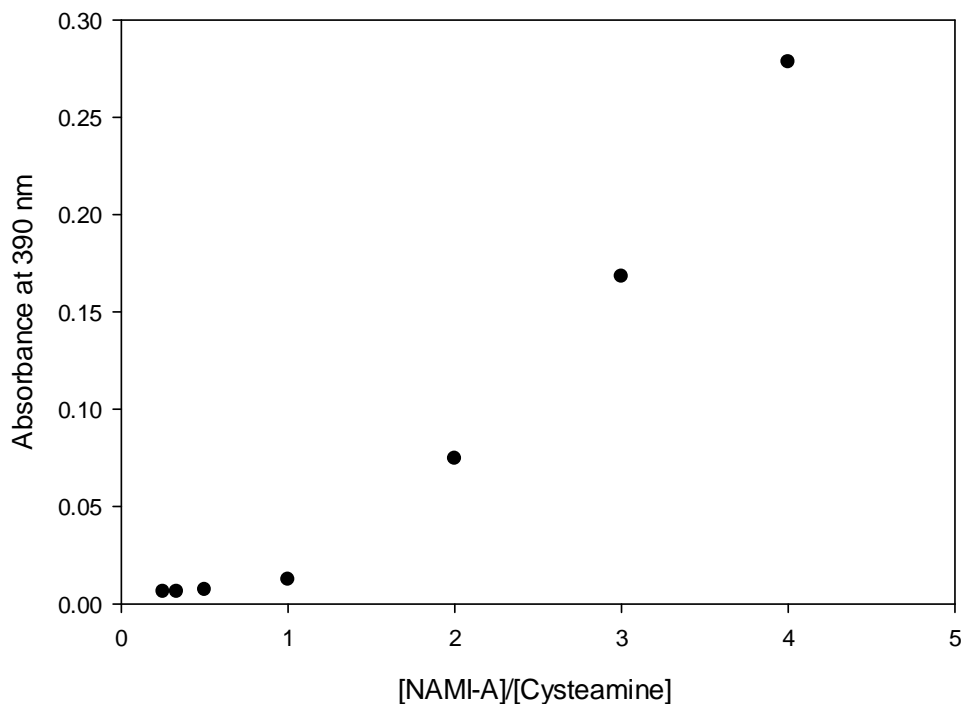
Figure 3-2: *Plot of Residual absorbance of NAMI-A against [NAMI-A]/[cysteamine] ratio revealing stoichiometric ratio beyond which residual absorbance persists. [NAMI-A]/[cysteine] = 0.25, 0.33, 0.5, 1.0, 2.0, 3.0 and 4.0.*

A full ESI-MS spectrum of equimolar concentrations of NAMI-A and cysteamine was taken within the first minute of the reaction in order to identify molecular species and possible intermediates involved in the reaction progress (see Figure 3-3). An ESI-MS peak corresponding to NAMI-A was observed at 389 m/z. The small relative abundance of this peak is expected since the reaction occurs in the order of ~ 4 s as recorded on the stopped-flow. The reaction is essentially complete on comparing the time scale of the reaction with that of ESI-MS experiment, although the sample was run with as short a time-lapse as possible from mixing time. Other peaks observed in the negative mode

spectrum demonstrate hydrolysis of NAMI-A involving two of the axial chloride ligands, 352 m/z, and loss of one or both of the apical ligands 274 and 209 m/z respectively. The peak at 180 m/z cannot be identified at this time, although its profile may suggest a non ruthenium-containing species.
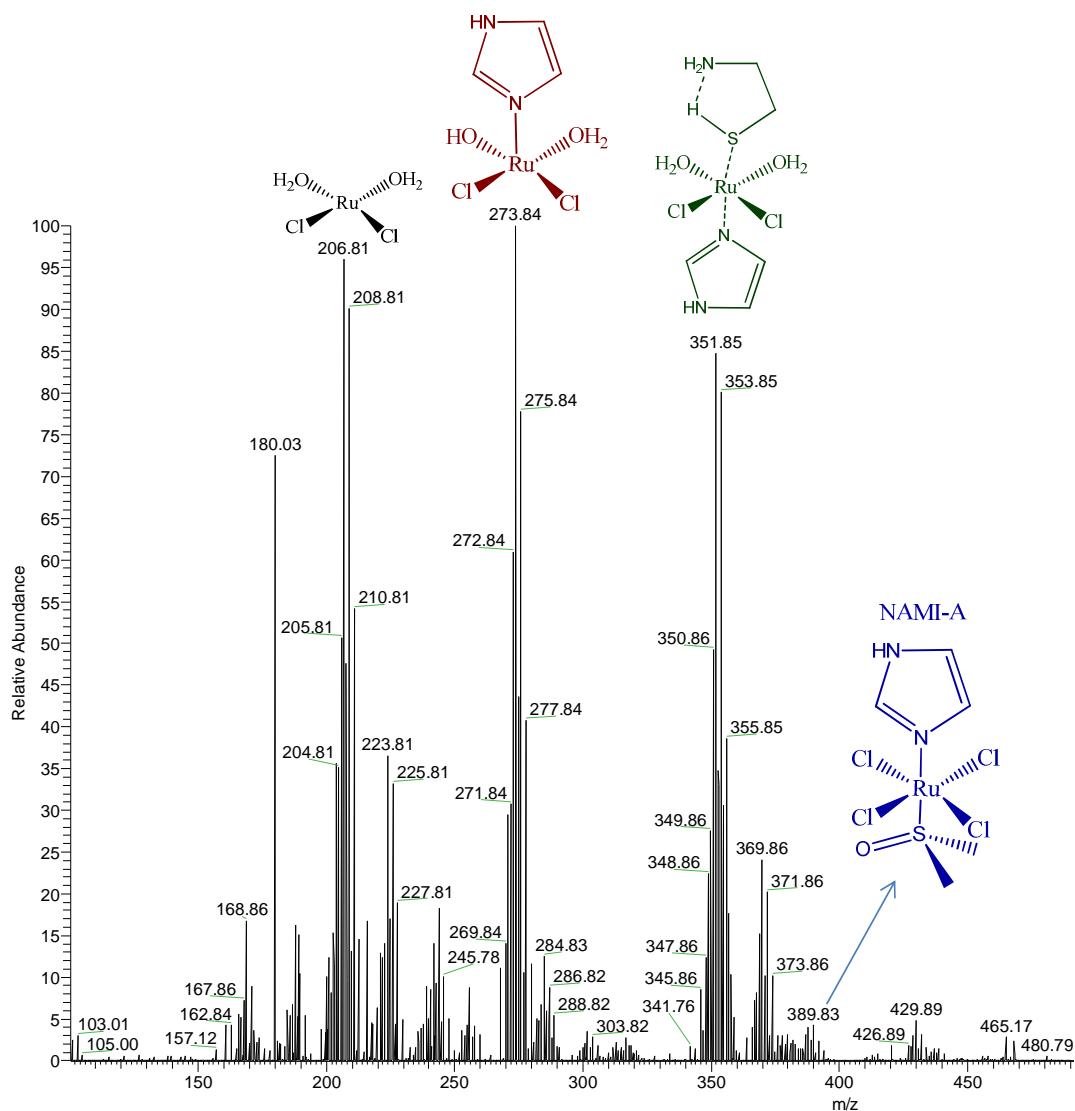
Figure 3-3: *Full ESI-MS (negative mode) spectrum of 1:1 ratio of NAMI-A to cysteamine taken within the first minute of the reaction in 50% methanol.*

37

Spectrum of the same reaction in the positive mode (Figure 3-4) features cystamine, disulfide of cysteamine at 153 m/z. This conforms to the expected result of a one-electron oxidation of cysteamine which should result in cystamine.
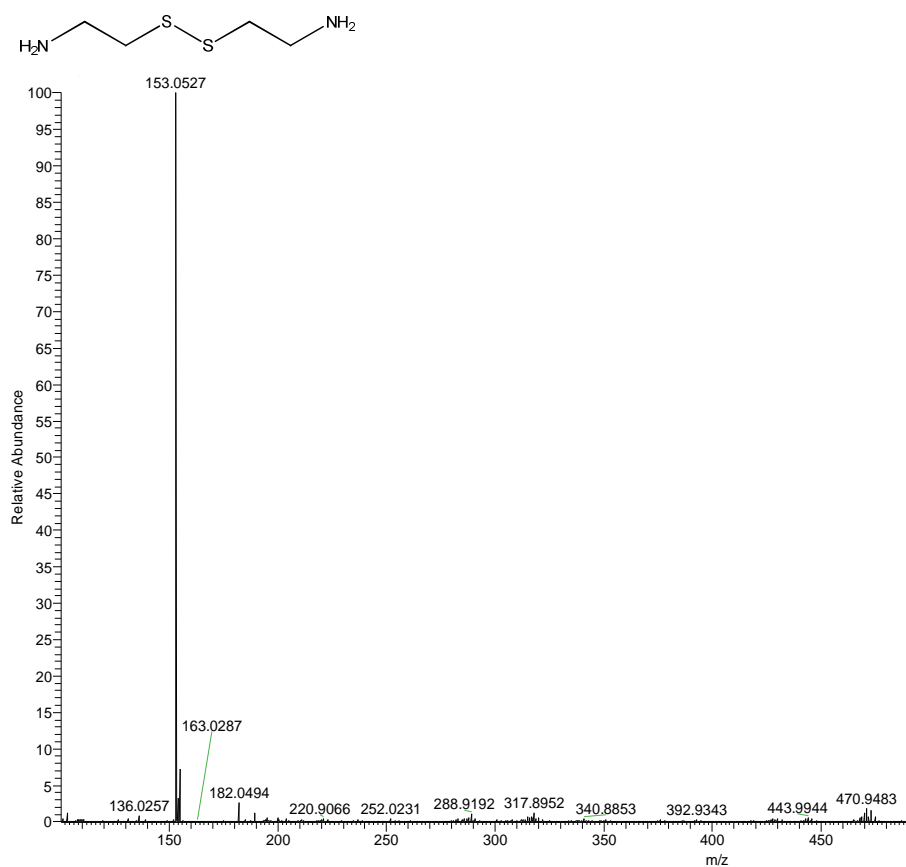
Figure 3-4: *Full ESI-MS (positive mode) spectrum of equimolar concentrations of NAMI-A and cysteamine taken within the first minute of the reaction in 50 % methanol. Spectrum shows cystamine as the product.*

3.2.2 Kinetics

3.2.2.1 NAMI-A dependence: Effect of varying initial concentrations of NAMI-A on the reaction in 0.05 M phosphate buffer at pH 7.4 was examined, (see Figure 3-5a). The rate of consumption of NAMI-A increased with increasing initial NAMI-A concentrations. Rate measurements were confined to the initial 2% of the reaction where determination of contributing species is fairly accurate before contributions from intermediates.
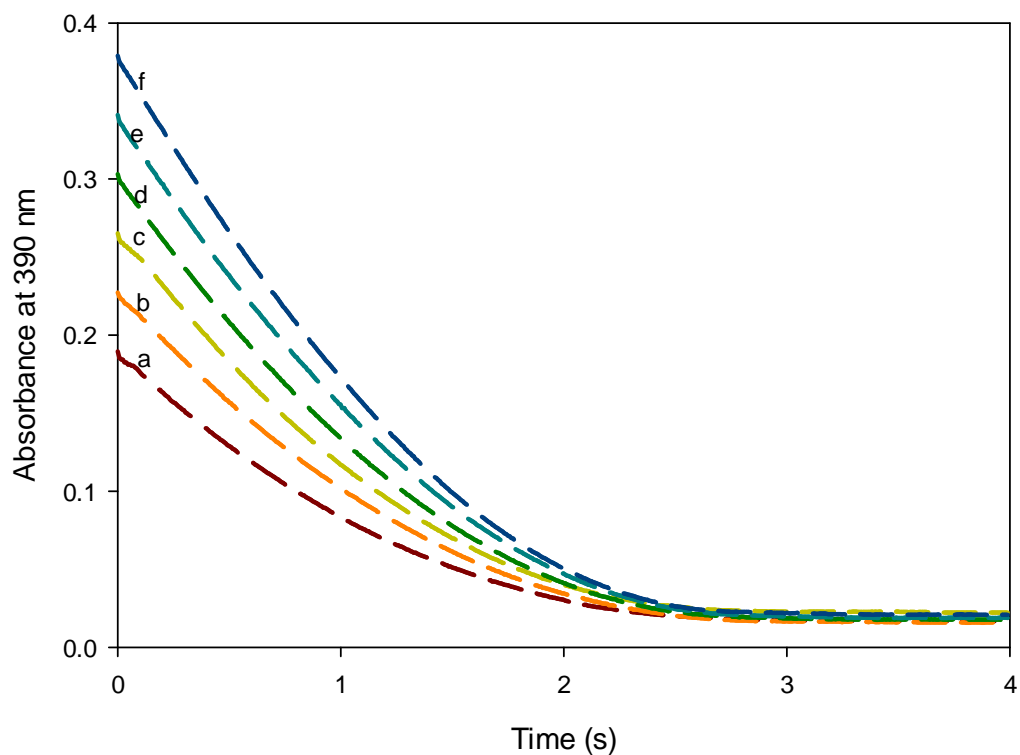
Figure 3-5a: *Kinetic traces of reaction in 0.05M phosphate buffer (pH 7.4) showing dependence on [NAMI-A] at its λ_{max}. [Cysteamine]$_o$ = 1.0 x 10^{-2}M; [NAMI-A]$_o$ = (a) 5.0 x 10^{-5} M (b) 6.0 x 10^{-5} M (c) 7.0 x 10^{-5} M (d) 6.0 x 10^{-5} M (e) 9.0 x 10^{-5} M (f) 1.0 x 10^{-4} M*

Plots of initial rates against initial NAMI-A concentrations gave straight lines, indicating a linear dependence on NAMI-A (Figure 3-5b). Since [cysteamine]$_o$ is much greater than [NAMI-A] $_o$, cysteamine concentration effectively remained unchanged during the reaction. The observed pseudo rate constant was then determined to be 6.85 x $10^{-1} \pm 0.03$ s^{-1}.
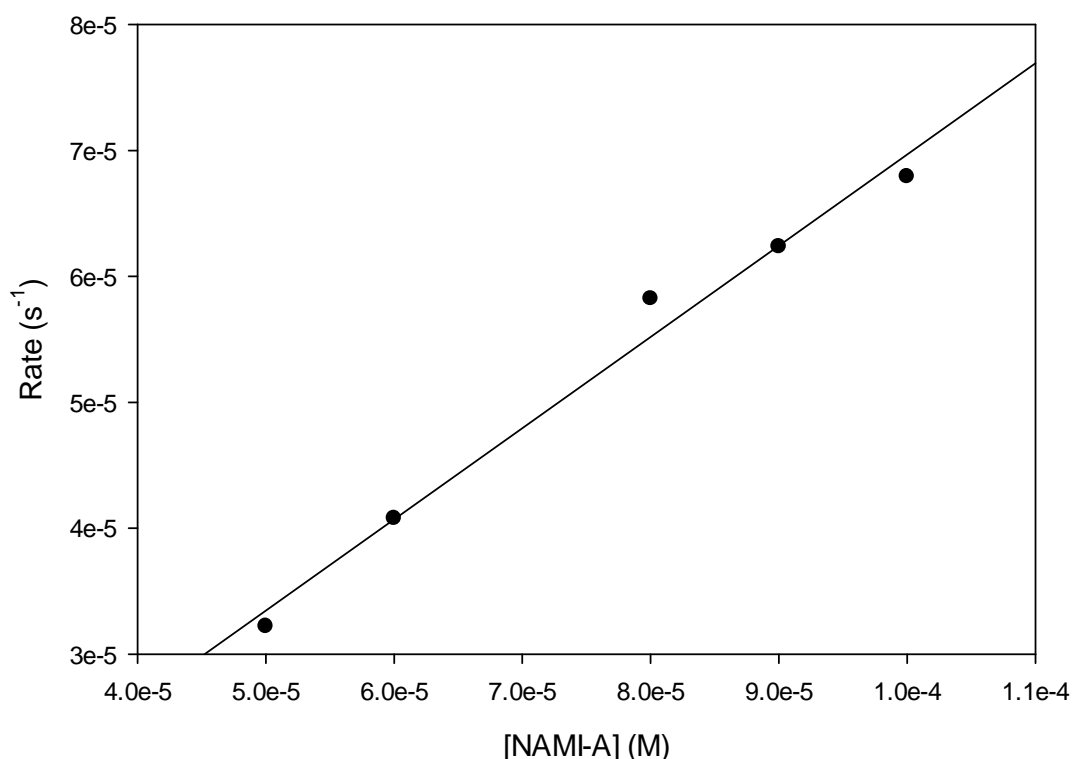
Figure 3-5b: *Initial rate plot derived from Figure 3-5a, showing linear dependence on NAMI-A. [Cys]$_o$ = 1.0 x 10^{-3}M; [NAMI-A]$_o$ = 5.0 x 10^{-5} M to 1.0 x 10^{-4} M*

3.2.2.2 Cysteamine dependence: Dependence of the reaction on initial concentrations of cysteamine (all other reaction conditions fixed) was monitored at 390 nm. Reaction rate increased with increasing concentrations of cysteamine (Figure 3-6a). The

sigmoidal-type traces, more pronounced at low cysteamine concentrations and later also observed at high temperatures, might suggest autocatalysis. Initial rate plots deduced from this plot are nonlinear (see Figure 3-6b) which might suggest adduct formation. Similar effects were observed at various temperatures vis-à-vis: 15, 20, 30 and 37 ^{o}C (Figure 3-6c) and are summarized in Figure 3-6d.
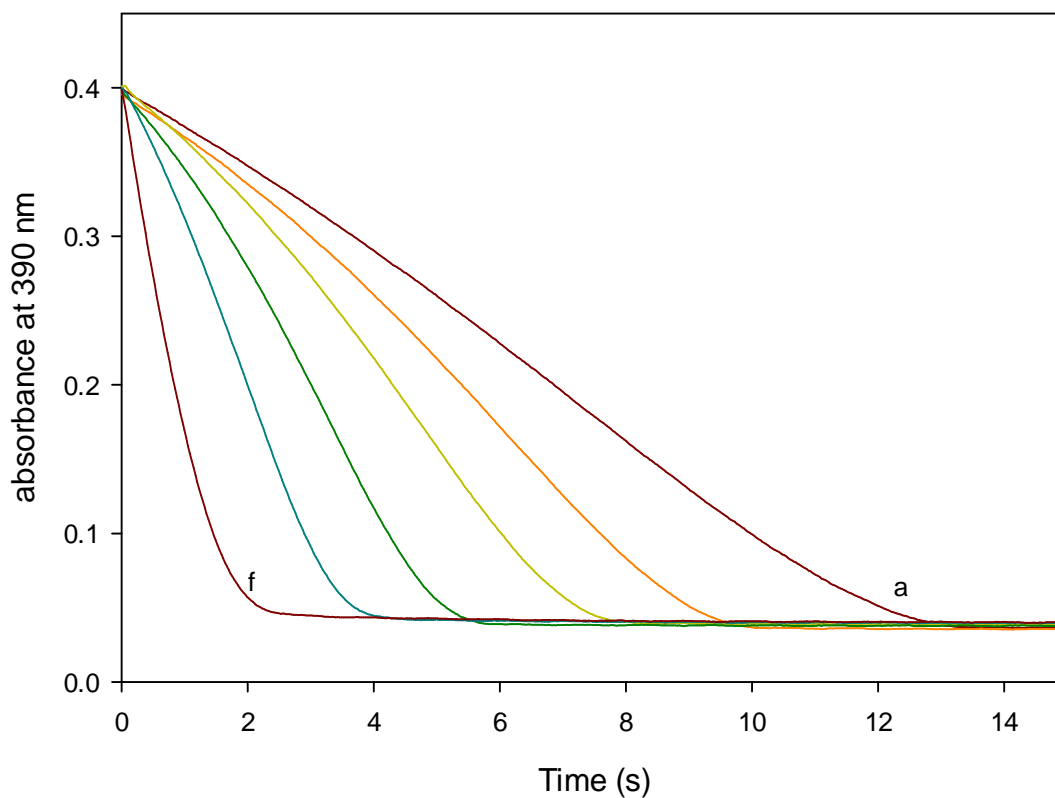
Figure 3-6a: *Effect of cysteamine variation on the consumption of NAMI-A at 390 nm. [NAMI-A]$_o$ = 1.0 x 10^{-4} M; [cysteamine]$_o$ = (a) 2.0 x 10^{-3} M (b) 3.0 x 10^{-3} M (c) 4.0 x 10^{-3} M (d) 6.0 x 10^{-3} M (e) 8.0 x 10^{-3} M (f) 1.0 x 10^{-2} M. Reaction rate increased with cysteamine concentration.*
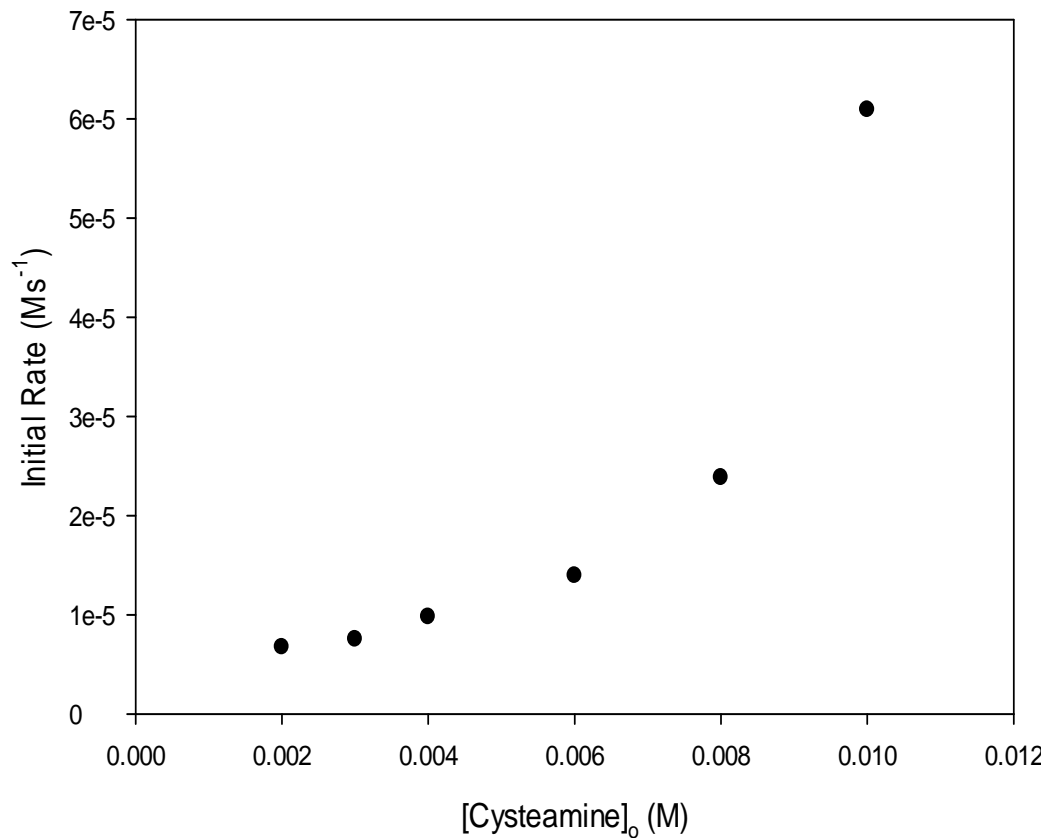
Figure 3-6b: *Initial rate plot derived from data shown in Figure 4a, showing nonlinear*

dependence on NAMI-A concentrations. $[NAMI-A]_o = 1.0 \times 10^{-4}$ M; $[cysteamine]_o = 2.0$

$\times 10^{-3}$ M to 1.0×10^{-2} M.
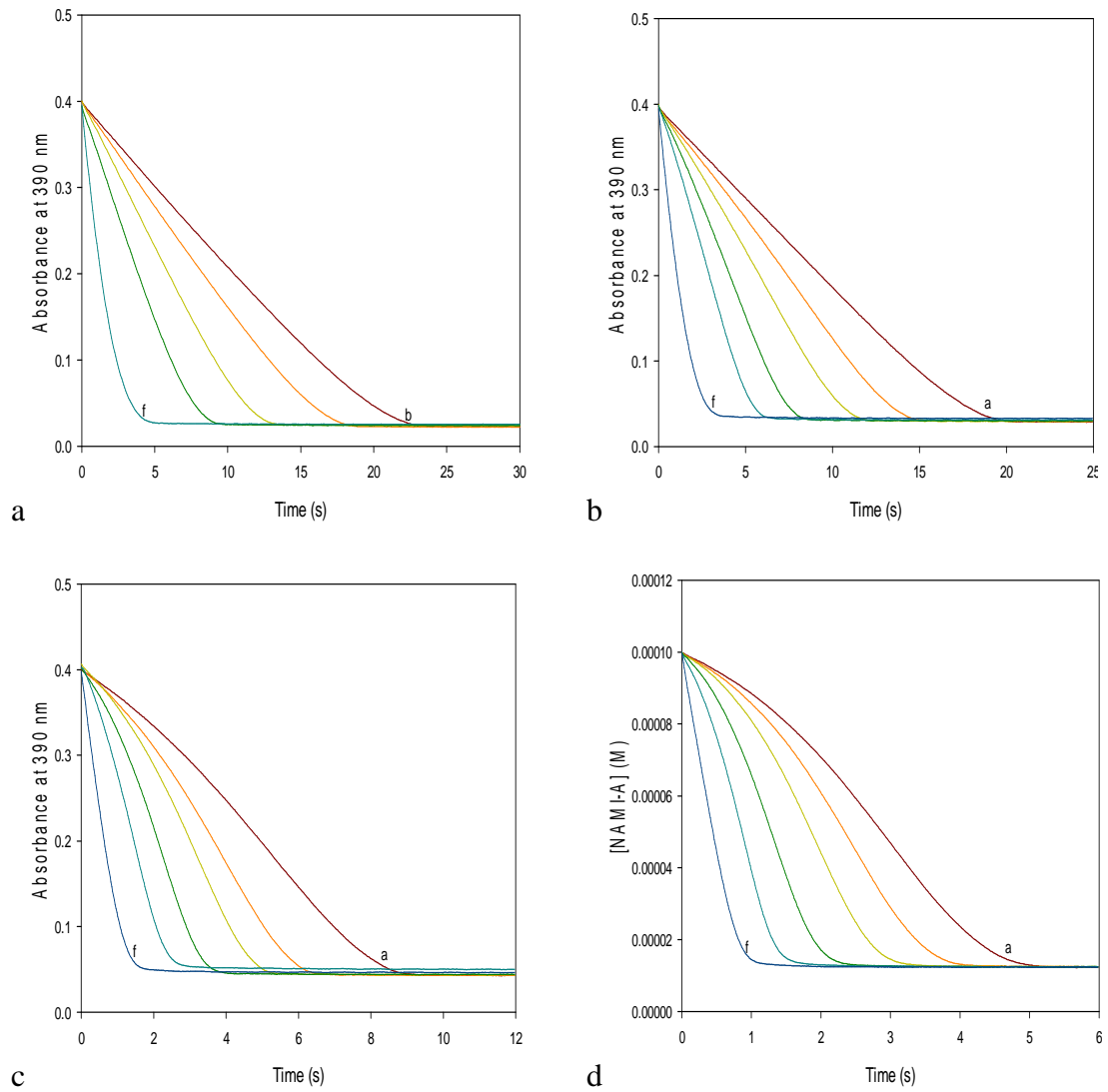
Figure 3-6c: *Effect of cysteamine variation at temperatures 15, 20, 30 and 37 ^{o}C from a*

through d respectively.
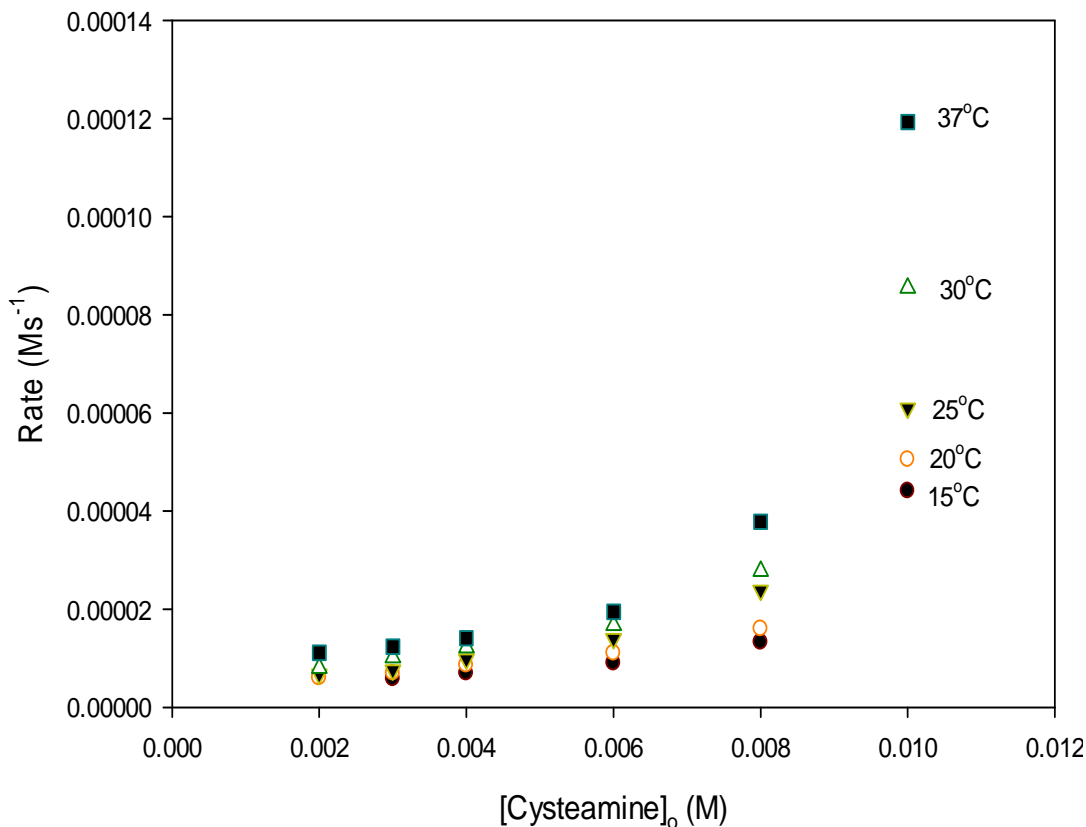
Figure 3-6d: *Summary of rate dependence on cysteamine at various temperatures.*

[NAMI-A]$_o$ = 1.0 χ 10^{-4} M; ΄[cysteamine]$_o$ = 2.0 χ 10^{-3} M το 1.0 χ 10^{-2} M.

3.2.2.3 Effect of ionic strength: The response of this reaction to changes in concentration of an inert salt (NaClO$_4$), at constant temperature and reactants concentrations, was monitored at pH 7.4 without a buffering environment. Increasing ionic strength slowed down the reaction rate in both cases as shown in the representative plot, Figure 3-7 (no buffer). This suggests that the rate determining step(s) involve species of different charges. Although, from pKa of cysteamine, appreciable amount of zwitterionic cysteamine exists in solution, the net positively charged species should be predominant in the rate determining step.

44
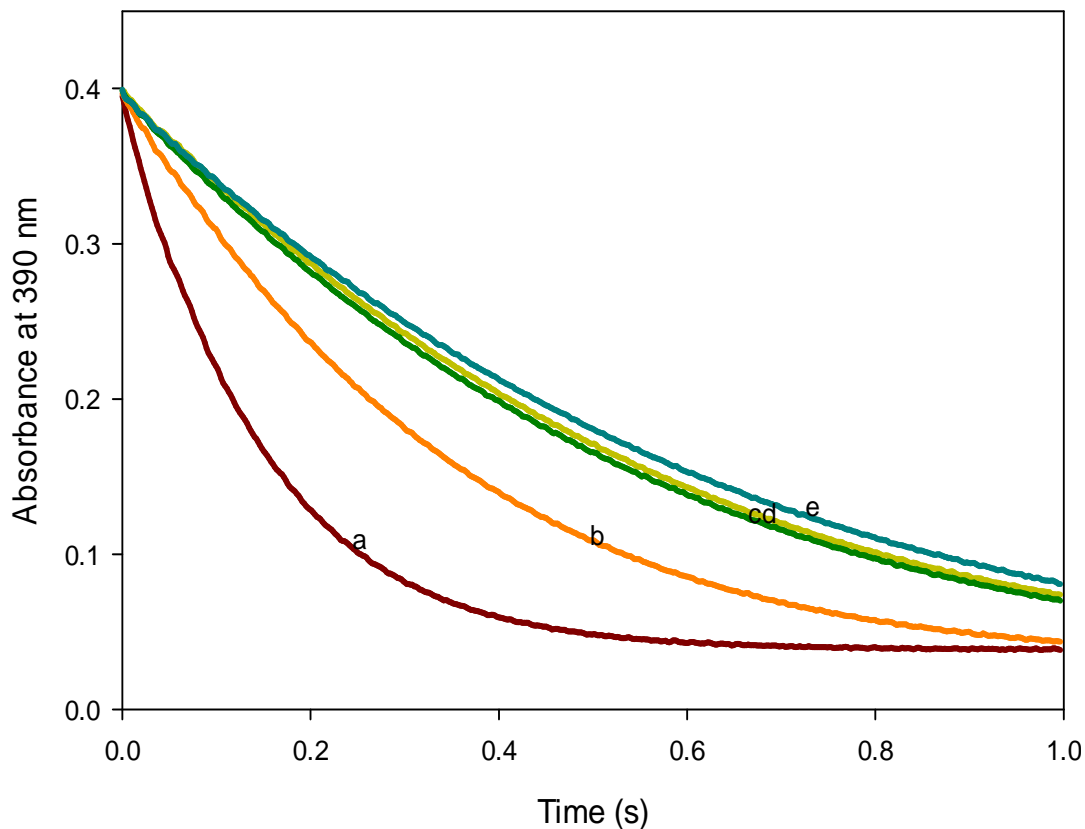
Figure 3-7: *Ionic strength dependence of cysteamine-NAMI-A reaction. [Cysteamine]$_o$ = 1.0 x 10^{-2} M; [NAMI-A]$_o$ = 1.0 x 10^{-4} M; [I]$_{NaClO4}$ = (a) 1.00 x 10^{-4} M (b) 0.15 M (c) 0.30 M (d) 0.45 M (e) 0.90 M*

3.2.2.4 Effect of chloride ion: The dependence of this reaction to changes in chloride ion concentrations at constant temperature and other reaction conditions (pH, reactants concentrations and ionic strength) was examined. Chosen chloride concentrations were corresponded to concentrations in the cytoplasmic matrix (~2 mM), blood/extracellular fluids (up to 100 mM) and in some experiments higher concentrations were used. The presence of small amounts of chloride ions retarded the reaction as seen in Figure 3-8, but increasing chloride ion concentrationsfurther, however, did not significantly affect

45

the overall rate of reaction. No observable difference was observed in the kinetics traces of solutions containing chloride concentrations of 0.02, 0.1, 1.0 M and higher.
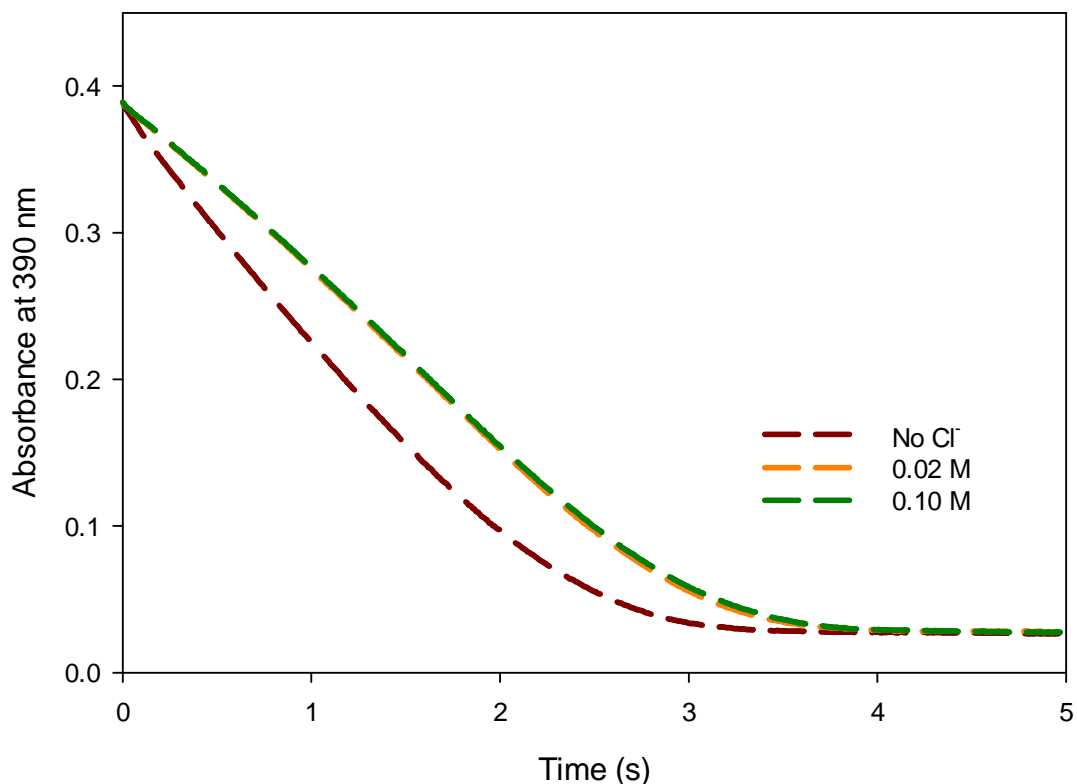
Figure 3-8: *Effect of varying initial chloride concentration.[cysteamine]$_o$ = 1.0 x 10^{-2} M; [NAMI-A]$_o$ = 1.0 x 10^{-4} M; [μ]$_{NaClO4}$ = 1.0 M; [Cl-] = 0.00 M to 0.10 M*

3.2.2.5 Thermodynamics and activation parameters: At fixed concentrations of substrate, oxidant and ionic strength, the effect of temperature on the reaction was evaluated. Reaction rate increased proportionally with increasing temperatures as expected (see Figure 3-9a). The data obtained were used to construct an Arrhenius plot (see Figure 3-9b).
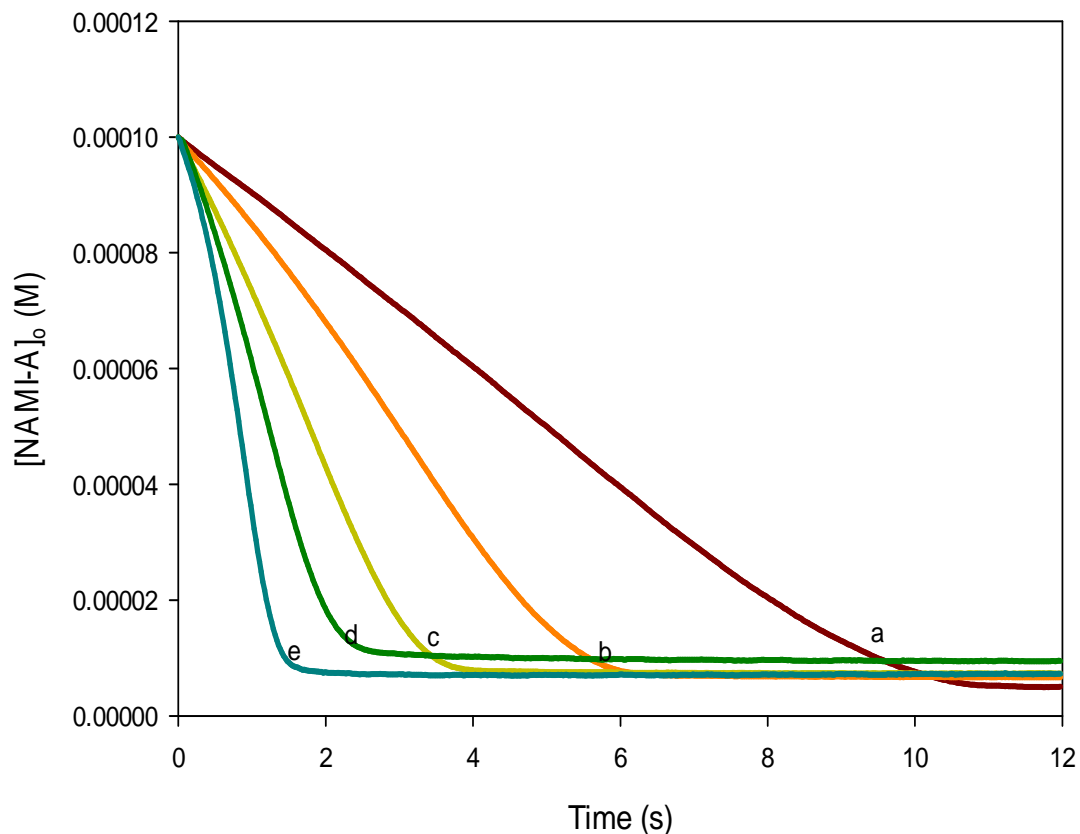
Figure 3-9a: *Temperature dependence of cysteamine-NAMI-A reaction. [NAMI-A]$_o$ = 1.0 x 10^{-4}M; [cysteamine]$_o$ = 1.0 x 10^{-2} M , Temperature = (a) 15 ^{o}C (b) 20 ^{o}C (c) 25 ^{o}C (d) 30 ^{o}C (e) 37 ^{o}C, pH 7.4; Ionic strength maintained at 1.0 M using NaCl*

The Arrhenius plot afforded these activation parameters: entropy of activation, $\Delta S^{\neq}$ = -117 J K^{-1} mol^{-1}, enthalpy of activation, $\Delta H^{\neq}$ = 41.5 kJ mol^{-1} and free energy of activation as $\Delta G^{\neq}$ = 76 kJ mol^{-1} (at 25 ^{o}C). Low positive enthalpy and distinctly negative entropy of activation suggests some degree of molecular ordering in the rate determining step. These parameters are indicative of an associative mechanism.
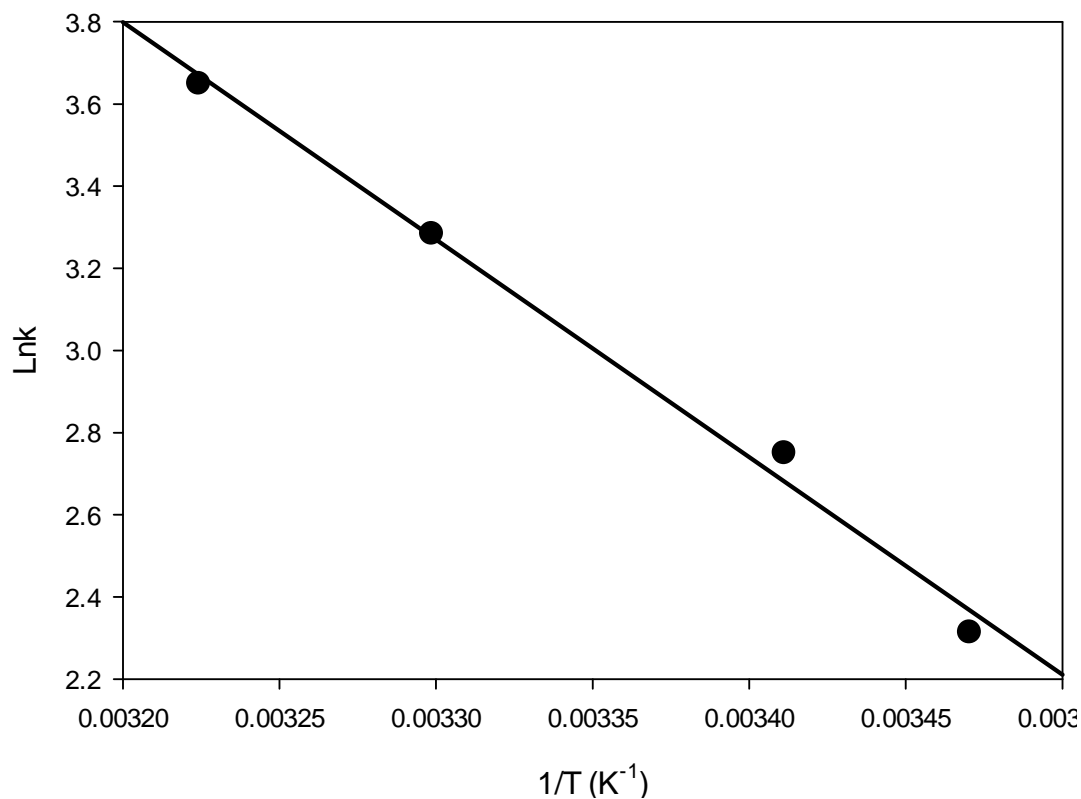
Figure 3-9b: *Temperature dependence of cysteamine-NAMI-A reaction. [NAMI-A]$_o$ = 1.0 x 10^{-4}M; [cysteamine]$_o$ = 1.0 x 10^{-2} M.*

3.3   Mechanism

3.3.1   Electron Transfer: Reactions were carried out at pH 7.4. At this pH, the amine functional group of cysteamine should be predominantly protonated since the thiol and amine pKa's are 8.27 and 10.53 respectively.[221]

$$H_2NCH_2CH_2SH \; \rightleftharpoons \; H_3N^+CH_2CH_2SH \; + \; H^+ \qquad\qquad K_b \qquad R1$$

Although cysteamine exists predominantly in the protonated form under these reaction conditions, appreciable amounts of zwitter-ionic form (see R2) are also present at 13 % of total cysteamine after using the Henderson-Hasselbach equation.

$$H_3N^+CH_2CH_2SH \; \rightleftharpoons \; H_3N^+CH_2CH_2S^- + \; H^+ \qquad\qquad K_{a1} \qquad R2$$
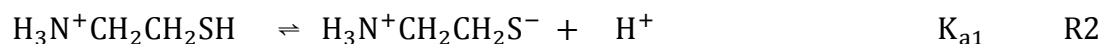
These species react with anionic NAMI-A to form an activated complex derived from reactions R3 and R4. The activated complex, sitting at the maximum energy point along the reaction coordinate, may, however, rearrange to form products or fall back to reactants. Activation parameters obtained are suggestive of an associative mechanism in which the activated complex is more ordered in comparison to the reactants.

$$H_3N^+CH_2CH_2SH + [ImRuCl_4DMSO]^-$$
$$\rightarrow \; [H_3N^+CH_2CH_2SH \ldots [ImRuCl_4DMSO]^-]^{\neq} \qquad k_1 \qquad R3$$

$$H_3N^+CH_2CH_2S^- + [ImRuCl_4DMSO]^-$$
$$\rightarrow \; [H_3N^+CH_2CH_2S^- \ldots [ImRuCl_4DMSO]^-]^{\neq} \qquad k_2 \qquad R4$$
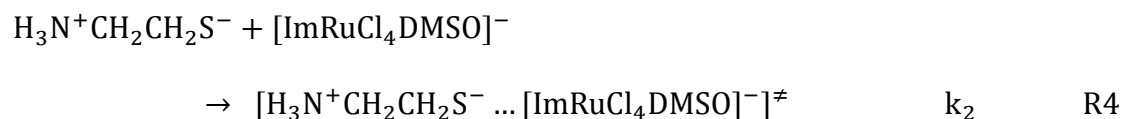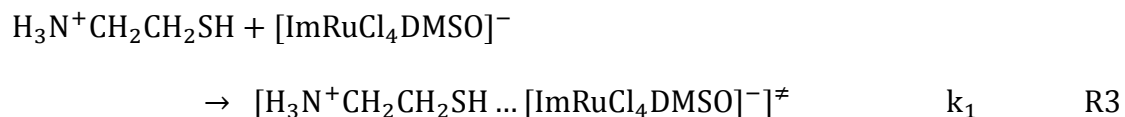
R3 and R4 estimate the nature of the activated complex in terms of composition only, specific molecular arrangement of the species cannot be determined at this time. R5 and R6 demonstrate formation of products: the reduced NAMI-A and cystamine from the activated complex.

$$2[H_3N^+CH_2CH_2SH \dots [ImRuCl_4DMSO]^-]^{\neq} \rightarrow H_2NCH_2CH_2SSCH_2CH_2NH_2$$

$$+ \; 2[ImRuCl_4DMSO]^{2-} \quad + \quad 4H^+ \qquad\qquad k_3 \qquad\qquad R5$$

$$2[H_3N^+CH_2CH_2S^- \dots [ImRuCl_4DMSO]^-]^{\neq} \rightarrow H_3N^+CH_2CH_2SSCH_2CH_2N^+H_3$$

$$+ \; 2[ImRuCl_4DMSO]^{2-} \quad + \quad 2H^+ \qquad\qquad k_4 \qquad\qquad R6$$
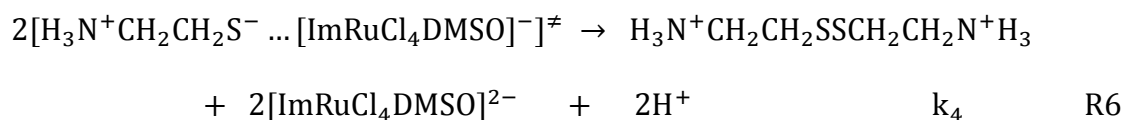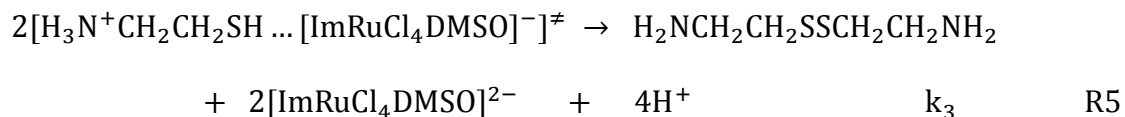
Redox interactions between reduced NAMI-A and cystamine were anticipated. The labile nature of the reduced complex however, with a half life of ~14 s[82] implies that reaction is effectively irreversible. This short half life taken together with reaction duration of ~4 s for electron transfer (measured by disappearance of charge transfer band of NAMI-A at 390 nm) might explain obvious absence of reduced NAMI-A from ESI-MS spectrum.

3.3.2 Ligand Exchange: Following electron transfer process, is a series of ligand exchange processes involving two chloride ligands and the apical ligands, imidazole and dimethyl sulfoxide as described by R7- R13.

$$[ImRuCl_4DMSO]^{2-} + H_2O \rightarrow [ImRuCl_3(H_2O)DMSO]^- + Cl^- \qquad R7$$

$$[ImRuCl_3(H_2O)DMSO]^- + H_2O \rightarrow [ImRuCl_2(H_2O)_2DMSO] + Cl^- \qquad R8$$

$$[ImRuCl_2(H_2O)_2DMSO] \rightarrow [ImRuCl_2(H_2O)(OH)]^- + H^+ + DMSO \qquad R9$$

50

$$[ImRuCl_2(H_2O)_2DMSO] \rightarrow [ImRuCl_2(OH)_2DMSO]^- + H^+ \qquad R10$$

$$[ImRuCl_2(H_2O)_2DMSO] + H_2O \rightarrow [ImRuCl_2(H_2O)_3] + DMSO \qquad R11$$

$$[ImRuCl_2(H_2O)_3] + H_3N^+CH_2CH_2S^-$$
$$\rightarrow [ImRuCl_2(H_2O)_3\,^-SCH_2CH_2N^+H_3] + H_2O \qquad R12$$

$$[ImRuCl_2(H_2O)_3] \rightarrow [RuCl_2(H_2O)_2] + H_2O + Im \qquad R13$$
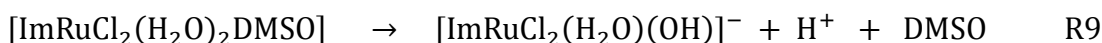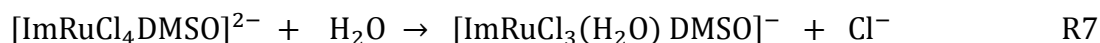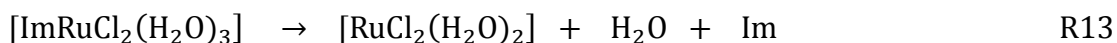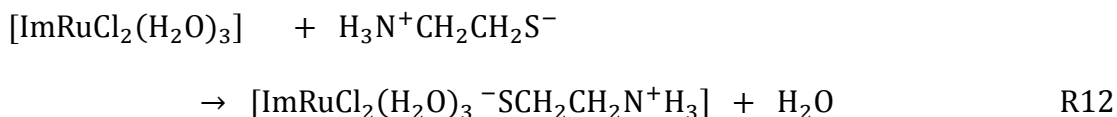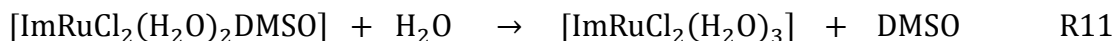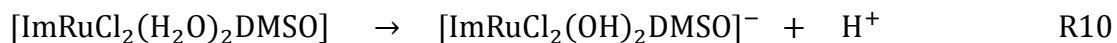
Results of influence of chloride ions on the reaction as seen in Figure 3.8 suggest that the chloride exchange reactions, R7 and R8) could be reversible. These interactions have been summarized graphically into Scheme 3-2. Structures labeled F and G were not observed on the ESI-MS spectra (refer to Figure 3.3), however, the presence of K and the 352 m/z with such high relative abundance strongly suggests formation of these species. The 352 m/z might be due to either J or L. Formation of J will require loss of acidic protons from coordinated water. Availability of protons (refer to R5 and R6) in the reaction mixture however, might make formation of J less viable. More so, the nonlinear dependence of reaction on cysteamine concentration might affirm adduct formation as was the case with respect to L.

Reaction scheme 3-2 exemplifies labilization and subsequent ligand exchange reactions that have been observed for metal-based anticancer prodrugs vis-à-vis; IndICR and platinum (IV) complexes[33;180] Consequently, reduction of NAMI-A by cysteamine should enhance reactivity of NAMI-A with biomolecules, this is in agreement with

reports of increased antimetastactic activity of NAMI-A and adduct formation with transferrin, human serum and albumin in the presence of cysteine and GSH.[222]
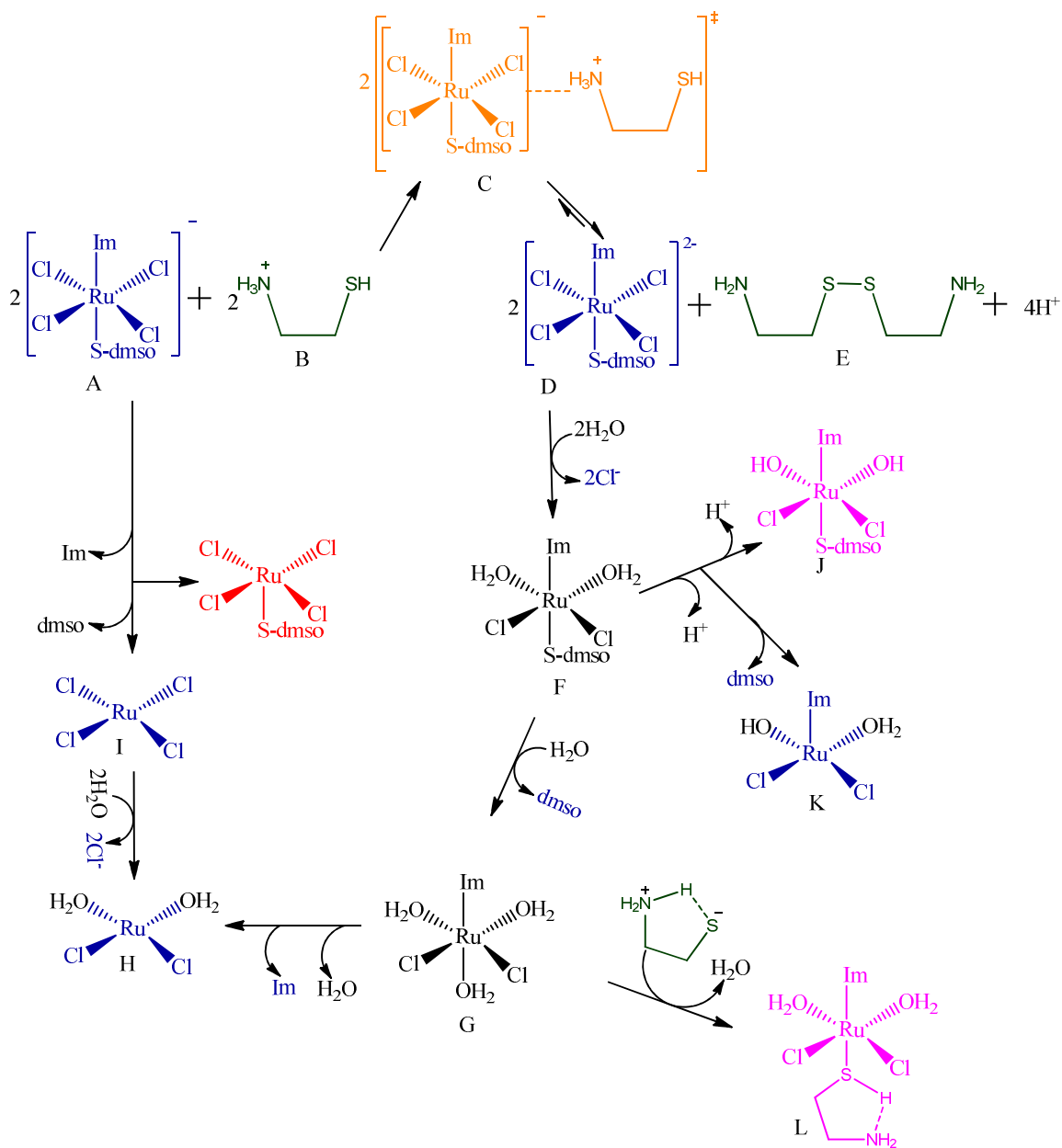
Scheme 3-2: *Proposed mechanism for the reduction of NAMI-A by cysteamine and subsequent ligand exchange process.*

CHAPTER FOUR

4.0 Kinetics and Mechanistic Investigation into the Possible Activation of NAMI-A by 2-Mercaptoethane sulfonate

4.1 Introduction

Cancer still poses a significant health threat mostly due to the inability of individual drugs to cure cancer at clinically tolerable doses.[223-225] The two exceptions to these are choriocarcinoma and Burtitt's lymphoma.[226] These factors have necessitated combination chemotherapy.

Imidazolium trans-[tetrachloro (dimethyl sulfoxide)(imidazole)ruthenate(III)], NAMI-A, is an experimental prodrug that shows low host toxicity and selectively targets metastatic cells.[74;177;181;227] NAMI-A, while being very active against metastases has relatively limited activity towards primary tumor.[228;229] This suggests that administration of NAMI-A in combination with drug(s) active against primary tumor might present more desirable chemotherapy outcome. Likely options for this purpose are widely used anticancer drugs shown in Table 1. These drugs form an integral part of chemotherapy regimens used in cancer treatment, for instance, cisplatin is used in 50-70% of all cancer patients most often in combination with other drug(s).[230] A notable disadvantage with these and other drugs is their induction of nephrotoxicity.[186;188;226] Most anticancer drugs and their metabolites are eliminated through the kidneys, thus, making the kidneys susceptible to injury.[185]

Alkylating Agents	Antimetabolites	Miscellaneous
Cisplatin	Azacitidine	Diaziquone
Carboplatin	Methotrexate	Clofarabine
Carmustine	6-Thioguanine	Mitomycin
Streptozocin	Pentostatin	Temsirolimus
Ifosfamise		
Cyclophosphamide		
Chloroethylnitrosoureas		

Table 4- 1: *Widely used chemotherapy drugs with inherent nephrotoxicity.*[185;186;188;226]

Antimetabolite: drug that interferes with normal metabolic processes within cells[231]

Alkylating agent: drug that causes DNA damage by addition of alkyl groups to specific bases.[232]

A combination, therefore, of NAMI-A and any of the above mentioned drugs will require a concurrent use of a chemoprotectant to prevent nephrotoxicity. Chemoprotection aims at prevention, mitigation or delay of toxicity, thereby increasing therapeutic index of chemotherapy without interfering with efficacy of applied drug.[233] These are all expected to improve patients' quality of life. Failure to provide adequate chemoprotection during therapy may mandate withdrawal or postponement of treatment and consequently lowers the probability of treatment success. Sodium-2-mercaptoethanesulfonate, MESNA, is a low molecular weight thiol in clinical use as a

chemoprotectant which inhibits the hemorrhagic cystitis and prevents bladder and kidney toxicities induced by cisplatin, ifosfamide and cyclophosphamide.[234-237] Chemoprotection by simultaneous administration of 100 mg/kg MESNA did not affect survival times observed with vincristine, 5-fluorouracil, doxorubicin, methotrexate, cisplatin, or cyclophosphamide.[237;238] This current clinical utility of MESNA suggests that an encounter with NAMI-A should be inevitable should NAMI-A be used as part of a combination regimen involving any nephrotoxic cancer drug. Interestingly, the disulfide of MENSA, BNP7787, is currently undergoing Phase III clinical trials for chemoprotection. Reports have revealed the involvement of MESNA in the mechanism of protection of cisplatin-induced nephrotoxicity as illustrated in Figure 4-1.[239-241] This further emphasizes the potential for interaction of MESNA with NAMI-A when administered in combination with cisplatin.
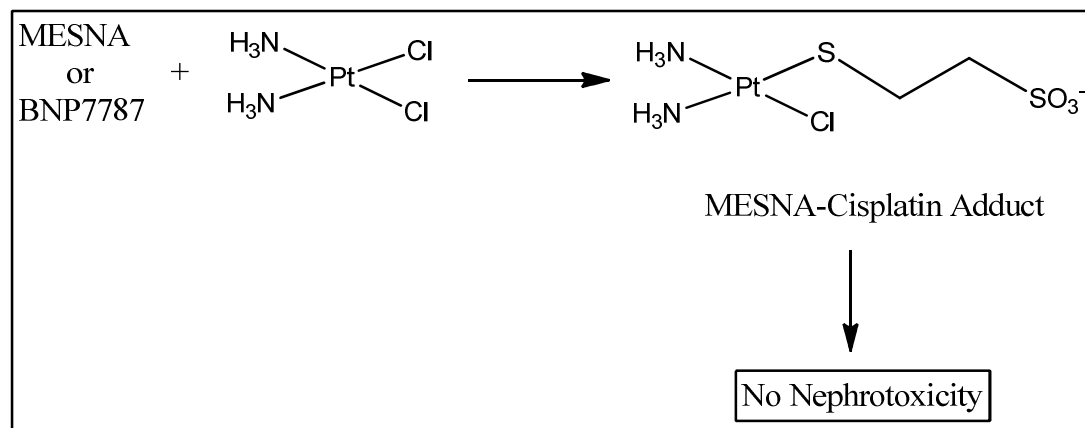
Figure 4-1: *Nephroprotection by BNP7787 showing involvement of MESNA.*[239]

A recent study reports cure of cancer in about 60% of the animals treated for lung metastasis using a combination of cisplatin and NAMI-A in mouse models.[242] This represents the most successful treatment reported for metastasis.[230] Presented here is a first report on kinetics and mechanism of interaction of NAMI-A with MESNA under physiologically-relevant conditions. An understanding of this interaction is important for optimizing clinical use of NAMI-A with high-dose nephrotoxic agents.

4.2   Results

4.2.1   Stoichiometry and Product Identification: Stoichiometry of reaction was found to be 1:1 with NAMI-A reacting with MESNA to give dimeric form of MESNA and reduced NAMI-A as represented in S1

$$2HSCH_2CH_2SO_3^- + 2[ImRuCl_4DMSO]^-$$

$$\rightarrow {}^-O_3SCH_2CH_2SSCH_2CH_2SO_3^- + 2[ImRuCl_4DMSO]^{2-} + 2H^+ \quad S1$$
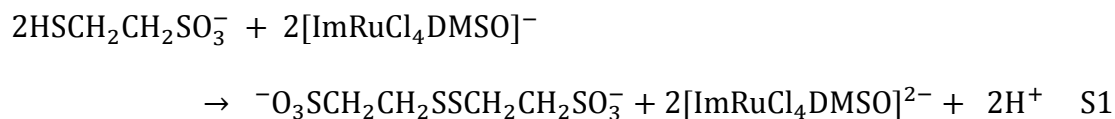
Figure 4-1 shows the spectral changes observed from a solution of MESNA and NAMI-A scanned at 30 second intervals. The charge transfer band of NAMI-A at 390 nm decreased as the reaction progressed showing one electron reduction of NAMI-A. The shoulder at 345 nm initially increased and then decreased towards the end of reaction. Absence of an isosbestic point indicates involvement of other absorbing species.
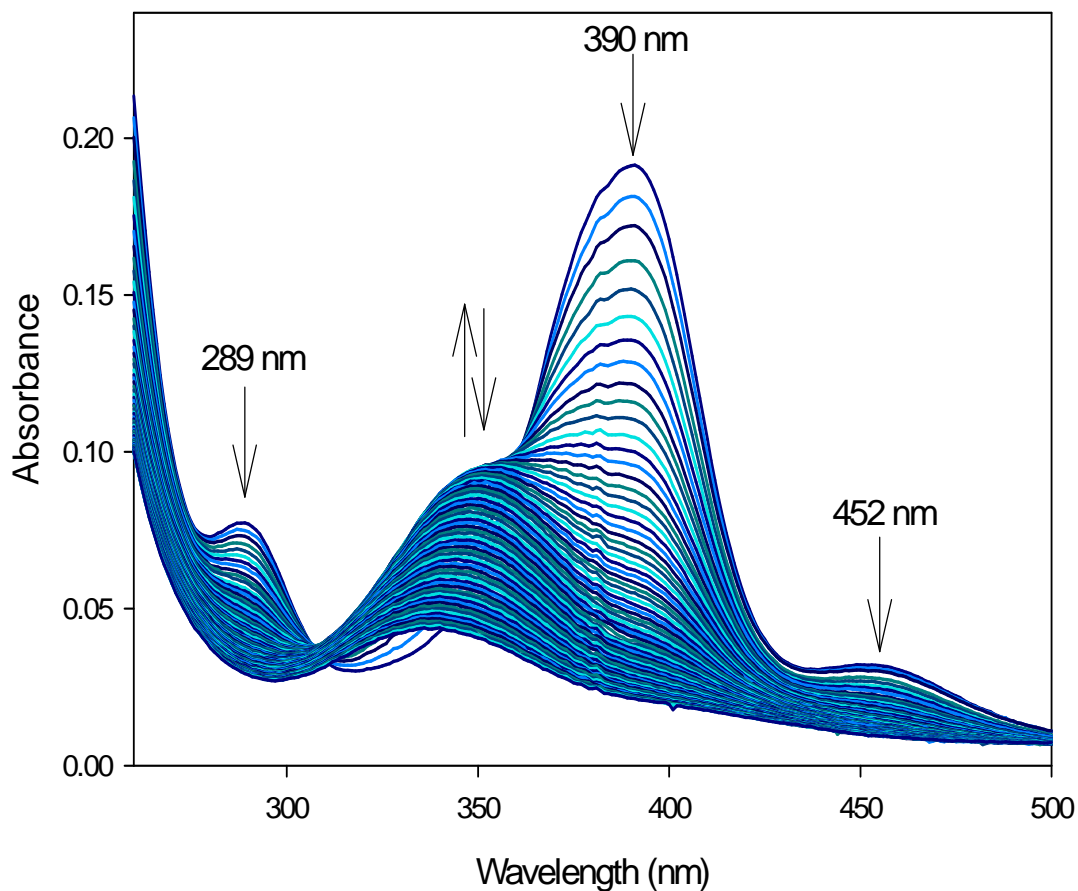
Figure 4-1: *Rapid spectral scan of aqueous solution of MESNA and NAMI-A taken at 30 s interval. $[MESNA]_o = 1.5 \times 10^{-4} M$; $[NAMI-A]_o = 5.0 \times 10^{-5} M$.*

Reduced form of NAMI-A, $[ImRuCl_4dmso]^{2-}$, has been reported to have a half life of approximately 14 s.[82] Upon formation, it is expected that this labile species will be rapidly hydrolyzed in these aqueous reaction conditions. A full electrospray ionization mass spectrum of the stoichiometric solution was taken in the negative mode within the first minute of reaction (Figure 4-2a). The spectrum features NAMI-A at m/z = 389 and MESNA at m/z = 140 being the most abundant. A small peak at m/z =

139.96 represents the already formed disulfide of MESNA. No peak was observed for the reduced NAMI-A at m/z = 194 since it is extremely labile.
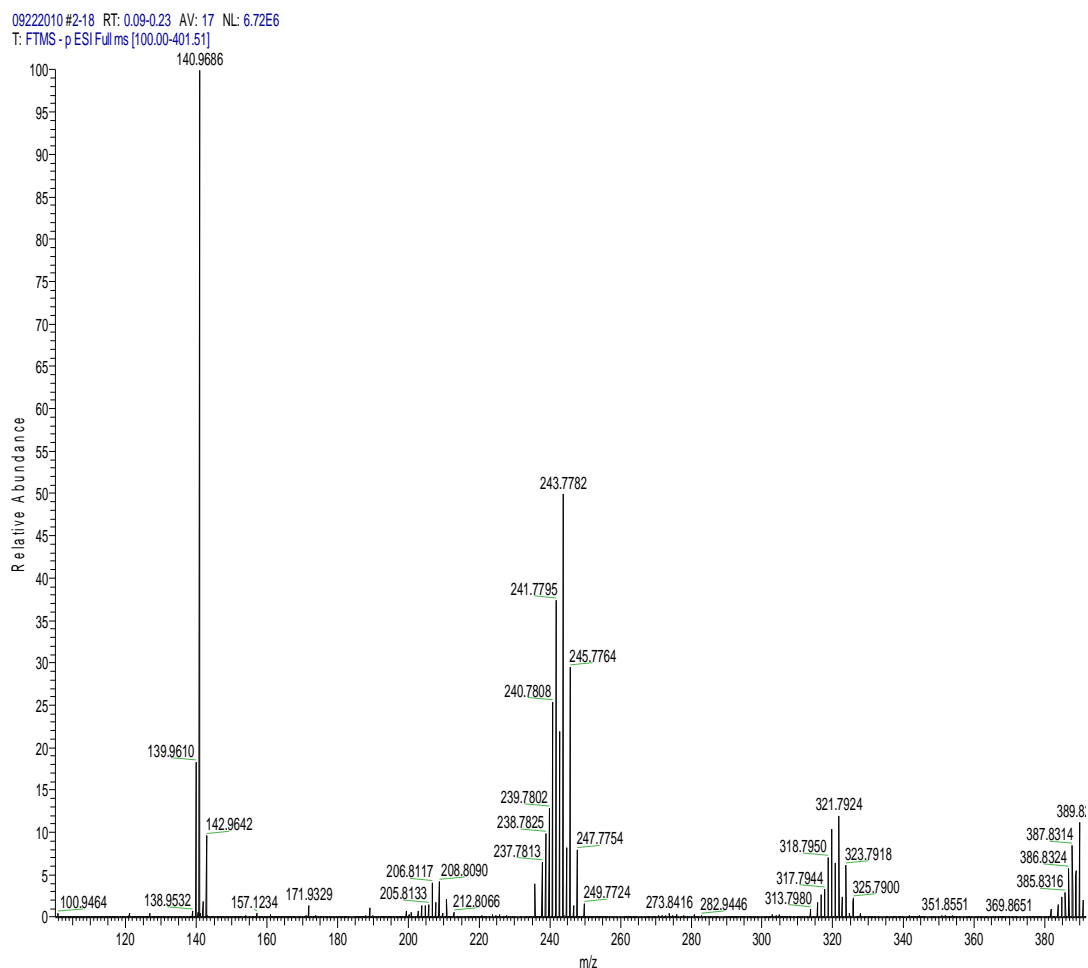
Figure 4-2a: *Negative ESI-MS spectrum of a stoichiometric solution of MESNA and NAMI-A within the first minute of start of reaction.*

Other crucial features of this spectrum are the group of peaks at m/z ~ 208, 243 and 321. The 208 m/z peaks might seem insignificant (5 % relative abundance) but evidence from other studies in this dissertation (Chapters 3 and 6) suggest these are ions

formed from reduced NAMI-A with a basic structure, [RuCl$_2$(H$_2$O)$_2$]. Figure 4-2a displays [RuCl$_2$(H$_2$O)$_2$+H] and [RuCl$_2$(H$_2$O)$_2$-H] with the same relative abundance. 243 and 321 m/z are due to ionization since NAMI-A without reductant shows these peaks.[82] Spectrum in Figure 4-2b, taken five minutes after Figure 4-2a shows decrease in both NAMI-A and MESNA peaks with simultaneous growth of the disulfide of MESNA.
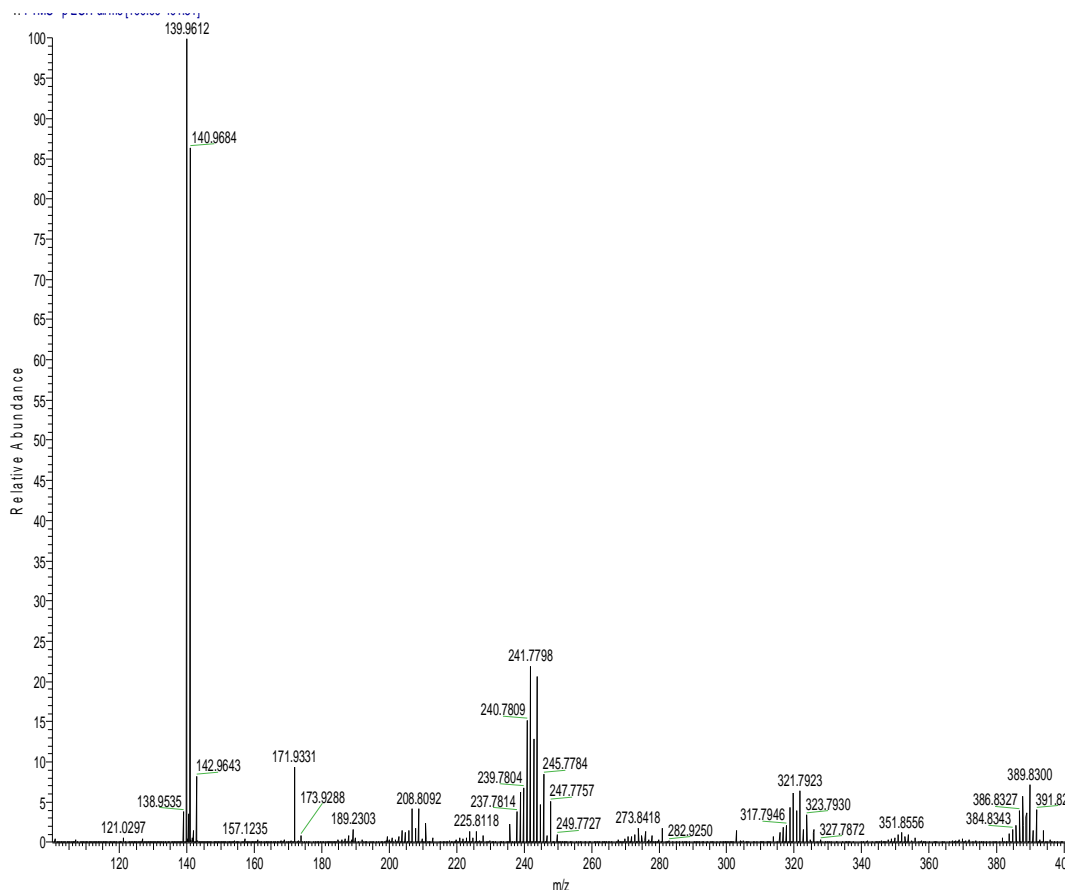
Figure 4-2b: *Negative ESI-MS spectrum of the same solution in Figure 4-2a taken five minutes later showing the depletion of both NAMI-A peak at 389.8300 m/z and MESNA peak at 140.9684 m/z with simultaneous growth of disulfide of MESNA at 139.9612 m/z and decay of MESNA.*

59

Figure 4-2c, taken at 5 minutes shows the disulfide as most abundant, demonstrating progress of the reaction towards completion, according to stoichiometric reaction S1.
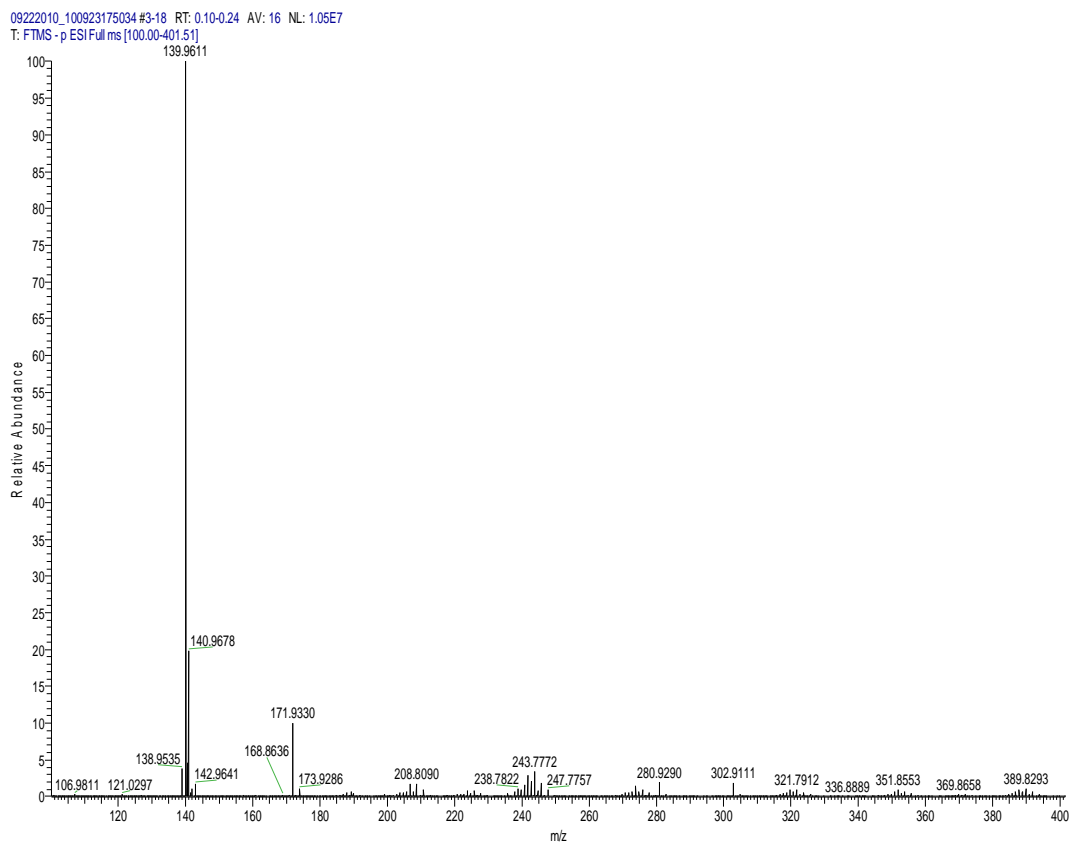
Figure 4-2c: *Negative ESI-MS spectrum of solution in Figure 3-2a taken ten minutes later showing disulfide of MESNA as the major peak.*

Of note is the nature of the product, dimeric form of MESNA (referred to as BNP7787),[239] and its relevance to cancer chemotherapy. BNP7787 has demonstrated chemoprotection that surpasses that of MESNA and may protect against cisplatin-

induced nephrotoxicity without interfering with efficacy, thus suggesting a more improved quality of life for patients.[241;243;244]

4.3   Kinetics

4.3.1   NAMI-A Dependence

Effect of varying initial concentrations of NAMI-A on the reaction in 0.1 M phosphate buffer at pH 7.4 was examined (see Figure 4-3a). The rate of consumption of NAMI-A increased with increasing initial NAMI-A concentrations. Absorbance traces at 390 nm in Figure 4-3a (and all other subsequent traces which monitor consumption of NAMI-A) show what might appear, erroneously, as mild autocatalysis. This peak at 390 nm is not entirely isolated and is influenced by contribution from a peak at 345 nm, which appears as a shoulder to the 390 nm peak. Since the peak at 345 nm initially increases, one expects a positive contribution, measured at 390 nm from this peak. As the reaction proceeds, however, the peak at 345 nm starts to fall, with a concomitant decrease in its contribution at 390 nm. Thus the observed rate of decrease of the peak at 390 nm will be enhanced, without necessarily an increased decrease in rate of loss of NAMI-A. There is no stoichiometric link between NAMI-A and the intermediate that absorbs at 345 nm, thus initial rates for all our kinetics determinations were confined to a very short initial part of the reaction before establishment of intermediates.
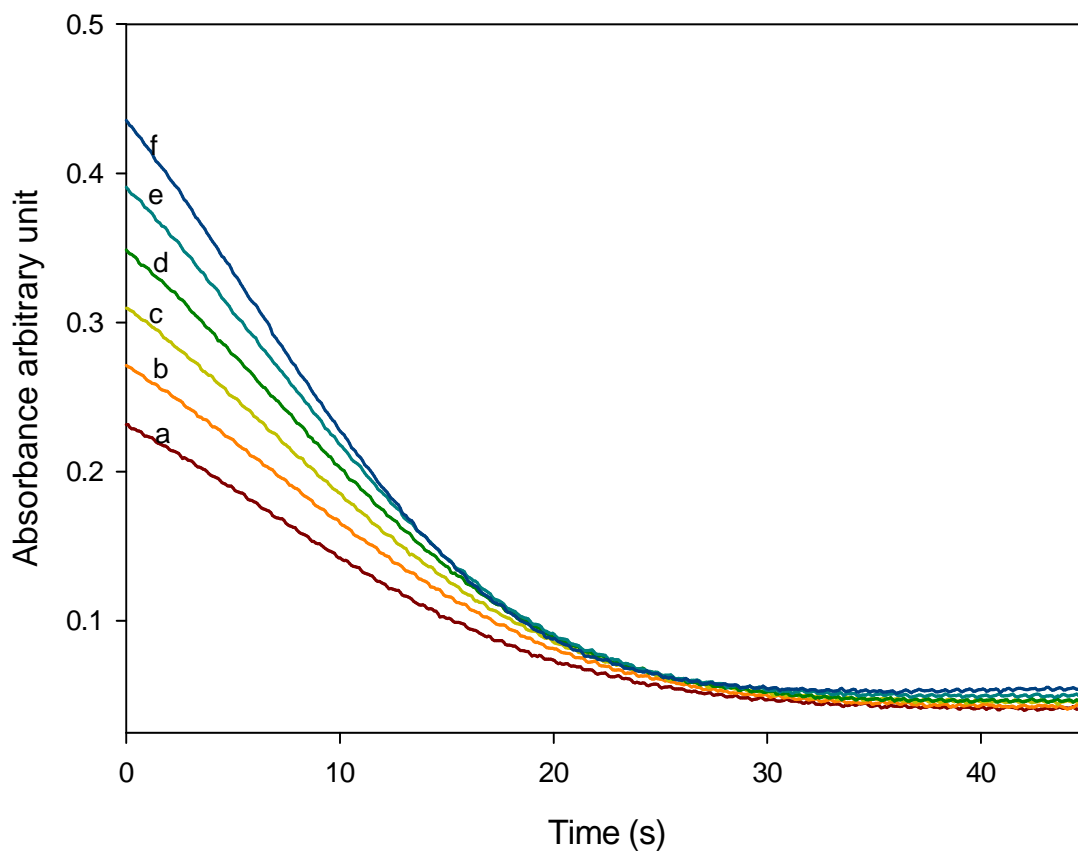
Figure 4-3a: *Kinetic traces of reaction in 0.1M phosphate buffer (pH7.4) showing dependence on [NAMI-A] at its λ_{max}. [MESNA]$_o$ = 5.0 x 10^{-2}M; [NAMI-A]$_o$ = (a) 5.0 x 10^{-5} M (b) 6.0 x 10^{-5} M (c) 7.0 x 10^{-5} M (d) 6.0 x 10^{-5} M (e) 9.0 x 10^{-5} M (f) 1.0 x 10^{-4} M*

Plot of initial rates against initial NAMI-A concentrations gives a straight line, with an intercept kinetically indistinguishable from zero, suggesting a linear dependence on NAMI-A (Figure 4-3b). A bimolecular rate constant of 7.07 x 10^{-1} $\pm$ 0.06 M^{-1}s^{-1} was deduced from the data shown in Figures 4-3a and b.
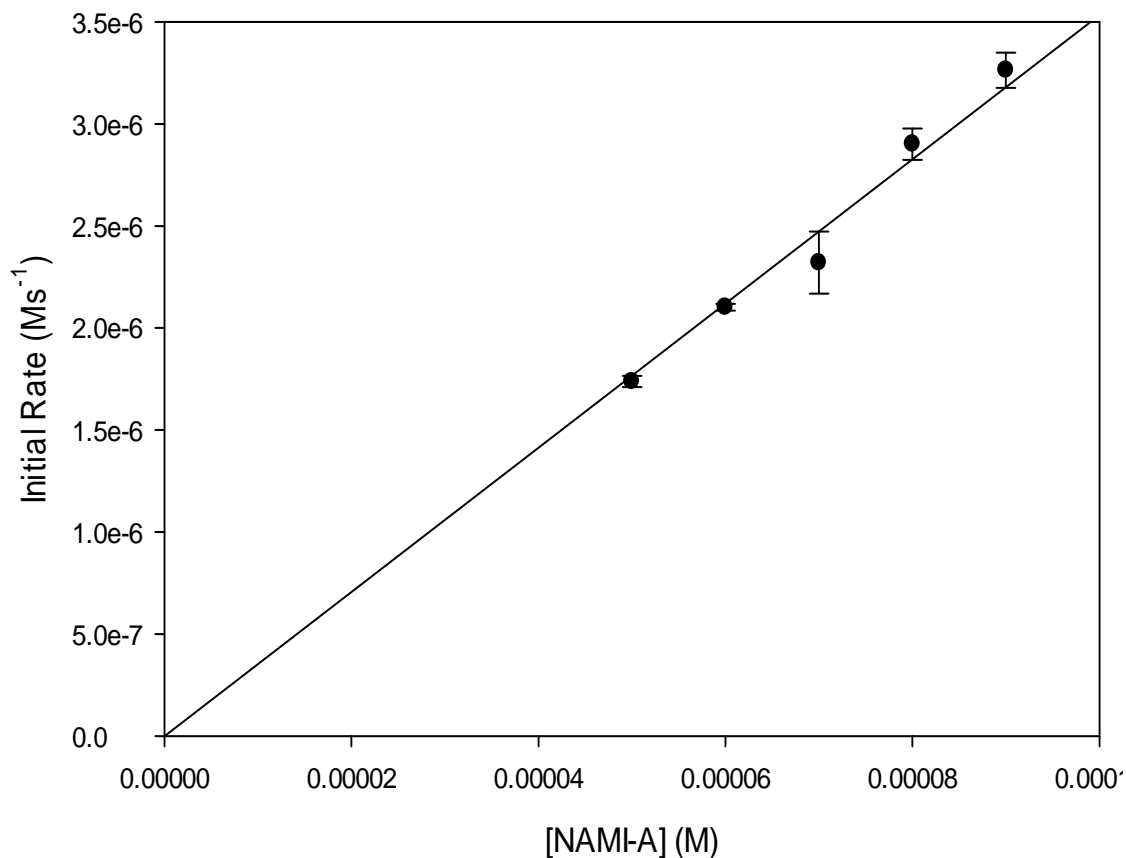
Figure 4-3b: *Initial rate plot derived from Figure 4-3a, showing linear dependence on NAMI-A. [MESNA]$_o$ = 2.0 x 10^{-3}M; [NAMI-A]$_o$ = 5.0 x 10^{-5} M to 9.0 x 10^{-5} M*

4.3.2 MESNA Dependence.

Effect of variation of initial concentrations of MESNA was also monitored at 390 nm. The reaction rate monotonically increased with increasing concentrations of MESNA with no apparent saturation but with an apparent slight increase in rate at high MESNA concentrations (Figure 4-4a). Initial rate plots deduced from this plot, Figure 4-4b, again show a linear dependence on MESNA concentrations. Increase in rate observed at the tail end of the traces is due to the aforementioned absorbance

contribution at 345 nm which magnifies rate of decrease in observed absorbance at 390 nm. Sigmoidal-type traces are much more pronounced at higher MESNA concentrations, and hence the expected deviations at high MESNA concentrations.
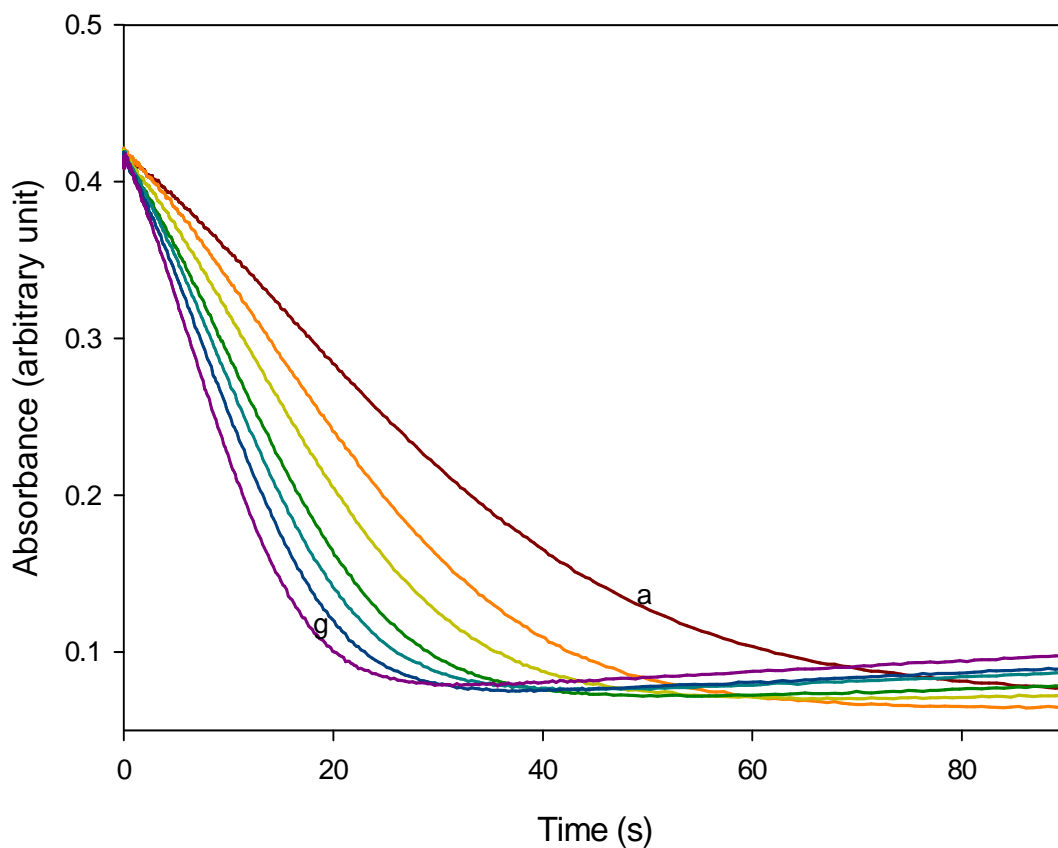
Figure 4-4a: *Effect of MESNA variation on the consumption of NAMI-A at 390 nm. [NAMI-A]$_o$ = 1.0 x 10^{-4} M; [MESNA]$_o$ = (a) 1.0 x 10^{-2} M (b) 2.0 x 10^{-2} M (c) 3.0 x 10^{-2} M (d) 4.0 x 10^{-2} M (e) 5.0 x 10^{-2} M (f) 6.0 x 10^{-2} M (g) 7.0 x 10^{-2} M.*
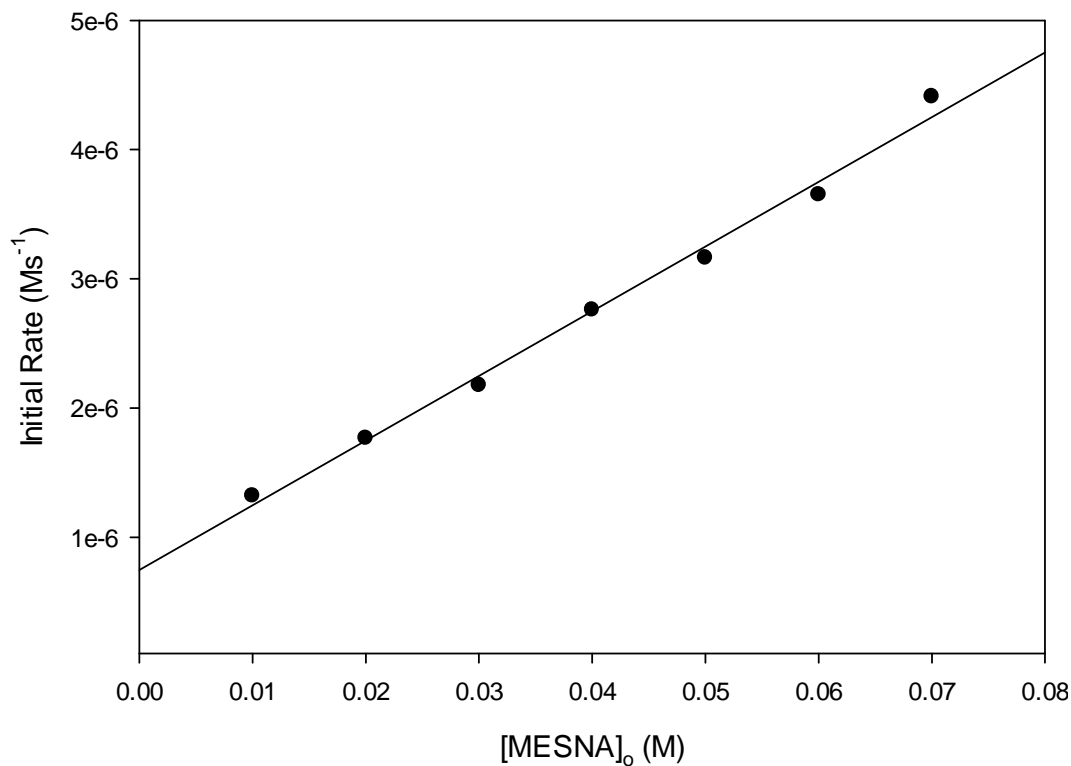
Figure 4-4b: *Initial rate plot derived from Figure 4-4a, showing linear dependence on [MESNA]$_o$*

4.3.3 Buffer and pH Effects.

In the absence of buffer ions, varying initial concentration of MESNA influenced the reaction in similar manner as were obtained when reaction was carried out at pH 7.4, compare Figures 4-4a and c. The slower rate in the absence of buffer might be due to reported stability of NAMI-A at lower pHs.[245] At much lower pH values of 5 through 3, lower rates were observed and sigmoidal characteristics on the traces became more pronounced as pH decreased, see Figure 4-4d.
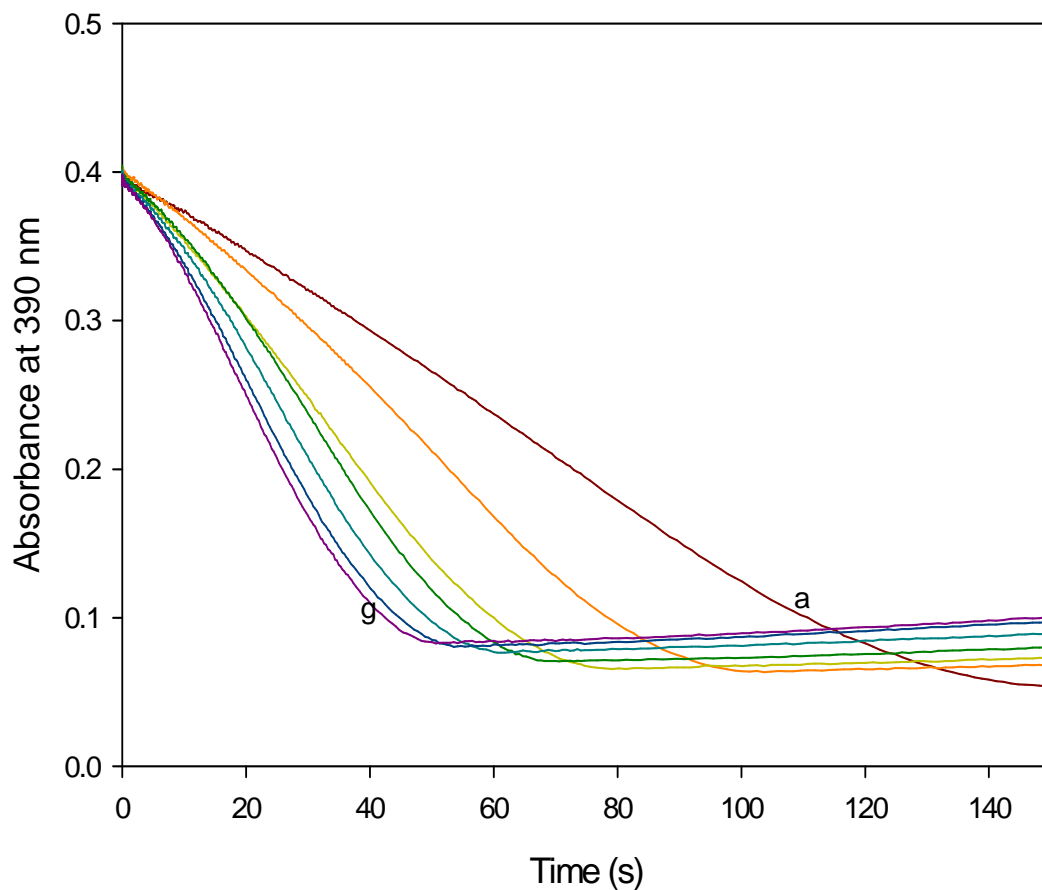
Figure 4-4c: *Effect of MESNA variation on the consumption of NAMI-A at 390 nm. Reaction not buffered. [NAMI-A]$_o$ = 1.0 x 10^{-4} M; [MESNA]$_o$ = (a) 1.0 x 10^{-2} M (b) 2.0 x 10^{-2} M (c) 3.0 x 10^{-2} M (d) 4.0 x 10^{-2} M (e) 5.0 x 10^{-2} M (f) 6.0 x 10^{-2} M (g) 7.0 x 10^{-2} M. Reaction is slower than observed at pH 7.4, compare Figure 4-4a.*
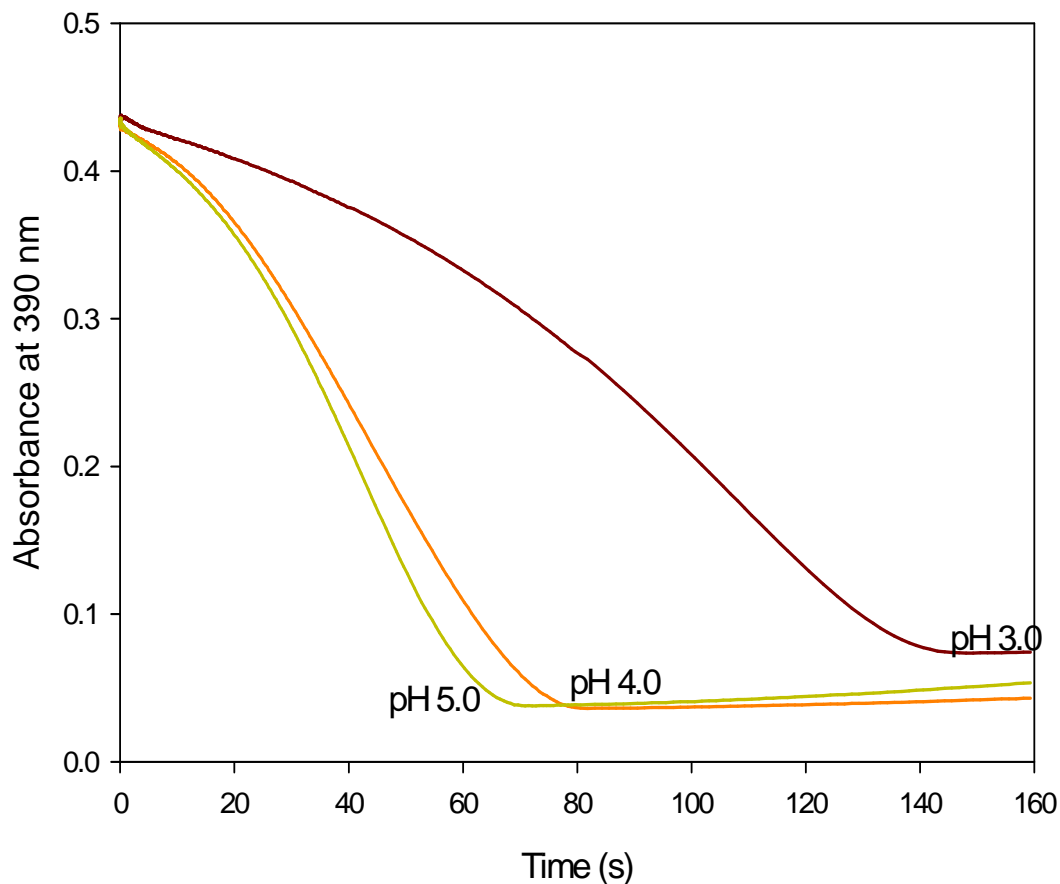
Figure 4-4d: *Influence pH on reaction rate. Reaction in 0.1 M phosphate buffered at pH 3.0 proceeded slowly compared to pH 4.0 and 5.0. [NAMI-A]$_o$ = 1.0 x 10^{-4}M; [MESNA]$_o$ = 5.0 x 10^{-2} M*

4.3.4 Temperature dependence.

At constant ionic strength, concentrations of NAMI-A and MESNA, the effect of temperature on the reaction was evaluated. Reaction rate increased proportionally with increasing temperatures as would be expected from standard Arrhenius kinetics (see Figure 4-5a), suggesting the existence of a single dominant rate-determining step. The data obtained were used to construct an Arrhenius plot (see Figure 4-5b).

67

Activation parameters deduced using information obtained from the Arrhenius plots are: entropy of activation, $\Delta S^{\neq} = -178.12 \pm 0.28$ J K^{-1}mol^{-1}, enthalpy of activation, $\Delta H^{\neq} = 20.64 \pm 0.082$ kJ mol^{-1} and free energy of activation as $\Delta G^{\neq} = 75.89 \pm 1.76$ kJ mol^{-1} at 37 ± 0.1 $^{\circ}$C and pH 7.4. The distinctly negative entropy of activation suggests some degree of molecular ordering in the rate determining step. These parameters are indicative of an associative mechanism.
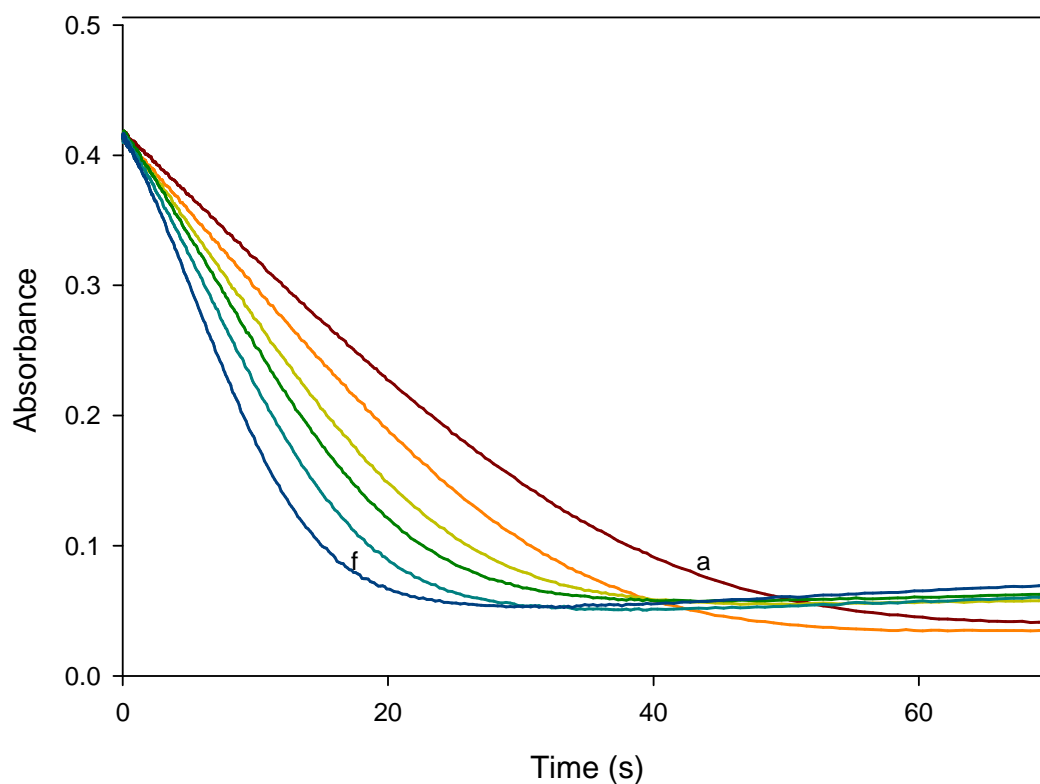
Figure 4-5a: *Temperature dependence of the reaction between NAMI-A and MESNA (0.1 M phosphate buffer, pH 7.4). Reaction rate increased with temperature increase. [MESNA]$_o$ = 5.0 x 10^{-2}M; [NAMI-A]$_o$ = 1.0 x 10^{-4}M; Temp = (a) 10° C (b) 15° C (c) 20° C (d) 25° C (e) 30° C (f) 37° C.*
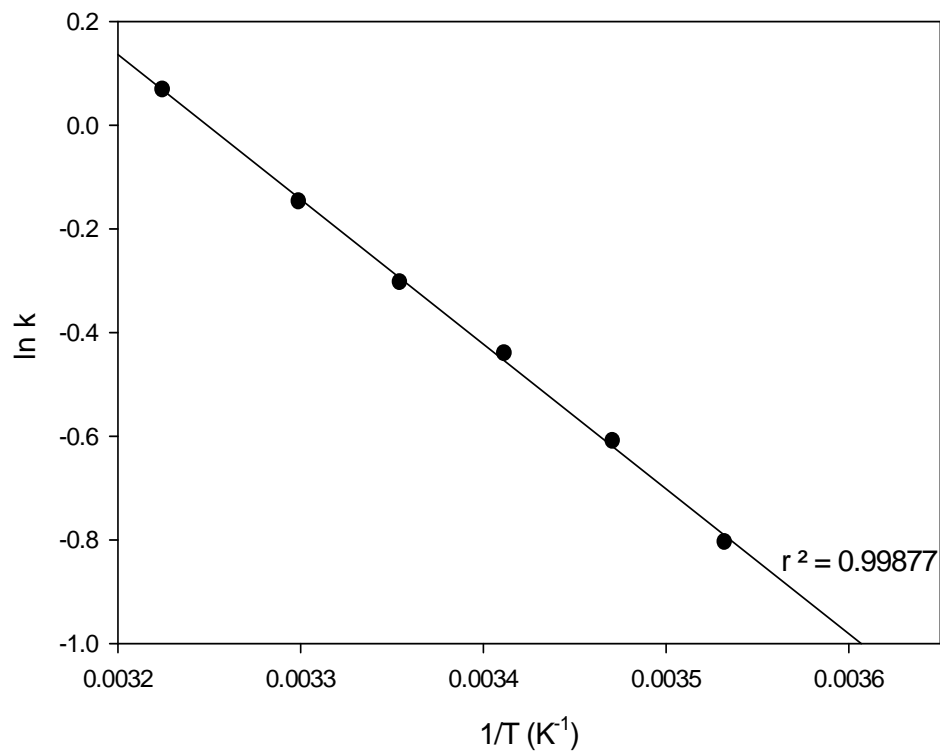
Figure 4-5b: *Arrhenius plot extracted from study of effect of temperature variation on the reaction for determination of activation parameters.*

4.3.5 Effect of ionic strength:

The response of the present reaction to changes in concentration of an inert salt, at constant temperature and reactants concentrations, was examined (Figure 4-6). Increasing ionic strength increased the rate of reaction. This might suggest that the rate determining step(s) contain species of similar charges.
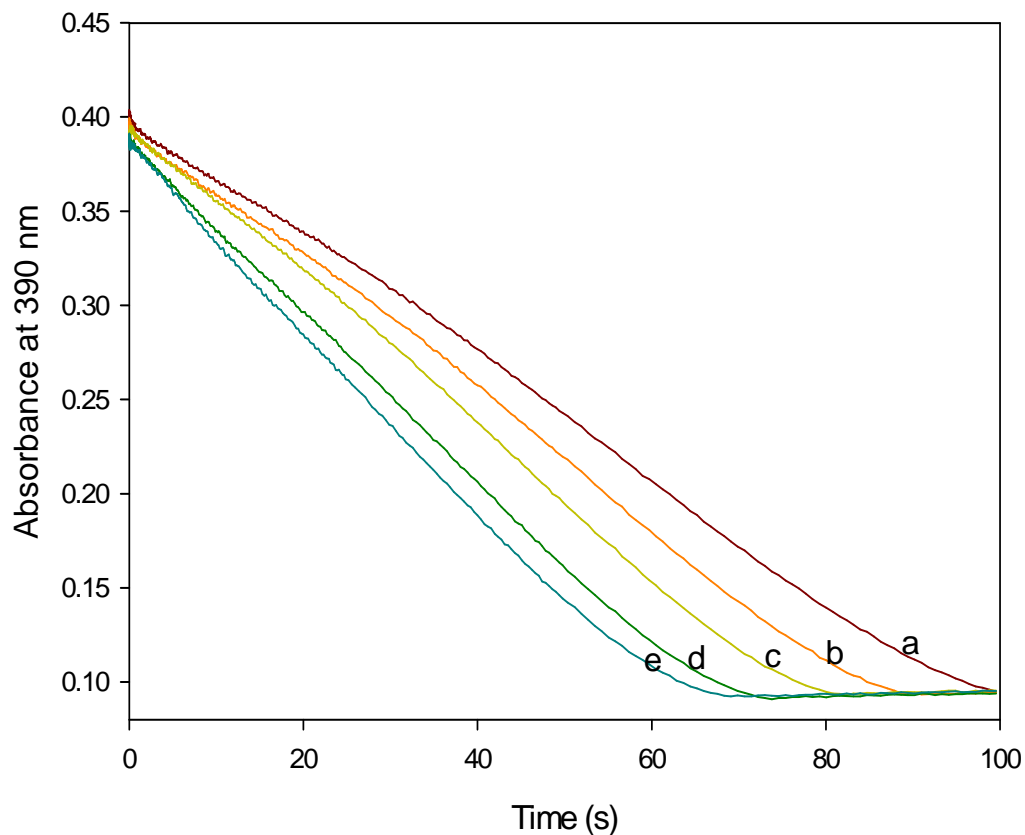
Figure 4-6: *Influence of ionic strength on reaction rate. Ionic strength increase from (a) to (e) increased the reaction rate as shown. $[NAMI\text{-}A]_o = 1.0 \times 10^{-4}M$; $[MESNA]_o = 5.0 \times 10^{-2}$ M; $[I]_{NaClO4} = $ (a) 0.05 M (b) 0.10 M (c) 0.20 M (d) 0.30 M (e) 0.40M.*

4.4   Mechanism

Ionization of MESNA in aqueous solution is represented in R1. Under reaction conditions of pH 7.4, predominant species is the monoanionic as seen in this reaction. Dianionic form (see R2) is expected to be present in quantifiable amounts based on the Henderson-Hasselbach equation.

$$HSCH_2CH_2SO_3Na \rightleftharpoons HSCH_2CH_2SO_3^- + Na^+ \qquad R1$$

$$HSCH_2CH_2SO_3^- \rightleftharpoons {}^-SCH_2CH_2SO_3^- + H^+ \qquad K_a \quad R2$$
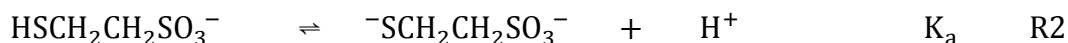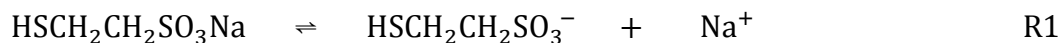
These species react with anionic NAMI-A to form associative complexes (see R3; R4) as indicated by deduced activation parameters. The activated complexes then proceed to form BNP7787 and reduced NAMI-A as products as shown in R5 and R6.

$$HSCH_2CH_2SO_3^- + [ImRuCl_4DMSO]^-$$

$$\rightarrow [HSCH_2CH_2SO_3^- ... [ImRuCl_4DMSO]^-]^{\neq} \qquad k_1 \qquad R3$$

$${}^-SCH_2CH_2SO_3^- + [ImRuCl_4DMSO]^-$$

$$\rightarrow [{}^-SCH_2CH_2SO_3^- ... [ImRuCl_4DMSO]^-]^{\neq} \qquad k_2 \qquad R4$$

$$2[HSCH_2CH_2SO_3^- ... [ImRuCl_4DMSO]^-]^{\neq}$$

$$\rightarrow {}^-O_3SCH_2CH_2SSCH_2CH_2SO_3^- + 2[ImRuCl_4DMSO]^{2-} \ 2H^+ \quad R5$$

$$2[{}^-SCH_2CH_2SO_3^- ... [ImRuCl_4DMSO]^-]^{\neq}$$

$$\rightarrow {}^-O_3SCH_2CH_2SSCH_2CH_2SO_3^- + 2[ImRuCl_4DMSO]^{2-} \qquad R6$$
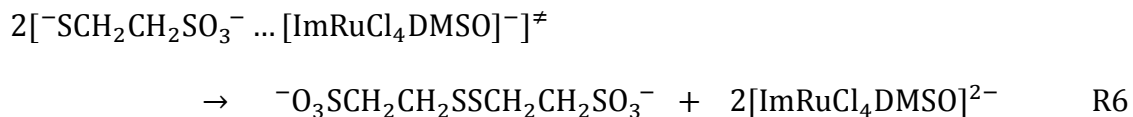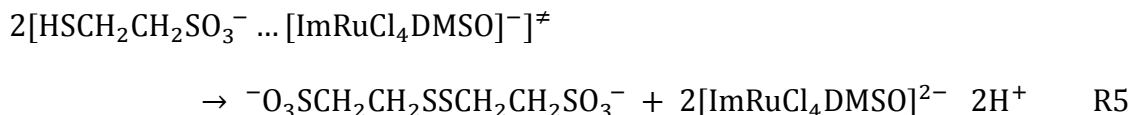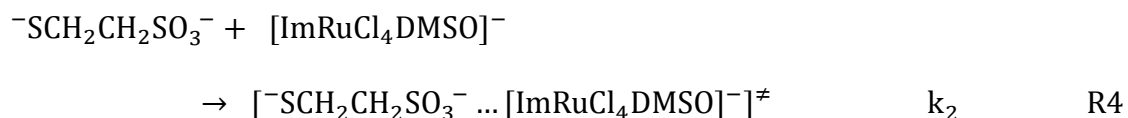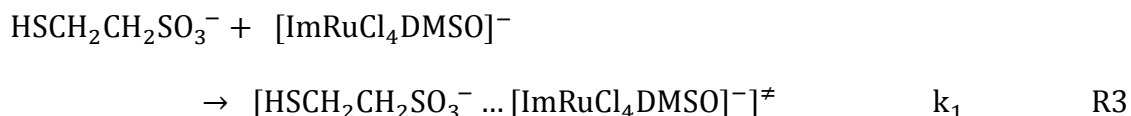
Results of the ESI-MS experiments (Figure 4-2a-c) suggests a clean conversion of NAMI-A to the reduced dianion form. The absence of an isosbestic point on the multiple UV/Vis spectra suggests involvement of multiple absorbing species. Redox

interaction between the products was anticipated, however, the nature of these species in terms of charge strongly indicate prevention of such interactions due to electrostatic repulsions.

Reaction rate measured as the rate of disappearance of [ImRuCl$_4$DMSO]$^-$, NAMI-A is defined as:

$$\text{Rate} = k_1[RSH][ImRuCl_4DMSO]^- + k_2[RS^-][ImRuCl_4DMSO]^- \qquad E1$$

where RSH and RS$^-$ represent protonated and deprotonated MESNA respectively as shown in R1 and R2. Results obtained from ionic strength effects demonstrate that the reaction of RS$^-$ is rate limiting thus indicating that $k_1 \gg k_2$ and E1 reduces to

$$\text{Rate} = k_2[RS^-][ImRuCl_4DMSO]^- \qquad E2$$

E2 can be expressed in terms of initial MESNA concentration which is distributed between RSH and RS$^-$. From mass balance,

$$[RSH]_o = [RSH] + [RS^-] \qquad E3$$

Combining E3 with Henderson-Hasselbach equation, a ratio of [RS$^-$] to [RSH] can be derived. Substitution for [RSH] using R2 results in the rate law;

$$\text{Rate} \quad = \quad \frac{Kak_2[\text{RSH}]_o[\text{ImRuCl}_4\text{DMSO}]^-}{[\text{H}^+](1 + 10^{\text{pH}-\text{p}Ka})} \qquad\qquad \text{E4}$$

which in conditions of overwhelming excess of MESNA can be written as

$$\text{Rate} \quad = \quad k_o[\text{ImRuCl}_4\text{DMSO}]^- \qquad\qquad \text{E5}$$

where

$$k_o \quad = \quad \frac{Kak_2[\text{RSH}]_o}{[\text{H}^+](1 + 10^{\text{pH}-\text{p}Ka})} \qquad\qquad \text{E6}$$

CHAPTER FIVE

5.0   Kinetics and Mechanism of interaction of NAMI-A with Glutathione

5.1   Introduction

Intracellular thiols are essential for maintenance of cellular redox homeostasis in living systems.[246] Glutathione (GSH) is the most abundant and most important cellular antioxidant in animal cells with concentrations up to 10 mM in the cytoplasm and 2 – 20 µM in extracellular fluids.[247;248] It performs cytoprotectivity against reactive oxygen and nitrogen species vis: hydrogen peroxide, peroxynitrite, lipid peroxyl, hydroxyl, nitric oxide and superoxide radicals.[249] These reactive species have been implicated in the pathogenesis of various disease states including atherosclerosis, hypertension, ischemia/reperfusion injury, cardiovascular disease, diabetes mellitus, neurodegenerative diseases (Alzheimer's and Parkinson's diseases), rheumatoid arthritis, cancer and ageing [246;250;251] Participation of GSH in various metabolism and regulatory processes such as synthesis of prostaglandins, cell proliferation and apoptosis is well documented.[248;252-254] Its direct and indirect involvement in various important biochemical processes is further illustrated in Figure 5-1,[255] where it is shown to act as a center wheel influencing all featured processes.

Interactions of a drug with biomolecules and other xenobiotics influence its absorption, distribution, metabolism, excretion and toxicity (ADMET) properties and ultimately its activity. These properties are determinants of a drug's clinical relevance. Drugs are metabolised either to active or inactive metabolites by interaction with proteins and non-protein biomolecules. Such interactions impact drug efficacy

positively or otherwise. Interaction of any xenobiotic with GSH invariably translates to potential for modulation of processes involving GSH.[256]
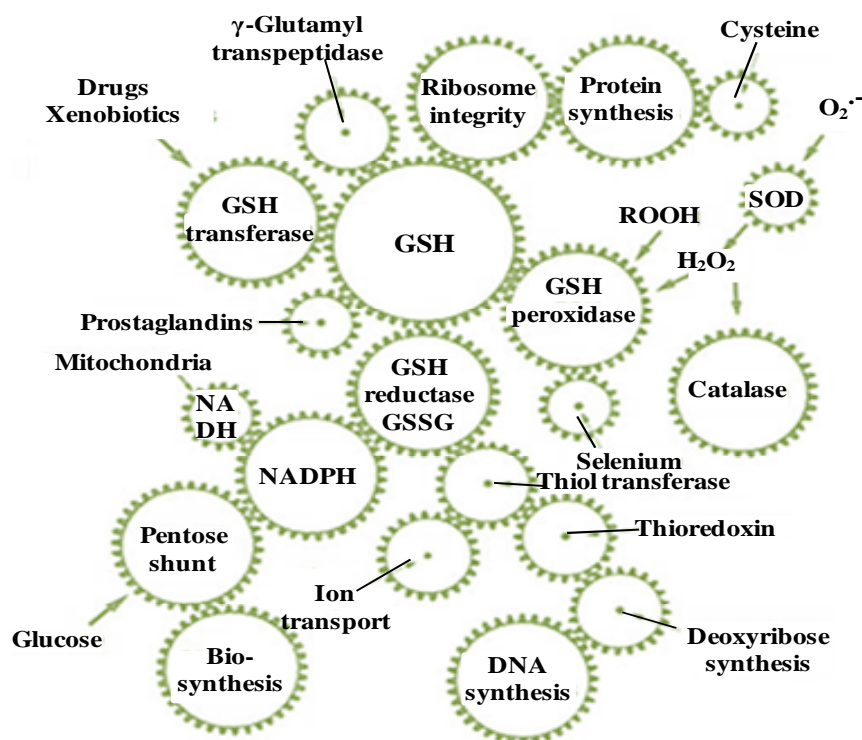
Figure 5-1: *A representation of the GSH involvement in important cellular processes. (Modified figure adapted from Mitchell, J.B. & Russo, A. 1987 Br. J. Cancer Suppl. 8:96-104)*[255]

Decrease in GSH levels impairs a cell's ability to protect itself thereby increasing sensitivity to effects of toxic substances. It is then not surprising that higher levels of GSH in cancer cells are associated with observed resistance to chemotherapeutic agents.[257-259] This is in agreement with mounting evidence that tumor cells have higher levels of GSH compared to normal healthy cells.[260-262]

There is great potential for interaction between NAMI-A and GSH considering the extent of GSH involvement in many processes of biological significance. In view of the above, this chapter reports on the investigation conducted on the reactivity of NAMI-A with GSH in hopes of better understanding of mechanism of action of this promising prodrug.

5.2   Results and Discussion

5.2.1   Stoichiometry and Product Identification: Absorbance measurement at 390 nm of varying ratios of NAMI-A to GSH afforded determination of reaction stoichiometry. A 1:1 ratio represented by R1 was obtained (GSSG stands for oxidized glutathione).

$$2GSH + 2[ImRuCl_4DMSO]^- \rightarrow GSSG + 2[ImRuCl_4DMSO]^{2-} + 2H^+ \qquad R1$$
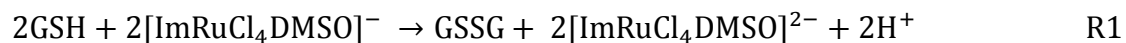
An absorption profile of a solution containing about 1:3 ratio of GSH to NAMI-A was recorded at 30 s intervals. Consumption of NAMI-A was observed as the reaction progressed as demonstrated by reduction at 390 nm (Figure 5-2a). The disappearance of this band occurred with concomitant formation of a new band at ~339 nm which progressively shifted to lower wavelength. Growth of the new peak represents conversion of reduced NAMI-A to a new absorbing form, supposedly through ligand exchange. Kinetic observation at ~339 nm could unveil some information regarding the species present. Several attempts to study reaction kinetics at this wavelength however,

demonstrated that consistent results could not be obtained under these reaction conditions. Contributions from multiple species might be responsible.
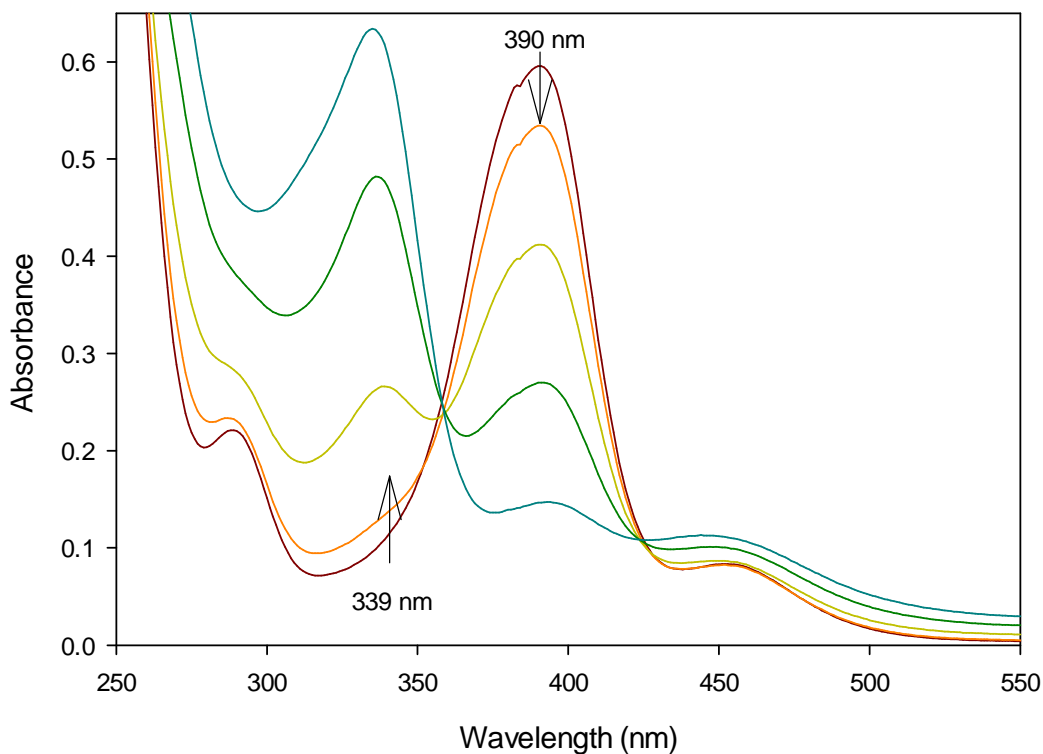
Figure 5-2a: *Multiple spectral scans showing absorption profile as reaction progressed of a GSH- NAMI-A reaction mixture. Spectral interval was 30 s. [NAMI-A]$_o$ = 1.5 x 10^{-4} M; [GSH]$_o$ = 5.0 x 10^{-4} M.*

A continuous spectral scan of the same solution as shown in Figure 5-2a revealed a decrease in the shifting 339 nm peak followed by an increase in absorption over the entire visible wavelength (Figure 5-2b). Blue shift in absorbance maximum and absence of well-defined isosbestic points might be suggestive of progress of reaction

towards product formation through various intermediates. Similar observations had been reported for GSH oxidation by chromium acetate cluster.[263]
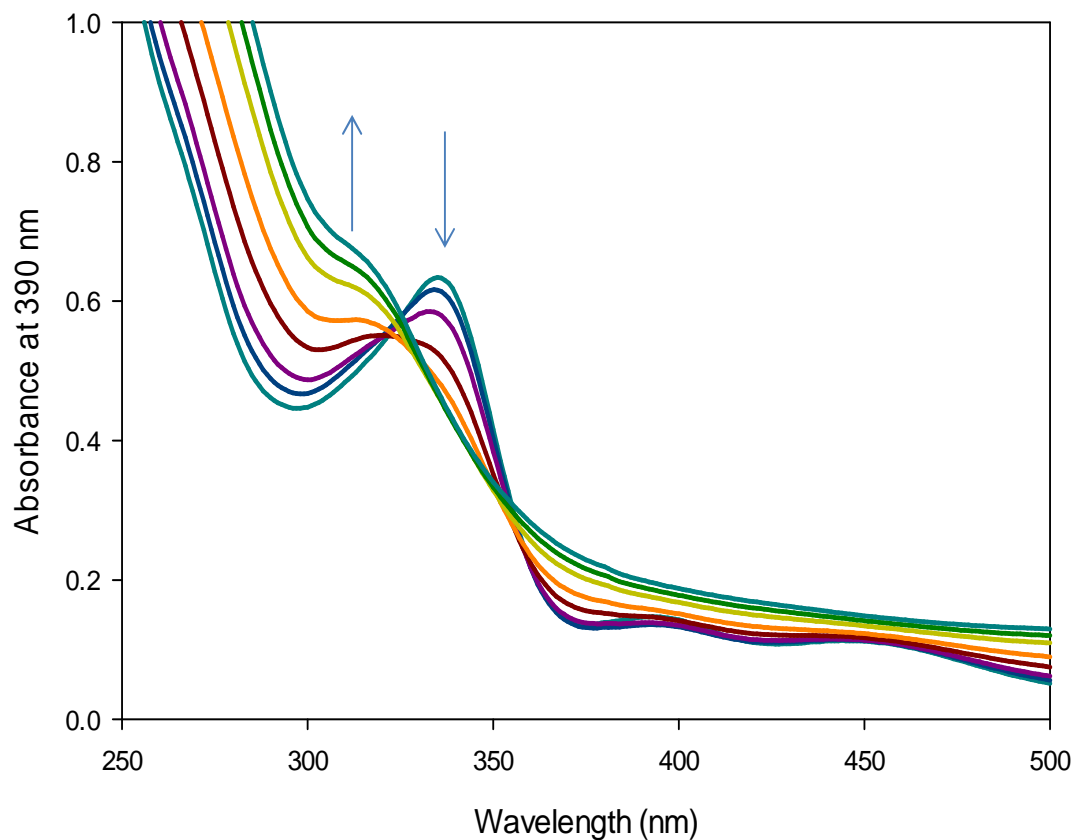
Figure 5-2b: *Multiple spectral scans of same solutions observed in Figure 5-2a. The new peak grew to a maximum and later decreased. Absorption over entire spectrum is observed with the disappearance of this peak.*

Identification of all observable molecular species present in a dynamic reaction mixture and after completion of reaction is key to establishing pathway for interaction of reactants to form products. A full ESI-MS spectrum of solution containing a stoichiometric ratio of NAMI-A and GSH was taken in the negative mode within the

first minute of the reaction in order to identify molecular species involved (Figure 5-3).

Observed ions were monoanionic NAMI-A, [RuCl$_4$DMSO]$^-$, [GSH-H]$^-$ and RuCl$_4$ at

389, 321 and 243 m/z respectively. One electron oxidation of GSH should result in

formation of dimeric GSH and dianionic NAMI-A.
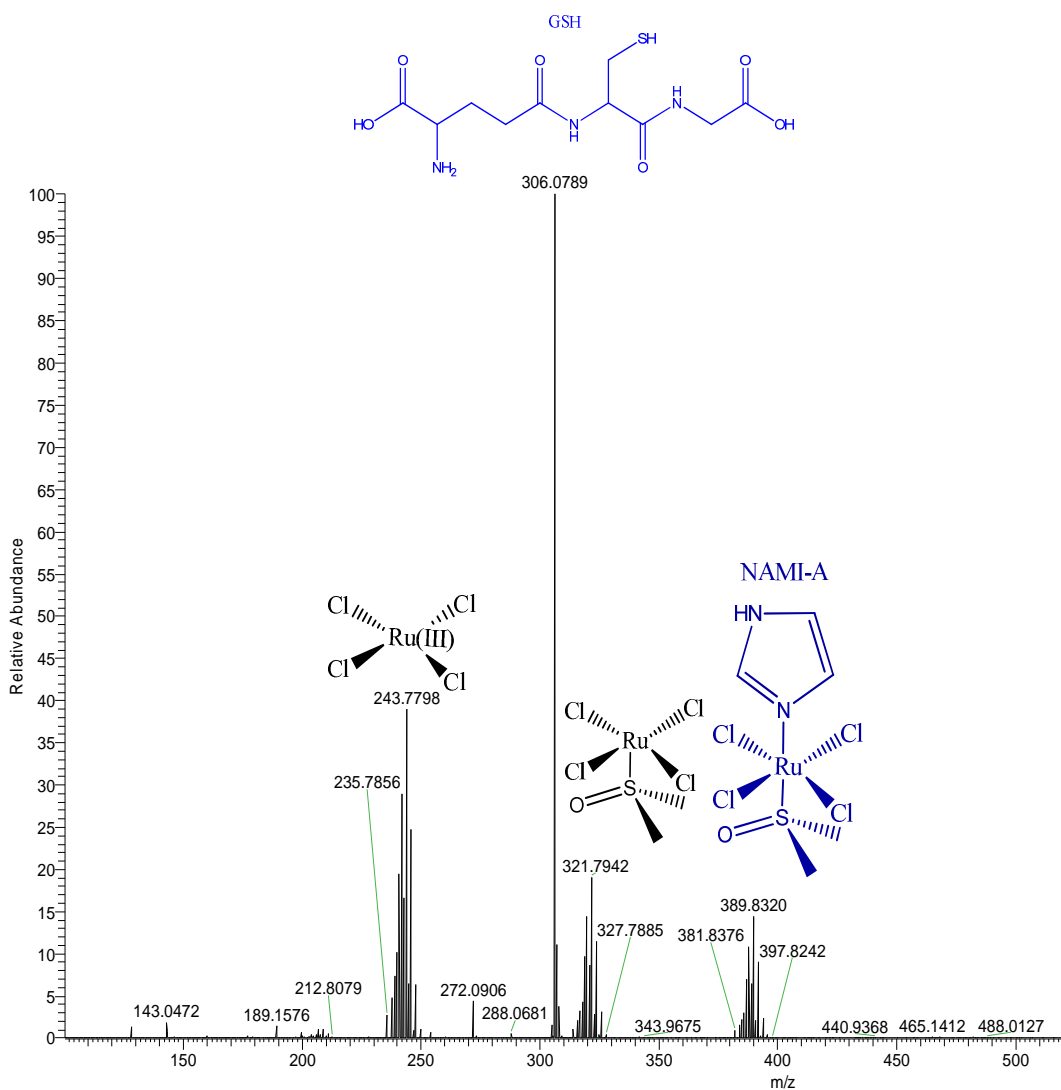
Figure 5-3: *Full ESI-MS spectrum of stoichiometric solution of NAMI-A and*

glutathione within the first minute of the reaction. (50% methanol, negative mode)

An ESI-MS spectrum of the same solution taken in the negative mode a minute later is shown in Figure 5-4. Same peaks as the ones observed in Figure 5-3 were present with the appearance of a new peak at 611 m/z displaying formation of dimeric GSH, GSSG.
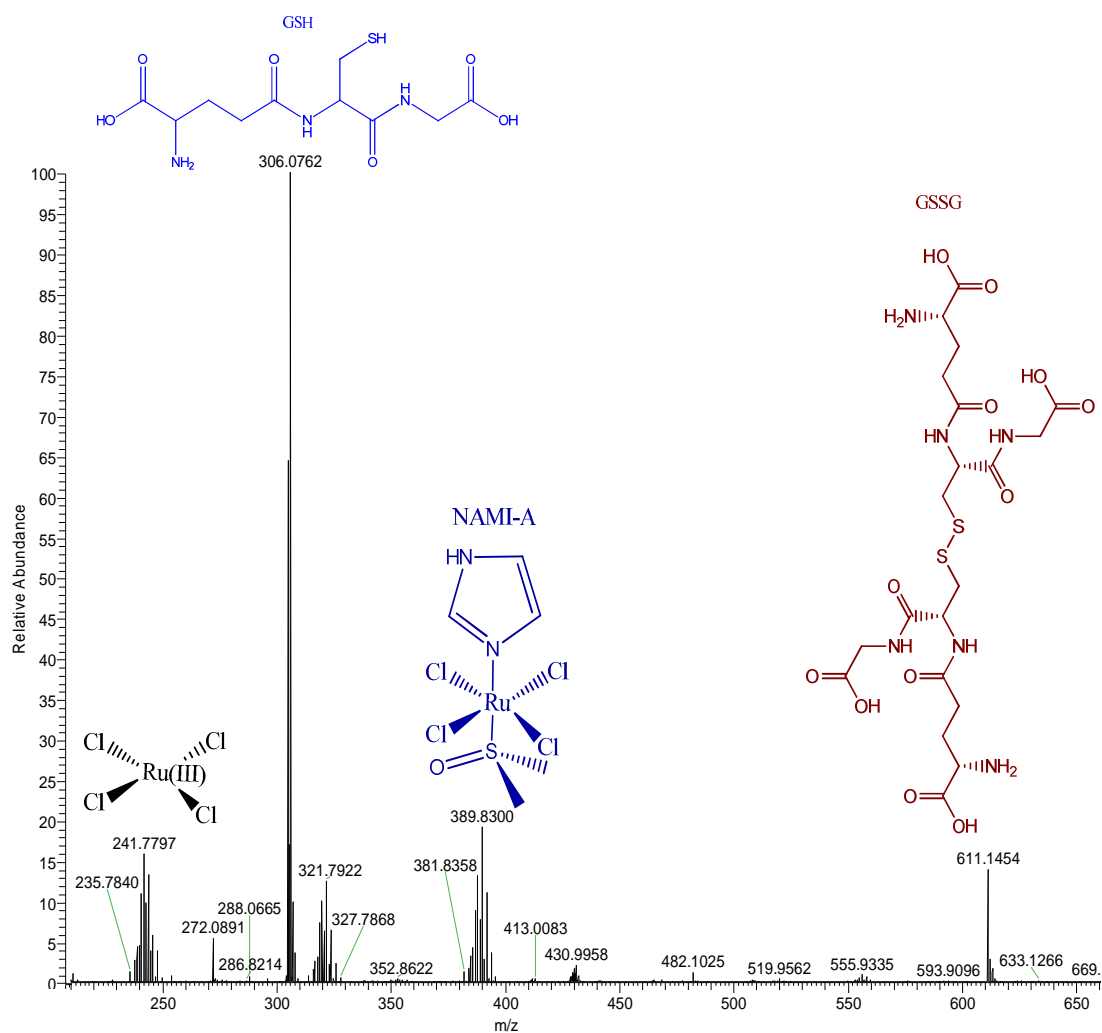
Figure 5-4: *Full ESI-MS spectrum of solution in Figure 5-1 taken a minute later. Formation of GSSG was observed. (50% methanol, negative mode)*

Dianionic NAMI-A was not observed, its obvious absence could be attributed to its short half life. No ions indicating aquation of any of the apical or axial ligands were observed. In the positive mode (Figure 5-5), only ions corresponding to GSH and GSSG were observed in significant relative abundances.
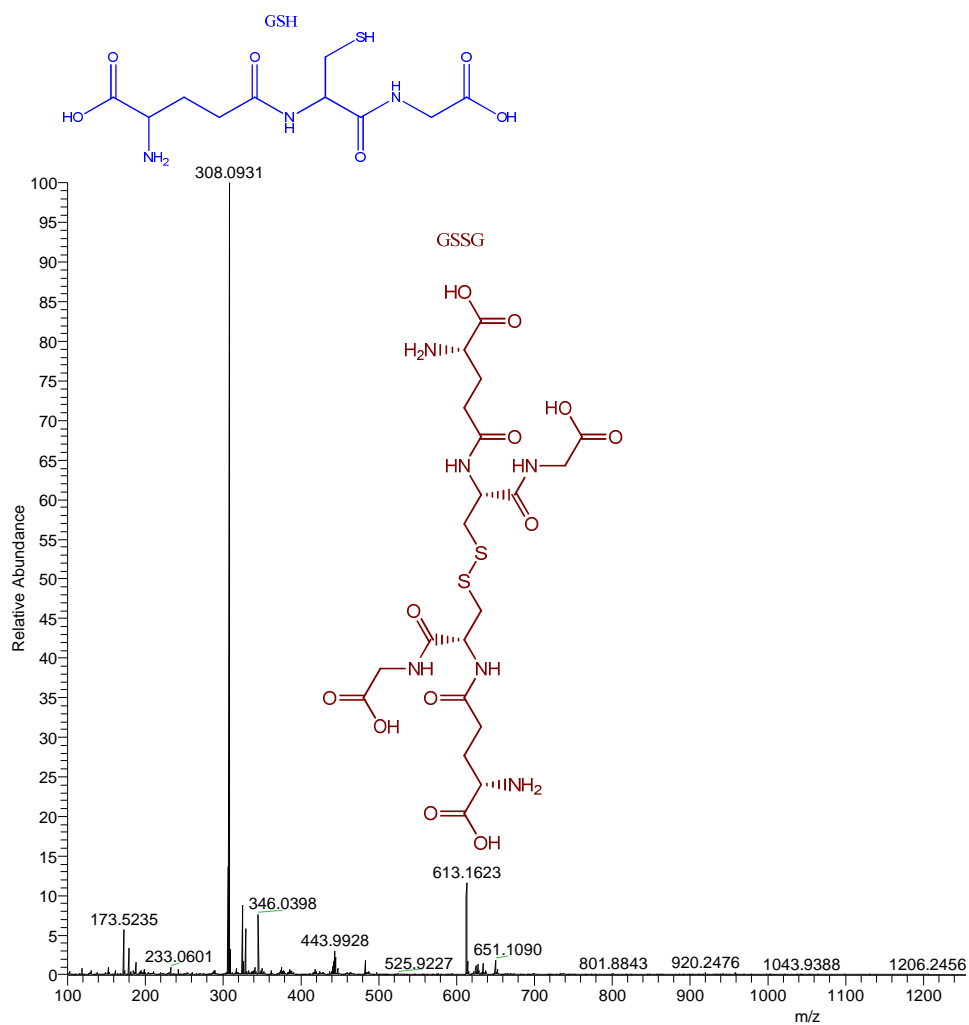
Figure 5-5: *Full ESI-MS spectrum of equimolar concentrations of NAMI-A and glutathione ran in the positive mode, showing formation of product, GSSG. (solvent-50% methanol)*

81

5.2.2 Kinetics

5.2.2.1 NAMI-A dependence: The peak serum concentration, C_{max}, of NAMI-A following administration of recommended safe dose of 300 mg/m^2/day ranged on the average between 1.58 x 10^{-4} M and 4.00 x 10^{-4} M for day 1 and day 5 respectively. Sets of initial NAMI-A concentrations were chosen such that highest concentration used is at least bioavailable. Under pseudo first-order conditions of excess GSH (100 – 200 fold), effect of varying initial concentrations of NAMI-A on the reaction at pH 7.4 was examined, see Figure 5-6a.
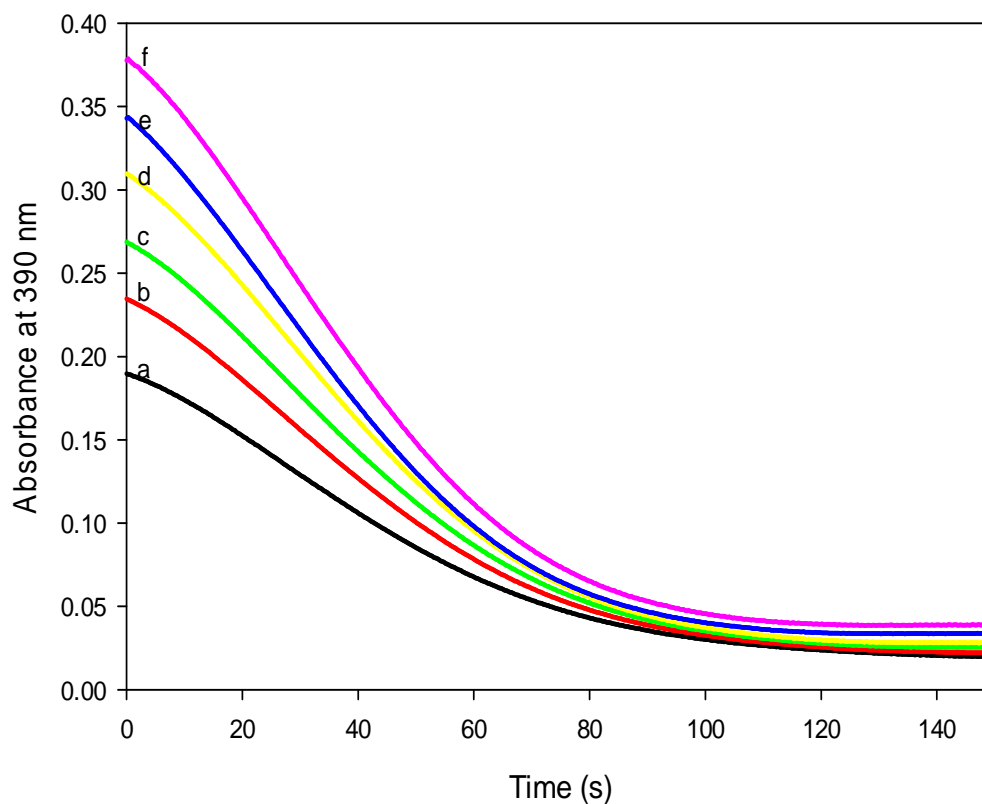
Figure 5-6a: *Kinetic traces of reaction in 0.1M phosphate buffer (pH 7.4) showing dependence on [NAMI-A] at its λ_{max}. [GSH]$_o$ = 1.0 x 10^{-2}M; [NAMI-A]$_o$ = (a) 5.0 x 10^{-5} M through (f) 1.0 x 10^{-4} M*

The rate of consumption of NAMI-A increased with increasing initial NAMI-A concentrations. Initial rates deduced from these data were employed to give Figure 5-6b, plot of initial rates against NAMI-A concentrations indicates a linear dependence on NAMI-A. Pseudo first-order rate constant was then deduced to be $7.42 \times 10^{-3} \pm 0.0004$ s^{-1}
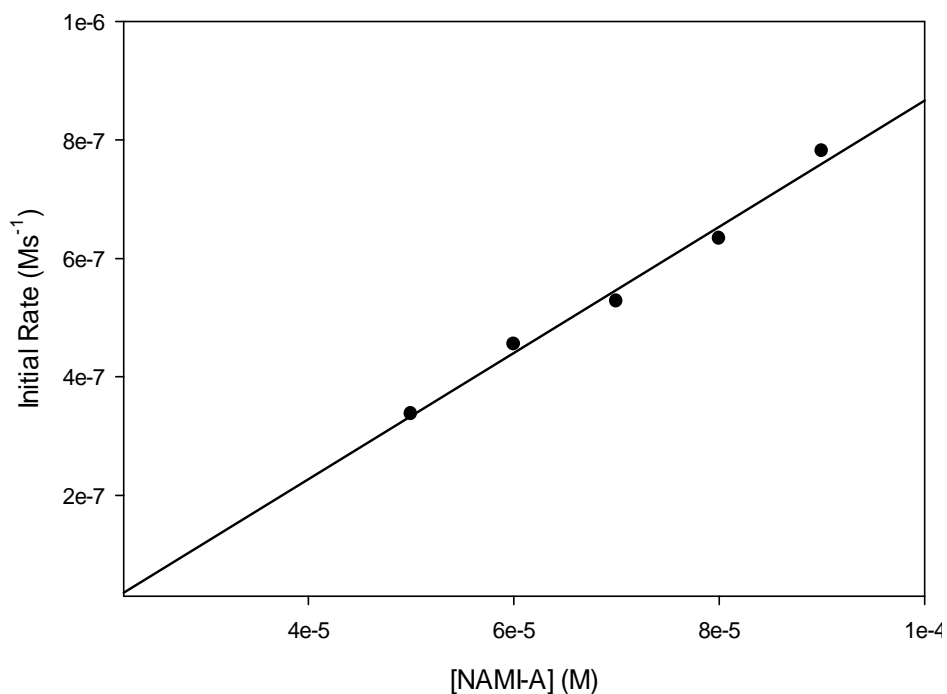
Figure 5-6b: *Initial rate plot derived from Figure 3.5a, showing linear dependence on NAMI-A. [GSH]$_o$ = 1.0 x 10^{-3}M; [NAMI-A]$_o$ = 5.0 x 10^{-5} M to 1.0 x 10^{-4} M*

5.2.2.2 GSH Dependence: Dependence of the reaction on initial concentrations of GSH (all other reaction conditions fixed) was monitored at 390 nm. Several independent runs of this experiment were performed to confirm the observed trend. A representative plot of the results, Figure 5-7, demonstrates independence of reaction rate on initial GSH

concentrations. The zero-order dependence of this reaction on GSH concentration thus renders the pseudo-first-order rate constant equivalent to overall reaction rate constant.
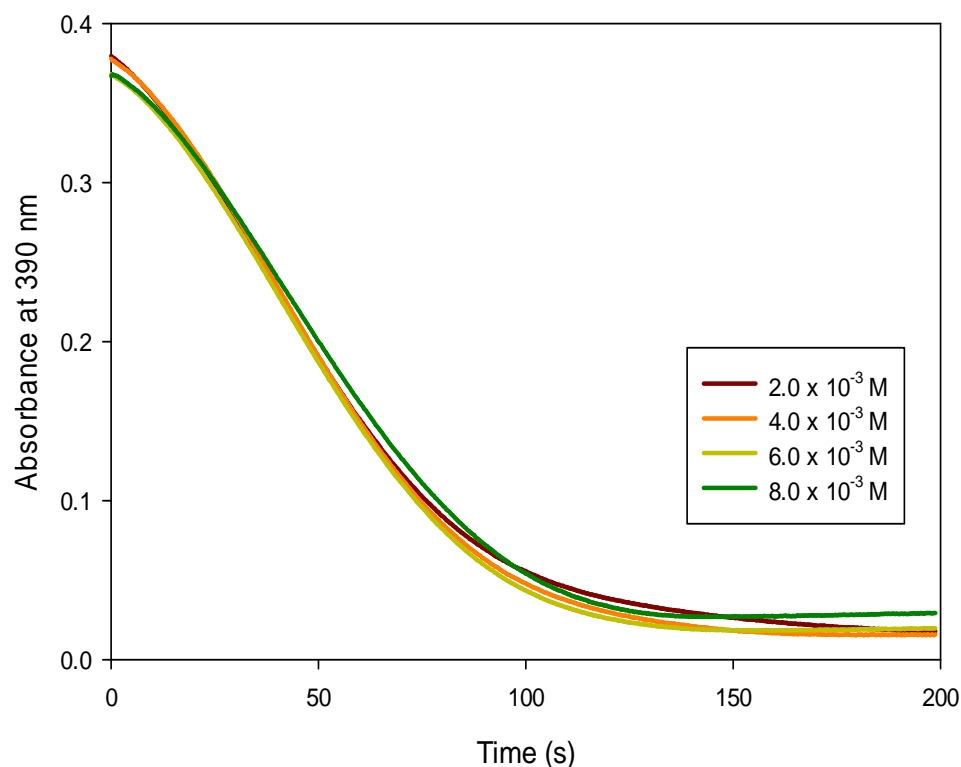
Figure 5-7: *Effect of increasing initial GSH concentration on the consumption of NAMI-A at 390 nm. [NAMI-A]$_o$ = 1.0 x 10^{-4}M; [I] = 1.0 M, [GSH]$_o$ varies from 2.0 x 10^{-3} M to 8.0 x 10^{-3} M*

This suggests that GSH is not involved in the rate-determining step and does not affect the transition state. This observation might be suggestive of a chelate formation process. GSH possesses multiple potential binding sites: carboxylic acid, amino, amide and sulfhydryl groups, all of which cannot be coordinated simultaneously to the ruthenium

84

center. Species demonstrating the formation of coordinated GSH were not observed on the ESI-MS.

5.2.2.3 Effect of ionic strength: Under unbuffered conditions of constant temperature, oxidant and reductant concentrations, the influence of varying concentrations of an inert salt (NaClO$_4$) was evaluated to establish effect of ionic strength on the reaction. Increasing ionic strength slowed down the reaction rate suggesting that the rate determining step contain species of opposite charges.

5.2.2.4 Thermodynamic and activation parameters: Temperature dependence of the reaction was isolated with all other reaction conditions were fixed. Reaction rate increased proportionally with increasing temperature (see Figure 5-8a). Rate constants for individual temperature conditions were obtained using initial rate plots shown in Figure 5-8b. The derived rate constants were used to construct an Arrhenius plot, Figure 5-8c, resulting in the following activation parameters: entropy of activation, $\Delta S^{\neq} = -100.6$ J K^{-1} mol^{-1}, enthalpy of activation, $\Delta H^{\neq} = 55.1$ kJ mol^{-1} and free energy of activation as $\Delta G^{\neq} = 85$ kJ mol^{-1}(25 ^{o}C). The distinctly negative entropy of activation suggests a more ordered activated transition state compared to the reactants and is indicative of an associative mechanism.
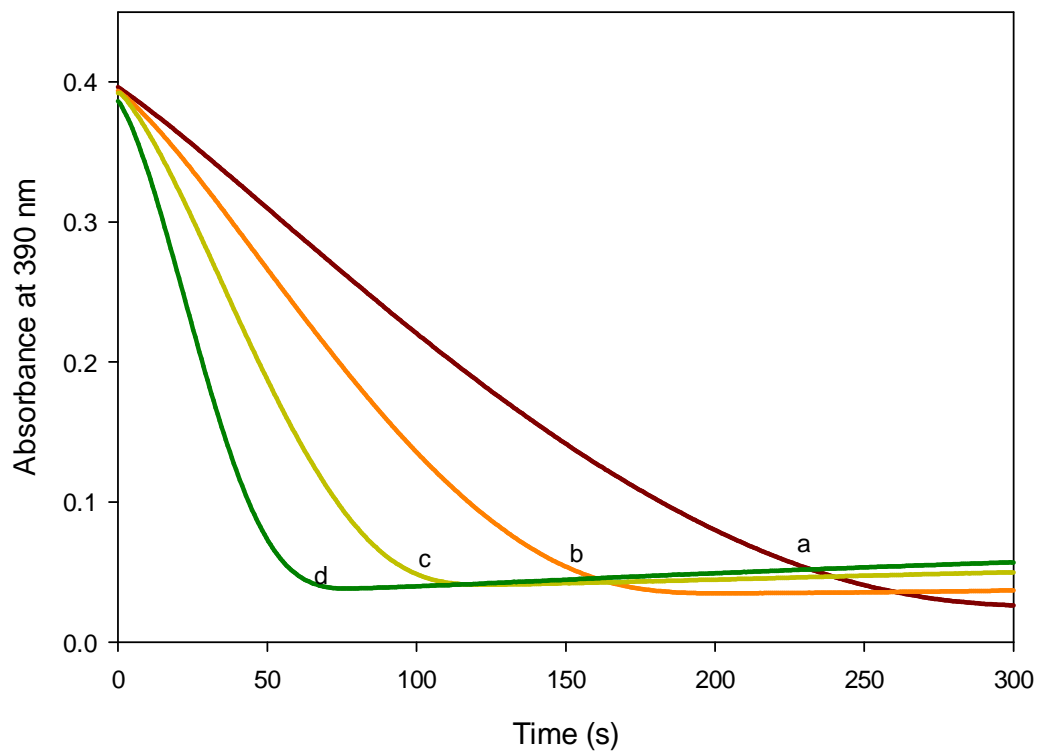
Figure 5-8a: *[NAMI-A]$_o$ = 1.0 x 10^{-4} M; [GSH]$_o$ = 5.0 x 10^{-2} M , Temperature = (a) 15*

^{o}C (b) 20 ^{o}C (c) 25 ^{o}C (d) 30 ^{o}C ; pH 7.4; Ionic strength maintained at 1.0 M using

NaCl
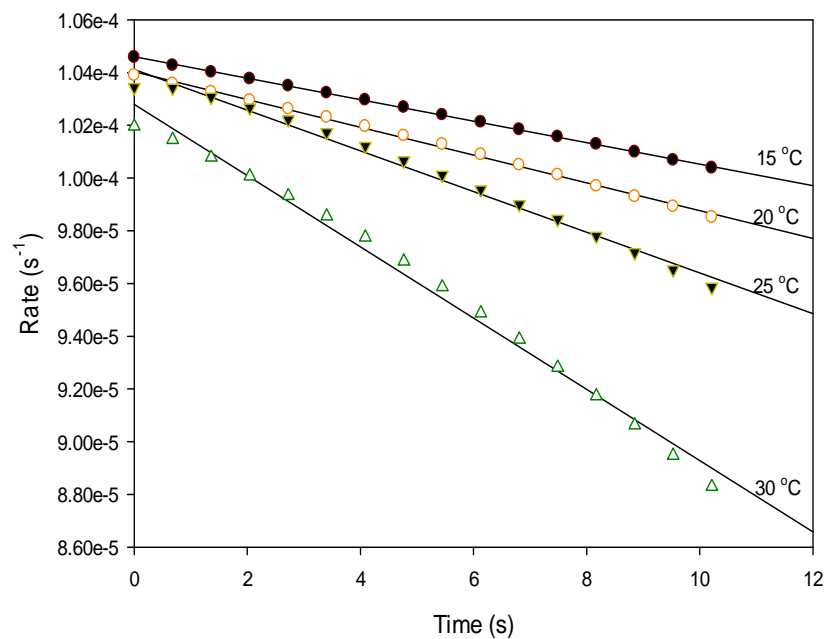
Figure 5-8b: *Rate plot from data shown in Figure 5-8a. All reaction conditions same as shown for Figure 5-8a.*
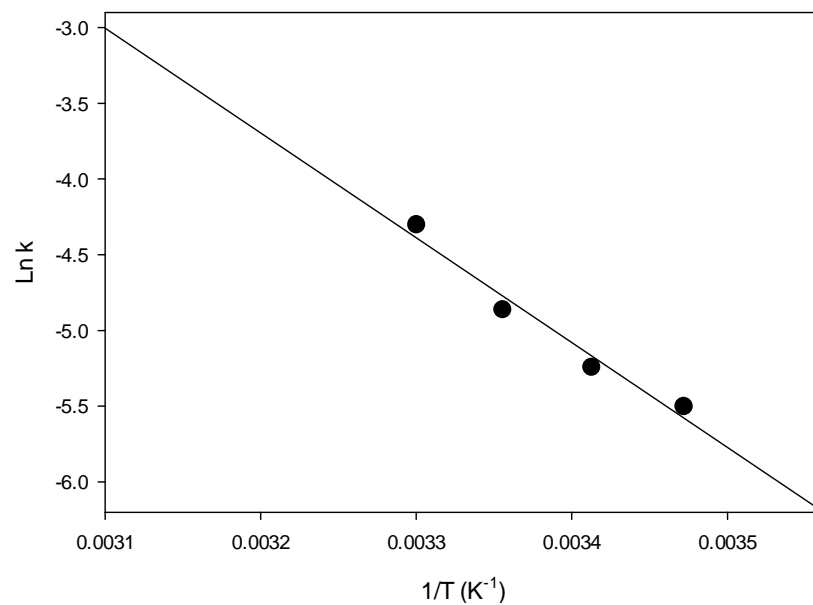
Figure 5-8c: *Arrhenius plot extracted from study of effect of temperature (Figure 5-8a) for determination of activation parameters.*

5.3   Mechanism

GSH has four pKa values: 2.12, 3.59, 8.75 and 9.65 for its carboxylic, thiol and amine functional groups. At pH 7.4, at which reactions were performed, both carboxylic groups are expectedly deprotonated while thiol and amine groups are protonated.[221] These dissociations are represented by R1-R3, where $HO_2CCH(NH_2)(SH)RCO_2H$ represents GSH.

$$HO_2CCH(NH_2)(SH)RCO_2H \; \rightleftharpoons \; {}^-O_2CCH(NH_2)(SH)RCO_2H \quad + \quad H^+ \quad K_{a1} \quad R1$$

$${}^-O_2CCH(NH_2)(SH)RCO_2H \; \rightleftharpoons \; {}^-O_2CCH(NH_2)(SH)RCO_2{}^- \quad + \quad H^+ \quad K_{a2} \quad R2$$

$${}^-O_2CCH(NH_2)(SH)RCO_2{}^- \; + \; H^+ \rightleftharpoons \; {}^-O_2CCH({}^+NH_3)(SH)RCO_2{}^- \quad K_b \quad R3$$
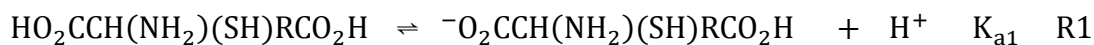
GSH will have a predominant net charge of -1. All of the different GSH forms will react with NAMI-A to form more ordered transition state, see R4 – R6.

$${}^-O_2CCH(NH_2)(SH)RCO_2H \; + \; [ImRuCl_4DMSO]^-$$
$$\rightarrow \quad [{}^-O_2CCH(NH_2)(SH)RCO_2H \ldots [ImRuCl_4DMSO]^-]^{\neq} \qquad\qquad k_1 \quad R4$$

$${}^-O_2CCH(NH_2)(SH)RCO_2{}^- \; + \; [ImRuCl_4DMSO]^- \; \rightarrow$$
$$[{}^-O_2CCH(NH_2)(SH)RCO_2{}^-\ldots [ImRuCl_4DMSO]^-]^{\neq} \qquad\qquad k_2 \quad R5$$

$${}^-O_2CCH({}^+NH_3)(SH)RCO_2{}^- \; + \; [ImRuCl_4DMSO]^-$$
$$\rightarrow \quad [{}^-O_2CCH({}^+NH_3)(SH)RCO_2{}^-\ldots [ImRuCl_4DMSO]^-]^{\neq} \qquad\qquad k_3 \quad R6$$
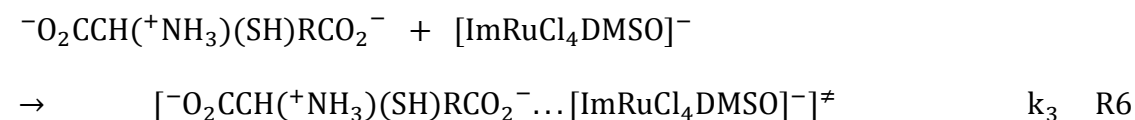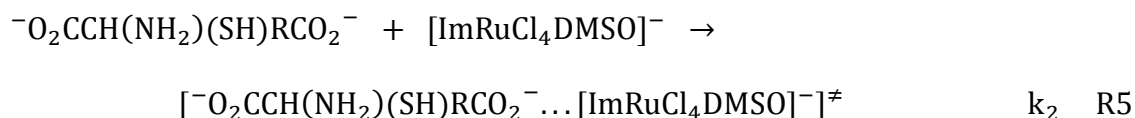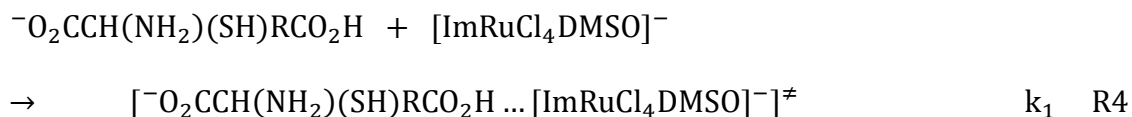
Representing all associative complexes by X and all different forms of glutathione by GSH_T, the reaction can be written as R7

$$[ImRuCl_4DMSO] \quad + \quad GSH_T \quad \rightleftharpoons \quad X \qquad\qquad K_4 \qquad R7$$

$$X \quad \rightarrow \quad Products \qquad\qquad k_5 \qquad R8$$
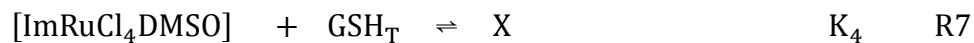
where products are oxidized GSSG and $[ImRuCl_4DMSO]^{2-}$. Rate of product formation can then be written as

$$Rate \quad = \quad k_5[X] \qquad\qquad E4$$

From R7,

$$K_4^{-1} \quad = \quad \frac{[ImRuCl_4DMSO][GSH]_T}{[X]} \qquad\qquad E5$$

From mass balance,

$$[ImRuCl_4DMSO^-] \quad = \quad [ImRuCl_4DMSO^-]_o \quad - \quad [X] \qquad\qquad E6$$

substituting for $[ImRuCl_4DMSO^-]$ in E5 implies

$$K_4^{-1} \quad = \quad \frac{([ImRuCl_4DMSO^-]_o - [X])[GSH]_T}{[X]} \qquad\qquad E7$$

and

$$[X] \quad = \quad \frac{[ImRuCl_4DMSO^-]_o[GSH]_T}{K_4 + [GSH]_T} \qquad\qquad E8$$

89

Substituting for [X] in the rate expression, E5,

$$\text{Rate} \quad = \quad \frac{k_5[\text{ImRuCl}_4\text{DMSO}^-]_o[\text{GSH}]_T}{K_4 + [\text{GSH}]_T} \qquad \text{E9}$$

The reaction shows a complex dependence on glutathione concentration as seen in E9. At low [GSH], where $[\text{GSH}]_T \ll K_4$, the rate becomes first order in [GSH] but at high [GSH], when $[\text{GSH}] \gg K_4$, rate becomes zero order in [GSH]. At high [GSH] under which reaction was performed,

$$\text{Rate} \quad = \quad \frac{k_5[\text{ImRuCl}_4\text{DMSO}^-]_o}{K_4} \qquad \text{E10}$$

which can be written as

$$\text{Rate} \quad = \quad k_o[\text{ImRuCl}_4\text{DMSO}^-]_o \qquad \text{E11}$$

where k_o is k_5/K_4. This is in agreement with experimental observation as demonstrated by Figure 5.7.

Ligand substitution reactions are expected to occur especially following formation of the reduced form of NAMI-A. Evidence is lacking however, on suggestion of possible structures.

In conclusion, independence of NAMI-A reaction with GSH on initial GSH concentrations might suggest that administration of NAMI-A will not adversely affect cellular detoxification (those dependent on GSH), in agreement with its reported low host toxicity.[162]

CHAPTER SIX

6.0   Kinetics and Mechanism of interaction of NAMI-A by L-Cysteine

6.1   Introduction

Cysteine is a non-essential amino acid that exists in various forms *in vivo* due to the different accessible oxidation states of sulfur, -2 to +6. It is the only sulfur contributor and the rate-limiting substrate in the biosynthesis of GSH, the most abundant non-protein antioxidant.[264] The ability of cysteine to undergo redox cycling is involved in many protein functions and redox-reactions in biological systems. Cysteine has been reported to be one of the few biological thiols that have inhibitory effects on direct acting and indirect-acting mutagens.[265]

Cysteine is a component responsible for many protein/enzyme structure and functions by modifications to the sulfhydryl functional group.[266] The most abundant protein found in plasma is Human serum albumin (HSA) which transports blood solutes to target organs and maintain pH and osmotic pressure. HSA contains 35 cysteine residues in the form of 17 pairs of intramolecular disulfides and one free thiol, Cys-34. It is noteworthy that this lone free thiol in HSA accounts for almost 80 % of plasma thiol and most of its antioxidant capacity.[267-269]

Mutation of tumor suppressor gene, p53, is a common characteristic of a wide variety of human cancers.[270-273] This is not surprising since p53 plays significant role in a wide range of biochemical processes including: cell cycle regulation, DNA repair, programmed cell death among others.[274] p53 protein contains 393 amino acids, modifications of cysteine residues in its central core (see Figure 6-1) critically affects its

functions. This is largely due to occurrence of most p53 interactions with target proteins in the central core.[274-276] Report has also shown involvement of cysteine residues in suppression of transactivation and transformation functions of p53.[277]
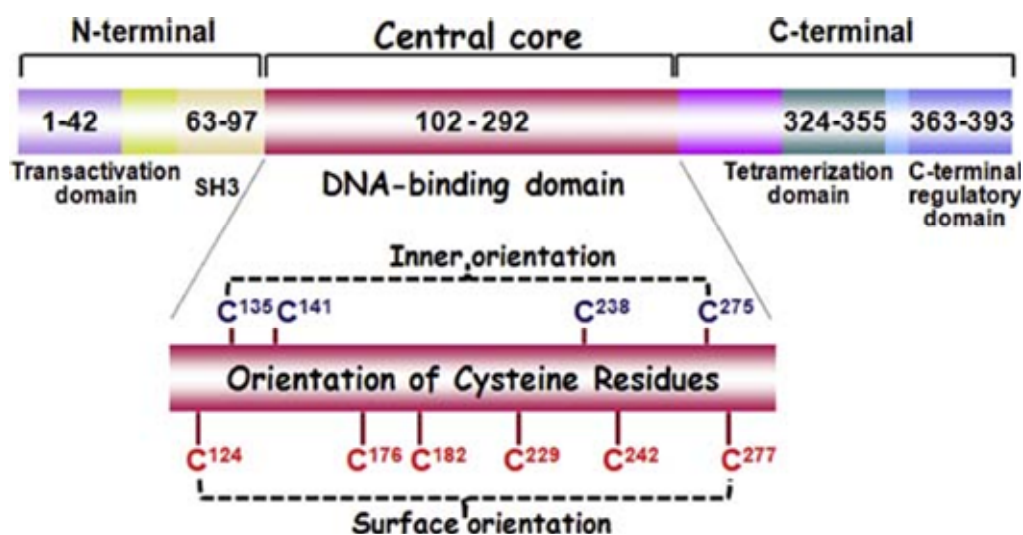
Figure 6-1: *Functional domains of p53. The DNA-binding domain contains 10 cysteine residues that affect its functions. (Adapted from Kim, D. et al [274])*

Also of importance is the role of cysteine in the activity of macrophage migration inhibitory factor, MIF, a protein involved in cell-mediated immunity, immuno-regulation, and inflammation. It effectively modulates p53 activities. It has been reported that a specific cysteine residue, 81, (Cys-81) plays a critical role in MIF-induced inhibition of p53 activity.[278]

Studying interaction of a drug candidate with cysteine can be regarded in one part, as investigating the reaction of the potential drug with a free amino acid and in another model the interaction of such drug candidate with all intracellular peptides,

proteins and enzymes containing cysteine residues. An investigation of the reactivity of NAMI-A with cysteine is therefore of high biological relevance. Results are thus presented in this chapter for the reactivity of NAMI-A with cysteine.

6.2   Results and Discussions

6.2.1   Stoichiometry and Product Identification: Reaction stoichiometry was determined using residual absorbance measurements of different ratios of NAMI-A to cysteine recorded within 10 minutes of solution preparation. The plot of residual absorbance at 390 nm against NAMI-A : cysteine ratio, Figure 6-2, clearly demonstrate significant residual NAMI-A in solution at ratios above the stoichiometry. Therefore, one mole of cysteine reacts with one mole of NAMI-A to form cystine (disulfide of cysteine) and reduced form of NAMI-A as shown in reaction R1. RSH, RSSR, [ImRuCl$_4$DMSO]$^-$ and [ImRuCl$_4$DMSO]$^{2-}$ represent cysteine, cystine, NAMI-A and reduced NAMI-A respectively.

$$2RSH + 2[ImRuCl_4DMSO]^- \rightarrow RSSR + 2[ImRuCl_4DMSO]^{2-} + 2H^+ \qquad R1$$
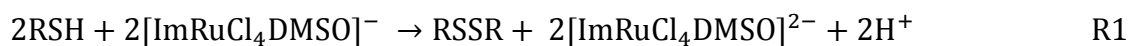
Figure 6-3 shows the spectral changes observed from a solution of cysteine and NAMI-A scanned at 30 second intervals. The characteristic absorption of NAMI-A at 390 nm decreased as the reaction progressed indicating conversion of [ImRuCl$_4$DMSO]$^-$ to [ImRuCl$_4$DMSO]$^{2-}$.
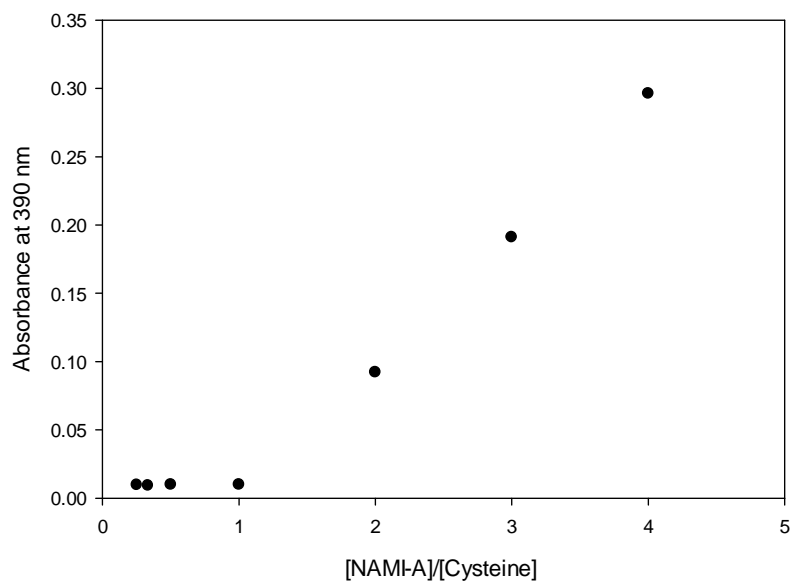
Figure 6-2: *Plot of Residual absorbance of NAMI-A against NAMI-A/cysteine revealing stoichiometric ratio beyond which residual absorbance persists. [NAMI-A]/[cysteine] = 0.25, 0.33, 0.5, 1.0, 2.0, 3.0 and 4.0.*
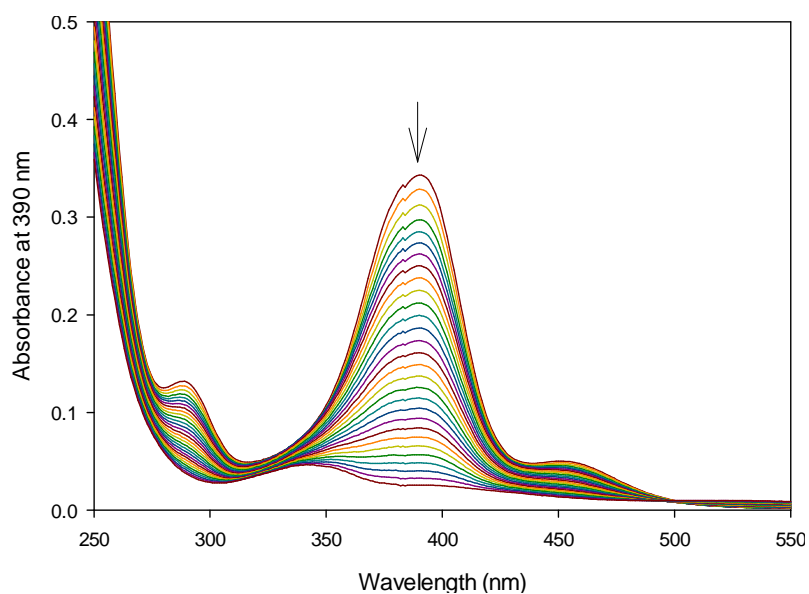
Figure 6-3: *Rapid spectral scan of solution of cysteine and NAMI-A taken at 5 s interval. $[cysteine]_o = 4.0 \times 10^{-4}$ M; $[NAMI-A]_o = 1.0 \times 10^{-4}$ M; no added buffer.*

Absence of clearly defined isobestic points might suggest involvement of intermediates of kinetic significance during this reduction reaction. A full electrospray ionization mass spectrum of stoichiometric solution was taken in the negative mode (Figure 6-4a) within the 60 s of mixing. Ions representing $[ImRuCl_4DMSO]^-$, $[RuCl_4DMSO]^-$, $[RuCl_4]^-$ and $[Cys-H]^-$ were observed at 390, 322, 244 and 120 m/z respectively. One electron oxidation of GSH should result in formation of cystine and dianionic NAMI-A. An ESI-MS spectrum of the same solution taken in the negative mode a minute later, Figure 6-4b, demonstrates cystine formation ([cystine-H] with 239 m/z). The peak at 209 m/z was not stable; compare Figure 6-4a and b. The m/z changed between scans, this could mean multiple ions with about the same m/z. Ions showing most abundance at this m/z have a basic structure, $[RuCl_2(H_2O)_2]$, switching between $[RuCl_2(H_2O)_2+H]$ and $[RuCl_2(H_2O)_2-H]$. These could arise from: loss of both apical ligands from reduced NAMI-A with exchange of two of the Cl^- for aquo ligands; or electron transfer to the Ru^{3+} center of 243 and 321 m/z from cysteine followed by appropriate ligand exchange. However, the lack of corresponding increase in relative abundance of the 209 peak with consumption of 243 and 321 m/z strongly support formation from reduced NAMI-A. In the positive mode, formation of cystine with 241 m/z is confirmed, Figure 6-4c.
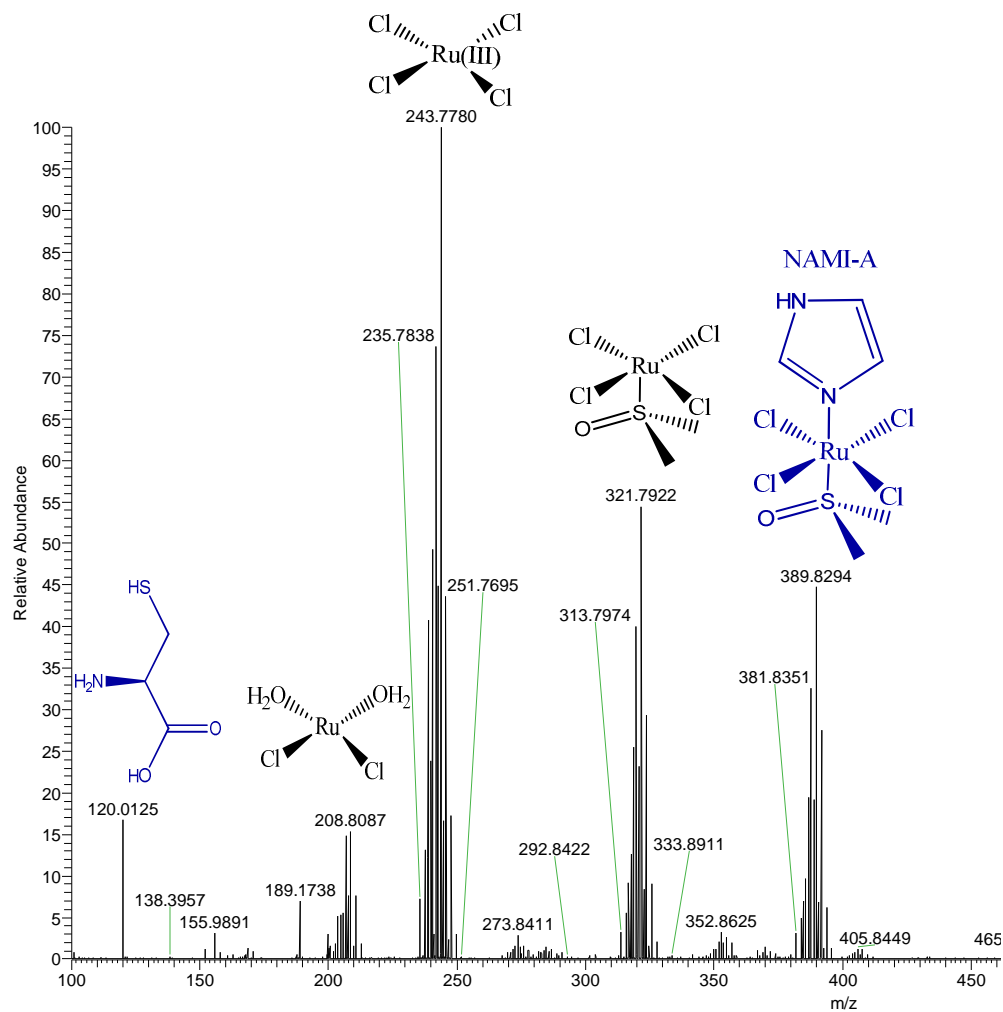
Figure 6-4a: *Full ESI-MS (negative mode) spectrum of 1:1 ratio of NAMI-A to Cysteine*

taken within the first minute of the reaction in 50% methanol.
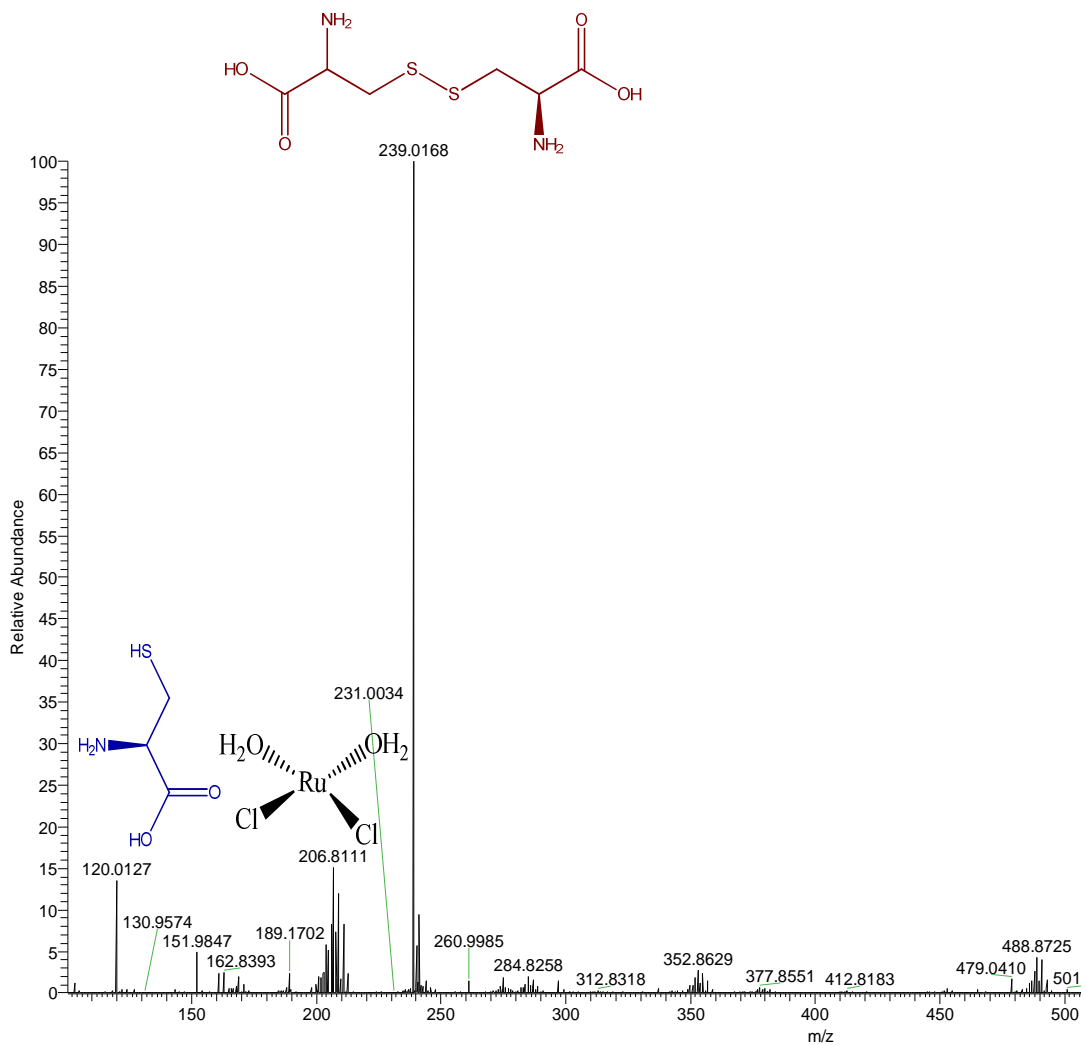
Figure 6-4b: *Full ESI-MS (negative mode) spectrum of 1:1 ratio of NAMI-A to Cysteine taken a minute later. Showing cystine and hydrolyzed NAMI-A (Solvent is 50% methanol).*
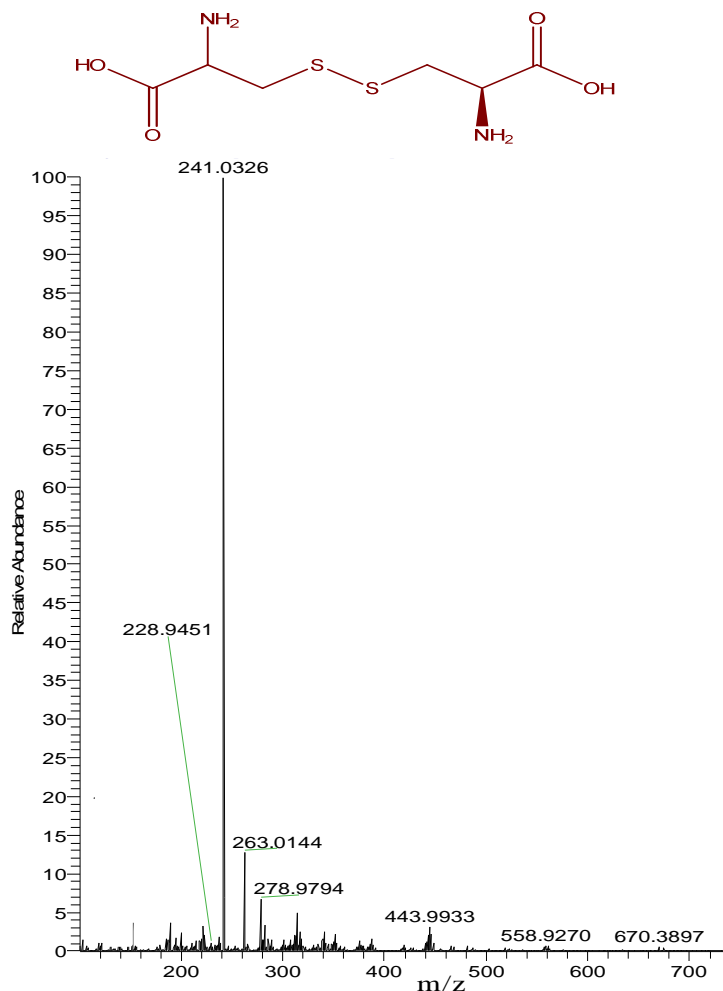
Figure 6-4c: *Full ESI-MS (positive mode) spectrum of product solution of 1:1 ratio of NAMI-A to Cysteine showing formation of cystine (t = 3 mins).*

6.2.2   Kinetics

6.2.2.1 NAMI-A Dependence: Under pseudo-first order conditions of excess cysteine, dependence of the present reaction on NAMI-A concentration was examined. Reaction rate increased with increase in initial NAMI-A concentrations as seen in Figure 6-7. Initial rate plot deduced from this confers a linear dependence on cysteine, see Figure 6-

7 inset. Under these reaction conditions, cysteine concentrations effectively remained unchanged during the reaction leading to deduction of an observed rate constant of 9.40 x $10^{-2} \pm 0.005$ s^{-1}.
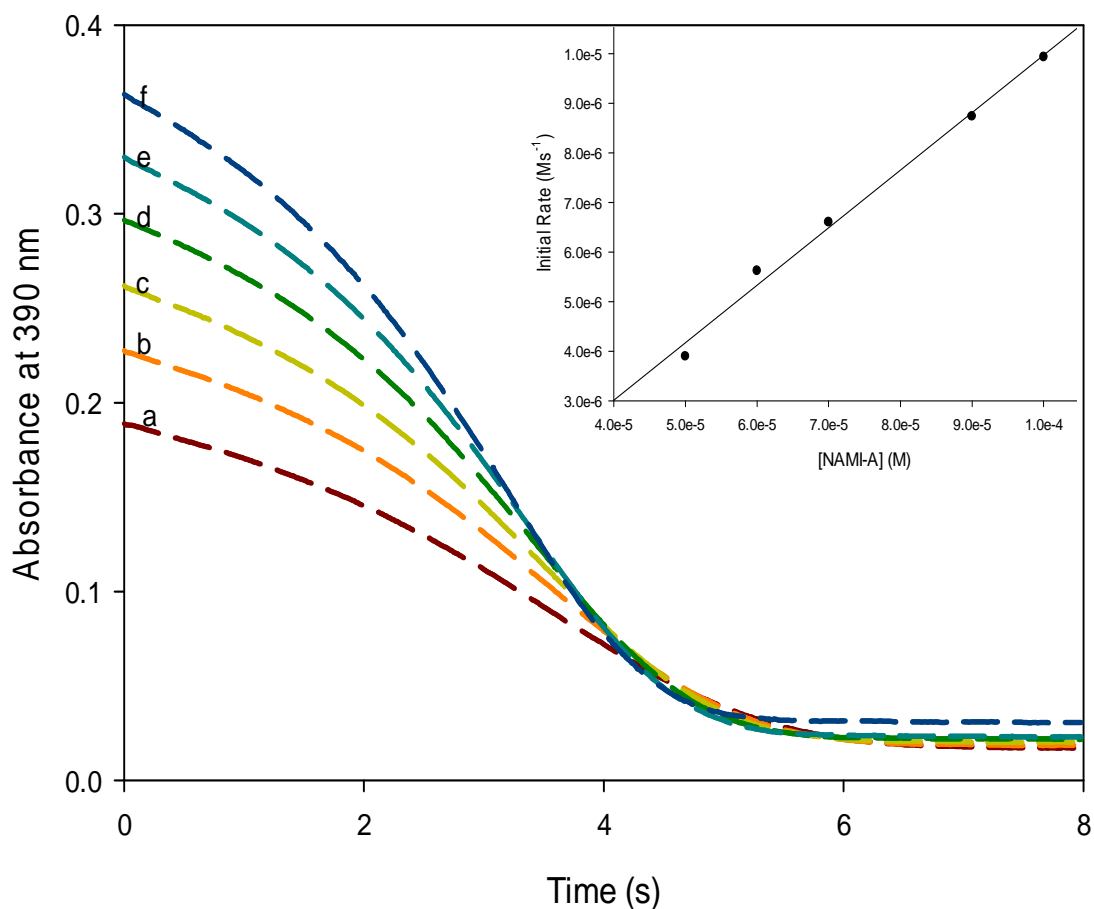
Figure 6-7: *Kinetic traces of reaction in phosphate buffer (pH 7.4) showing dependence on [NAMI-A] at its λ_{max} , 390 nm. [cysteine]$_o$ = 5.0 x 10^{-2}M; [NAMI-A]$_o$ = (a) 5.0 x 10^{-5} M (b) 6.0 x 10^{-5} M (c) 7.0 x 10^{-5} M (d) 6.0 x 10^{-5} M (e) 9.0 x 10^{-5} M (f) 1.0 x 10^{-4} M. Inset: Initial rate plot showing linear dependence on NAMI-A.*

6.2.2.2 Cysteine Dependence: Influence of varying initial concentration of cysteine was examined under pH 7.4 and in condition of no added buffer. Rate of reaction increased with increasing initial cysteine concentration as seen in Figures 6-8a and b. Reactions rates were faster at pH 7.4 than no added buffer conditions.
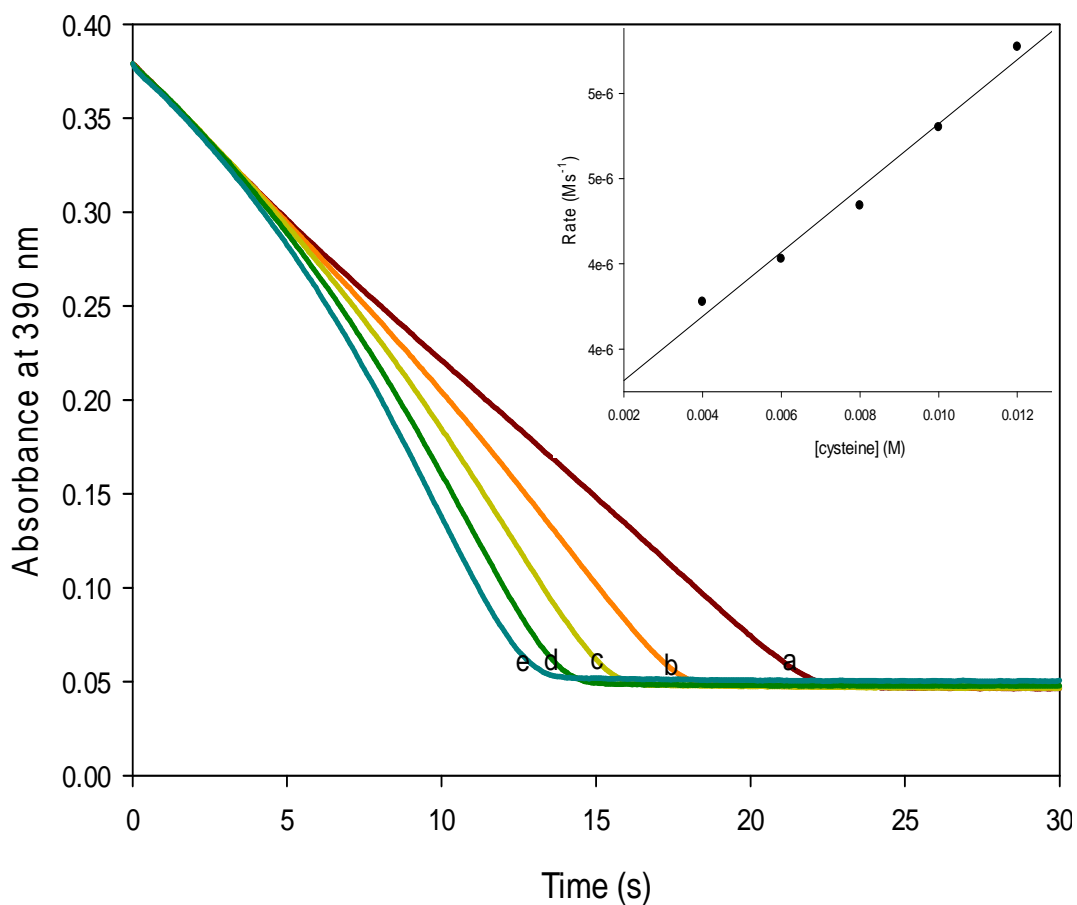
Figure 6-8a: *Effect of changing initial concentrations of cysteine on NAMI-A-cysteine reaction at pH 7.4. [NAMI-A]$_o$ = 1.0 x 10^{-4} M; [Cysteine]$_o$ = (a) 4.0 x 10^{-3} M (b) 6.0 x 10^{-3} M (c)8.0 x 10^{-3} M (d) 1.0 x 10^{-2} M (e) 1.2 x 10^{-2} M. Inset: Plot of initial rate deduced from cysteine dependence conferring a linear dependence on cysteine.*

Documented stability of NAMI-A at lower pH should be considered responsible for this observation.[84;245] Difference is only expected in rates under the two conditions.
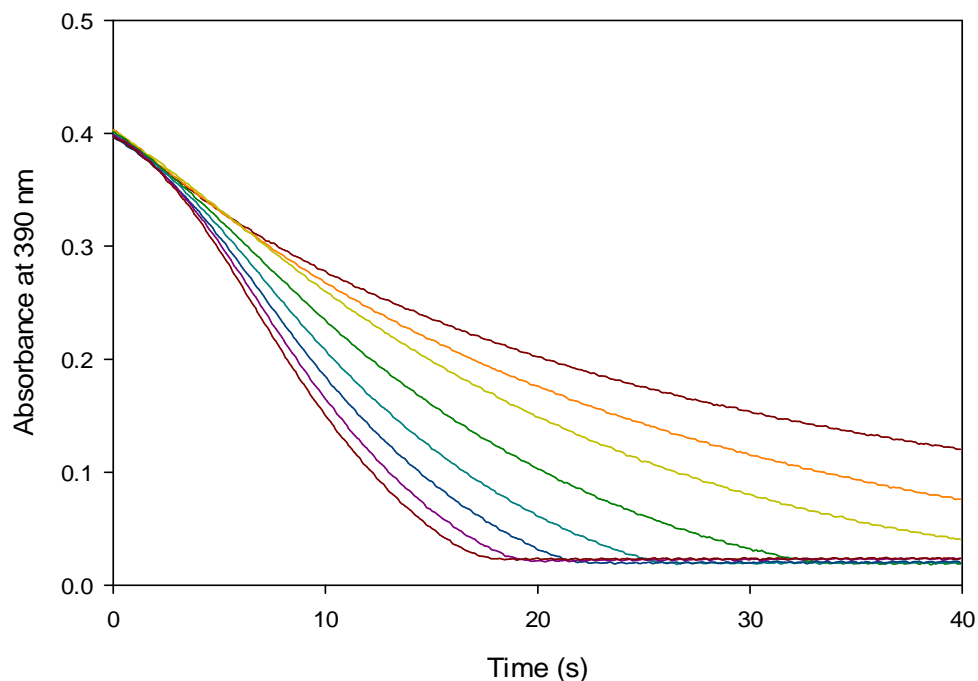
Figure 6-8b: *Effect of changing initial concentrations of cysteine on NAMI-A-cysteine reaction under same reaction conditions with Figure 6-8a except for the absence of buffer.*

6.2.2.3 Effect of ionic strength: Reaction rate is often affected by ions of reactants. This is corrected for by maintaining constant ionic strength, however, the effect of ionic strength can be isolated by varying amounts of an added inert salt. With reactant concentrations and other reaction conditions maintained constant, response of cysteine-NAMI-A reaction was evaluated. A positive salt effect was observed, see Figure 6-9. This is suggestive of involvement of similarly charged ions in the rate limiting step.

102
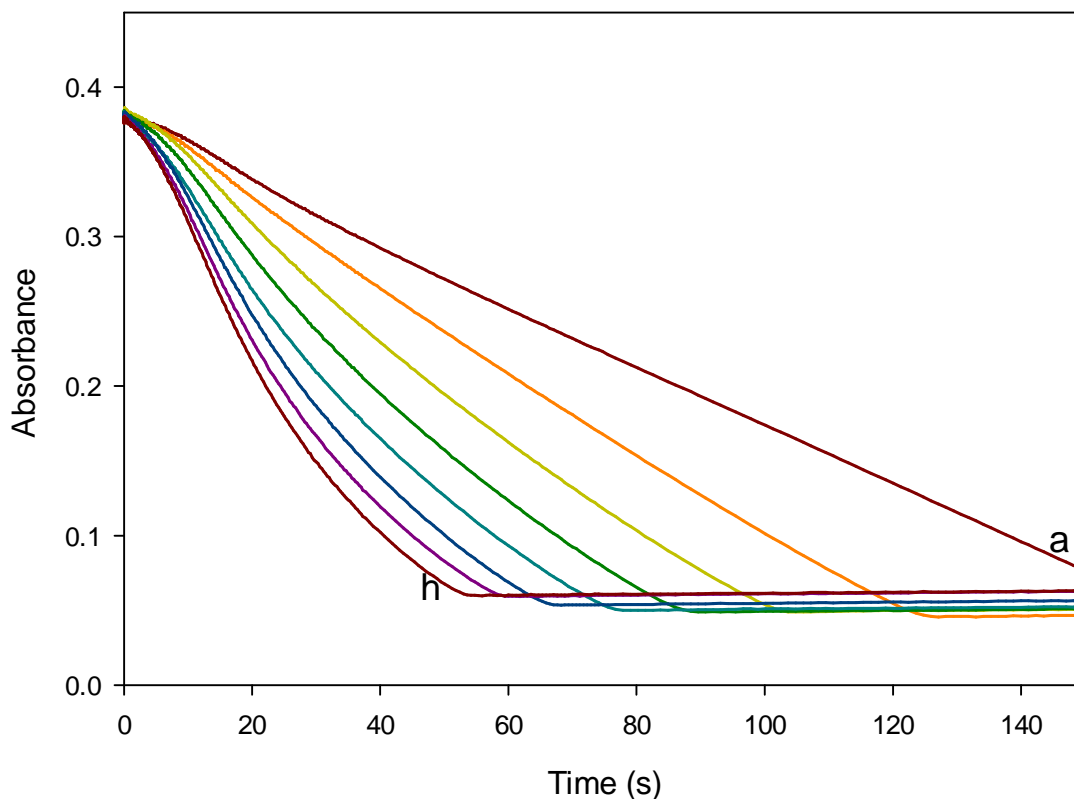
Figure 6-9: *Effect of changing ionic strength on NAMI-A-cysteine reaction. [NAMI-A]$_o$ = 1.0 x 10^{-4} M; [Cysteine]$_o$ = 4.0 x 10^{-3} M; Ionic strength maintained by addition of NaClO$_4$= (a) no added NaClO$_4$ (b) 0.1 M (c) 0.2 M (d) 0.3 M (e) 0.4 M (f) 0.5 M (g) 0.6 M (h) 0.7 M. Reaction rate increased with increasing ionic strength.*

6.2.2.4 Thermodynamic and activation parameters: Effect of varying temperature was evaluated under conditions of constant ionic strength, substrate and oxidant concentrations and pH of 7.4 (phosphate). Reaction rate increased with increasing temperatures as expected (see Figure 6-10a). The data obtained were used to construct an Arrhenius plot (see Figure 6-10b). Activation parameters calculated from this Arrhenius plot at 25 °C are: entropy of activation, $\Delta S^{\neq}$ = -200.6 J K^{-1} mol^{-1}, enthalpy of

103

activation, $\Delta H^{\neq} = 19.0$ kJ mol^{-1} and free energy of activation as $\Delta G^{\neq} = 78.8$ kJ mol^{-1}. These parameters are indicative of an associative mechanism.
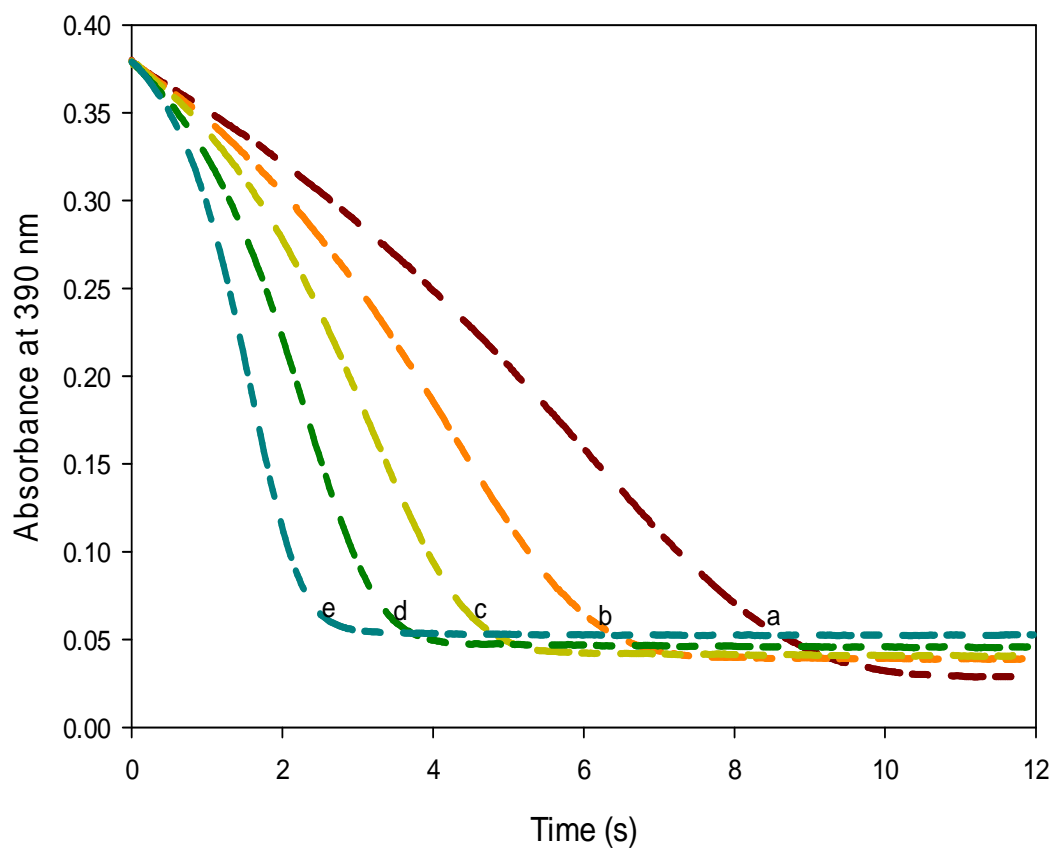
Figure 6-10a: *Temperature dependence of cysteine-NAMI-A reaction. Increase in rate observed with temperature increase. [Cysteine]$_o$ = 5.0 x 10^{-2}M; [NAMI-A]$_o$ = 1.0 x 10^{-4}M; Temp = (a) 10° C (b) 15° C (c) 20° C (d) 25° C (e) 37° C*
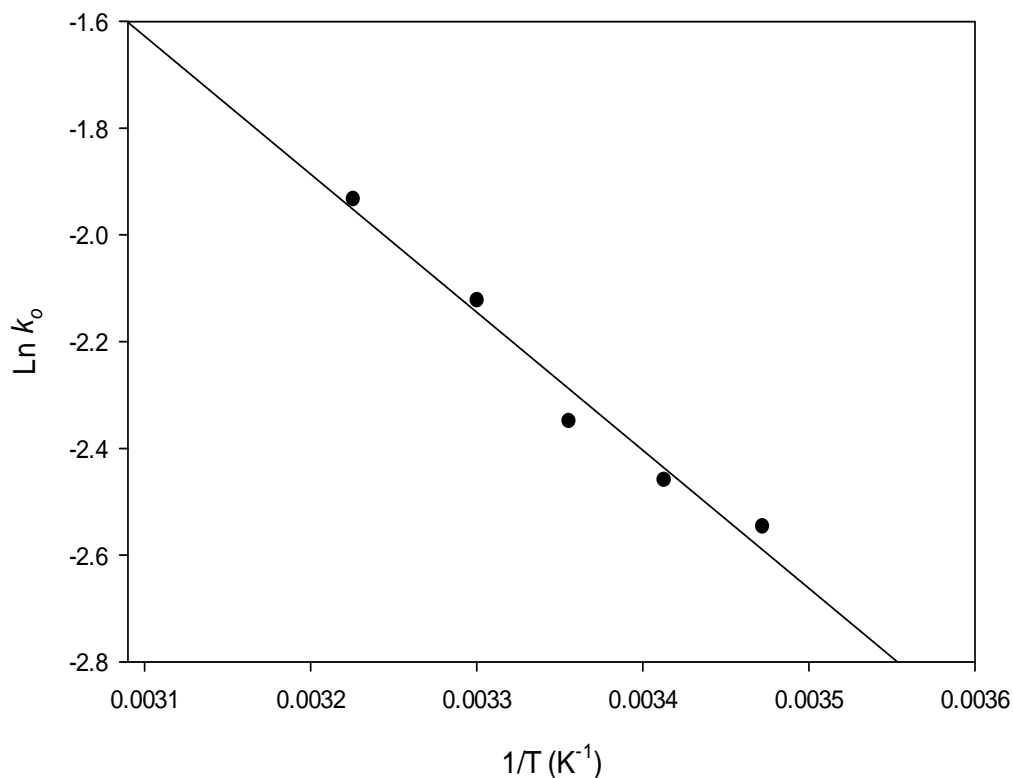
Figure 6-10b: *Arrhenius plot extracted from study of effect of temperature (Figure 5-8a) for determination of activation parameters.*

6.3 Mechanism

6.3.1 Electron Transfer: Considering the pKas for cysteine ionization,[221] a solution buffered at pH 7.4 will have cysteine ionized as represented in R2 and R3 where $H_2OC(NH_2)CHCH_2SH$ is cysteine. Some thiolate form will also exist in solution although in low concentration compared to the zwitter ionic form as represented by R4.

$$HO_2C(NH_2)CHCH_2SH \; \rightleftharpoons \; {}^-O_2C(NH_2)CHCH_2SH \;\; + \;\; H^+ \qquad K_{a1} \quad R2$$

$$^-O_2C(NH_2)CHCH_2SH \;\; + \;\; H^+ \; \rightleftharpoons \; {}^-O_2C({}^+NH_3)CHCH_2SH \qquad K_b \quad R3$$

$$^-O_2C(^+NH_3)CHCH_2SH \rightleftharpoons {}^-O_2C(^+NH_3)CHCH_2S^- + H^+ \qquad K_{a2} \qquad R4$$
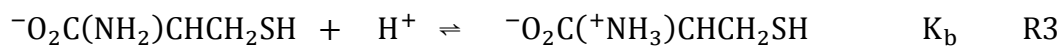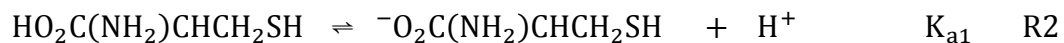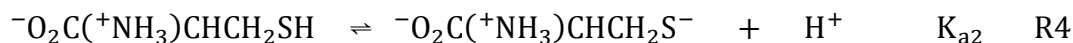
Zwitter ionic cysteine is expected to be the predominant species in solution. All of the different cysteine forms will react with NAMI-A to form products through a more ordered transition state, see R5 – R10.

$$^-O_2C(NH_2)CHCH_2SH + [ImRuCl_4DMSO]^- \rightarrow$$
$$[^-O_2C(NH_2)CHCH_2SH\ldots[ImRuCl_4DMSO]^-]^{\neq} \qquad k_1 \qquad R5$$

$$^-O_2C(^+NH_3)CHCH_2SH + [ImRuCl_4DMSO]^- \rightarrow$$
$$[^-O_2C(^+NH_3)CHCH_2SH\ldots[ImRuCl_4DMSO]^-]^{\neq} \qquad k_2 \qquad R6$$

$$^-O_2C(^+NH_3)CHCH_2S^- + [ImRuCl_4DMSO]^- \rightarrow$$
$$[^-O_2C(^+NH_3)CHCH_2S^-\ldots[ImRuCl_4DMSO]^-]^{\neq} \qquad k_3 \qquad R7$$

$$2[^-O_2C(NH_2)CHCH_2SH\ldots[ImRuCl_4DMSO]^-]^{\neq} \rightarrow$$
$$HO_2C(NH_2)CHCH_2SSCH_2CH(NH_2)CO_2H + 2[ImRuCl_4DMSO]^{2-} \qquad k_4 \qquad R8$$

$$2[^-O_2C(^+NH_3)CHCH_2SH\ldots[ImRuCl_4DMSO]^-]^{\neq} \rightarrow$$
$$HO_2C(NH_2)CHCH_2SSCH_2CH(NH_2)CO_2H + 2[ImRuCl_4DMSO]^{2-} + 2H^+ \qquad k_5 \quad R9$$

106

$$2[^-O_2C(^+NH_3)CHCH_2S^- \dots [ImRuCl_4DMSO]^-]^{\neq} \rightarrow$$

$$HO_2C(NH_2)CHCH_2SSCH_2CH(NH_2)CO_2H \ + \ 2[ImRuCl_4DMSO]^{2-} \qquad k_6 \quad R10$$

Describing the reaction rate, υ, in terms of disappearance of NAMI-A;

$$\upsilon = [ImRuCl_4DMSO]^- (k_1[^-O_2C(NH_2)CHCH_2SH] + k_2[^-O_2C(^+NH_3)CHCH_2SH] +$$

$$k_3 {}^-O_2C \ {}^+NH_3CHCH_2S^- \qquad\qquad E1$$

Results obtained from ionic strength effects demonstrate that species of similar charges are involved in the rate limiting step, thus indicating that k_2, involving the zwitter ionic cysteine does not contribute significantly to the rate ($k_2 \gg k_1, k_3$). Including k_2 anyway, results in a rate that is linearly dependent on [H$^+$] which contradicts observation of reduced rate at lower pH. E1, therefore, reduces to

$$\upsilon = [ImRuCl_4DMSO]^- (k_1[^-O_2C(NH_2)CHCH_2SH] + k_3[^-O_2C(^+NH_3)CHCH_2S^-] \quad E2$$

E2 can be expressed in terms of initial cysteine concentration, [H$_2$OC(NH$_2$)CHCH$_2$SH]$_o$ which is distributed between [$^-$O$_2$C(NH$_2$)CHCH$_2$SH], [$^-$O$_2$C($^+$NH$_3$)CHCH$_2$SH] and [$^-$O$_2$C($^+$NH$_3$)CHCH$_2$S$^-$];

$$\upsilon = [H_2OC(NH_2)CHCH_2SH]_o[ImRuCl_4DMSO]^- \left(\frac{Kak_1}{[H^+]} + Ka_2K_bk_3 \right) \qquad E3$$

107

which in conditions of overwhelming excess of MESNA can be written as

$$\text{Rate} \quad = \quad k_o[\text{ImRuCl}_4\text{DMSO}]^- \qquad\qquad\qquad \text{E4}$$

where

$$k_o \quad = \quad [\text{HO}_2\text{C(NH}_2)\text{CHCH}_2\text{SH}]_o \left(\frac{Kak_1}{[\text{H}^+]} + Ka_2K_bk_3 \right) \qquad\qquad \text{E5}$$

6.3.2 Ligand Exchange: Series of ligand substitution reactions are expected to occur especially following formation of the labile NAMI-A dianion, $[\text{ImRuCl}_4\text{dmso}]^{2-}$. Reactions R11 and R12 describe ligand exchange for supported by ESI-MS results (Figures 6-4a and b) for the loss of imidazole and dimethyl sulfoxide ligands with exchange of two chloride ligands.

$$[\text{ImRuCl}_4\text{DMSO}]^{2-} + 2\text{H}_2\text{O} \rightarrow [\text{ImRuCl}_2(\text{H}_2\text{O})_2\text{DMSO}] + 2\text{Cl}^- \qquad \text{R11}$$

$$[\text{ImRuCl}_2(\text{H}_2\text{O})_2\text{DMSO}] \qquad \rightarrow \quad [\text{RuCl}_2(\text{H}_2\text{O})_2] + \text{Im} + \text{DMSO} \qquad \text{R12}$$
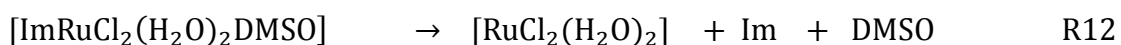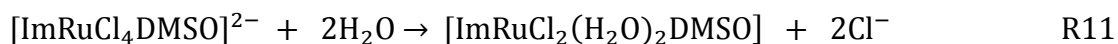
Greater reactivity of $[\text{ImRuCl}_4\text{dmso}]^{2-}$ is an indication that R11 and R12 are fast and would not influence the rate determining step. The overall reaction is summarized in Figure 6-11. H, $[\text{RuCl}_2(\text{H}_2\text{O})_2]$, attempts structural arrangement of the aquated product. Substitution could be on any two of the Cl⁻ ligands, depending on activation enthalpy and free energy of the different configurations. Higher calculated energy values have

been reported for second aquation step of NAMI-A leading to a trans configuration.[279;280]
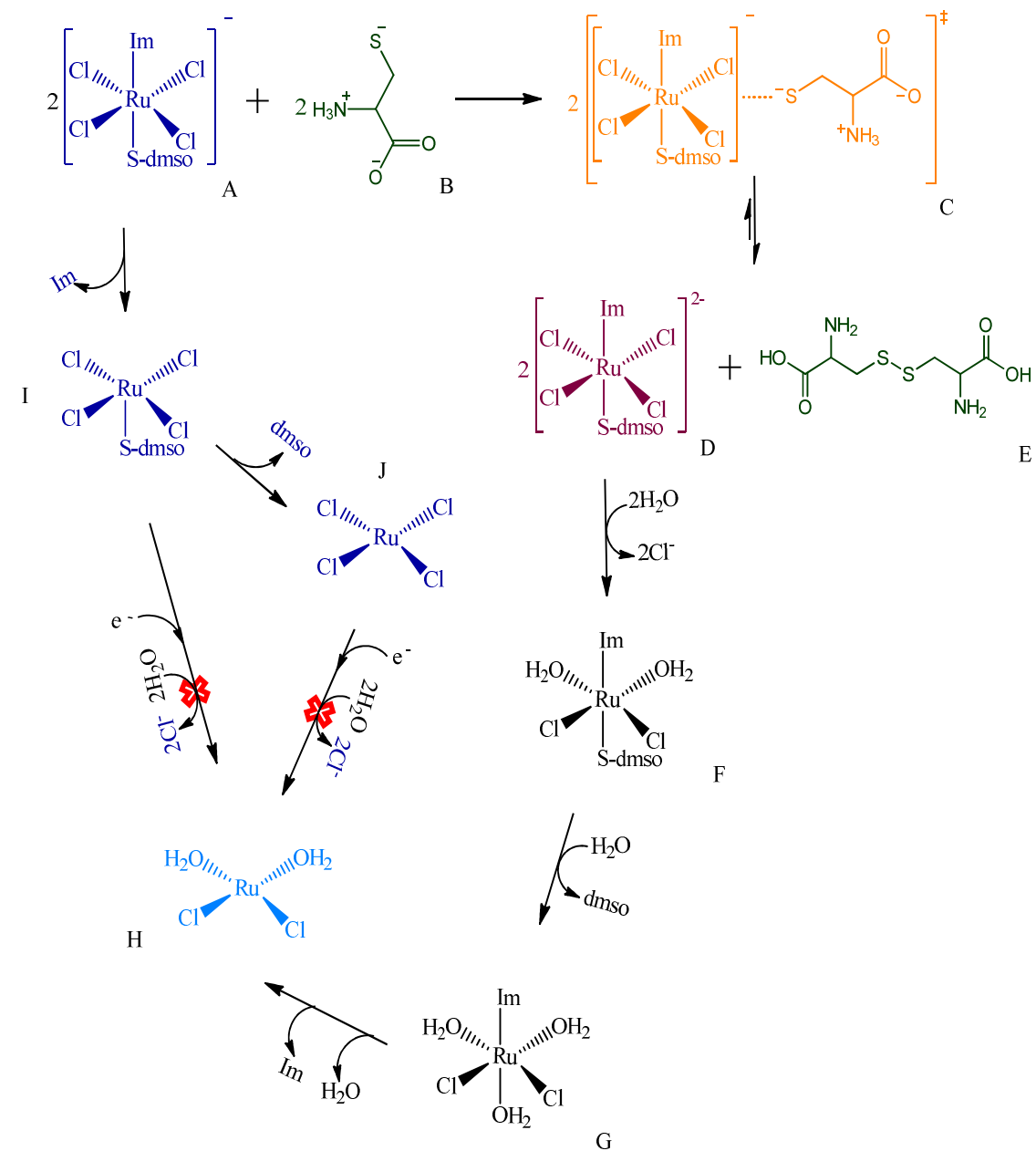
Scheme 6-1: *Proposed mechanism for the reduction of NAMI-A by cysteine and subsequent hydrolysis.*

Orders of magnitude lower rate constants than obtained in this study have been reported for experimental and theoretical hydrolysis of NAMI-A.[245 281;282] This is in support of our proposed formation of aquated product through reduced NAMI-A.
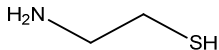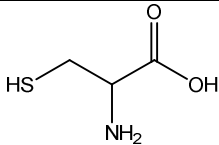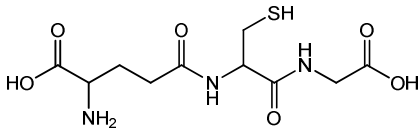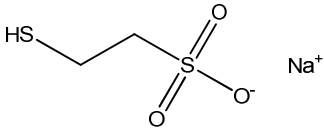
CHAPTER SEVEN

7.0   Summary and Conclusions

Decline in cancer mortality rates acknowledges improvements and advances in cancer treatment. For instance, surgical removal of primary tumors is becoming highly successful, however, afore-mentioned characteristics of metastasis warrant chemotherapy. Lack of effective therapeutics towards metastasis adequately maintain interest in drug candidates with antimetastatic potential such as NAMI-A. Studies of interactions of NAMI-A with bio-relevant molecules are of considerable interest due to the promising pharmacological benefits of this experimental drug in cancer therapy.

Solution chemistry of NAMI-A is quite interesting and this study has demonstrated that its interaction with biologically-relevant thiols can be as interesting and complex especially past the electron transfer process. Stoichiometry for the overall electron transfer reactions obtained in this study demonstrates a 1:1 ratio of oxidant to reductant which culminates in ligand exchange with water as described in chapters 3, 4 and 6. Initial reactions were centered on sulfur atoms of thiols investigated, there was no evidence for interactions on the nitrogen or oxygen atoms. In all cases, reactions were dependent on NAMI-A to the first order. There was no clear evidence for binding of thiol to NAMI-A or any of the aquated species observed, though, our results demonstrate complex interactions with respect to cysteamine and GSH. Formation and identification of such species could be determined using time dependent NMR and LC-MS. Further clarification of origin of $[RuCl_2(H_2O)_2]$ species could be done using a Q-band EPR which will show some signal for Ru^{3+} but would be EPR silent for Ru^{2+}.

111

Results of kinetics analysis of reactions of NAMI-A with select thiols yields effective rate constant, k_o, which are reported in Table 7-1 for the purpose of comparison.

Thiol	Structure	S-H pKa	Pseudo first-order rate constant, k_o/s^{-1}
Cysteamine		8.27[a]	$6.85 \pm 0.3 \times 10^{-1}$
Cysteine		8.7[a]	$9.40 \pm 0.5 \times 10^{-2}$
GSH		8.75[a]	$7.42 \pm 0.4 \times 10^{-3}$
MESNA		9.2[b]	$3.63 \pm 0.3 \times 10^{-2}$

Table 7-1: *Comparison of observed rate constants in relation to thiol pKa. [a] S-H pKa adapted from Handbook of Chemistry and Physics.*[221]   *[b] 283;284*

GSH exhibits the lowest rate determined, an explanation might be drawn from its molecular structure where the thiol might not be necessarily accessible due to steric

hindrance compared to other thiols studied. Also, the simple molecular structure of cysteamine might account for the observed high reactivity. This is not surprising since similar trends have been observed for kinetics analysis of reactions of GSH, MESNA and WR-1065 with metabolites of cyclophosphamide (4-hydroperoxycyclophosphamide and acrolein).[285] 4-hydroperoxycyclophosphamide and acrolein have high reactivity towards MESNA and GSH than NAMI-A on the basis of reported rate constants[285] which are orders of magnitude higher than those obtained in this study. A clinical indication of comparing our results with those obtained for 4-hydroperoxycyclophosphamide and acrolein is that NAMI-A could not compete with these metabolites for the studied thiols provided rate constants are similar within and outside the cell.

A negative correlation of k_o with thiol pKa was observed. Higher pKa corresponds to lower reaction rate with NAMI-A except for MESNA. Thiol with the lowest pKa should have higher amount of deprotonated sulfhydryl group (thiolate anion) and thus reacts faster at physiological pH 7.4. A Brønsted plot derived from data presented in Table 7-1 shows linearity as seen in Figure 7-1. Brønsted equation is log k_o = -1.4pKa + 11. The plot demonstrates a positive slope when molecular weights of the thiols were factored in i.e. plot of log (MW/k_o) vs pKa linear with positive slope. This correlation is indicative of significant contribution of thiolate anions of the different thiols in their reactivity with NAMI-A. Similar observations have been made in the reactions of thiols with Cytochrome c, a heme protein.[286] WR-1065 has a lower pKa for thiol ionization of 7.7 and should have thiolate species up to 22 % at pH 7.4, one could

113

predict that WR-1065 will have a higher rate compared to cysteine, MESNA and GSH. In all, our results suggest that NAMI-A interactions with any of the thiols investigated should not interfere with the protective effect of amifostine or MESNA when used in a therapy regimen combining NAMI-A with any anticancer drug for which chemoprotection is necessary.
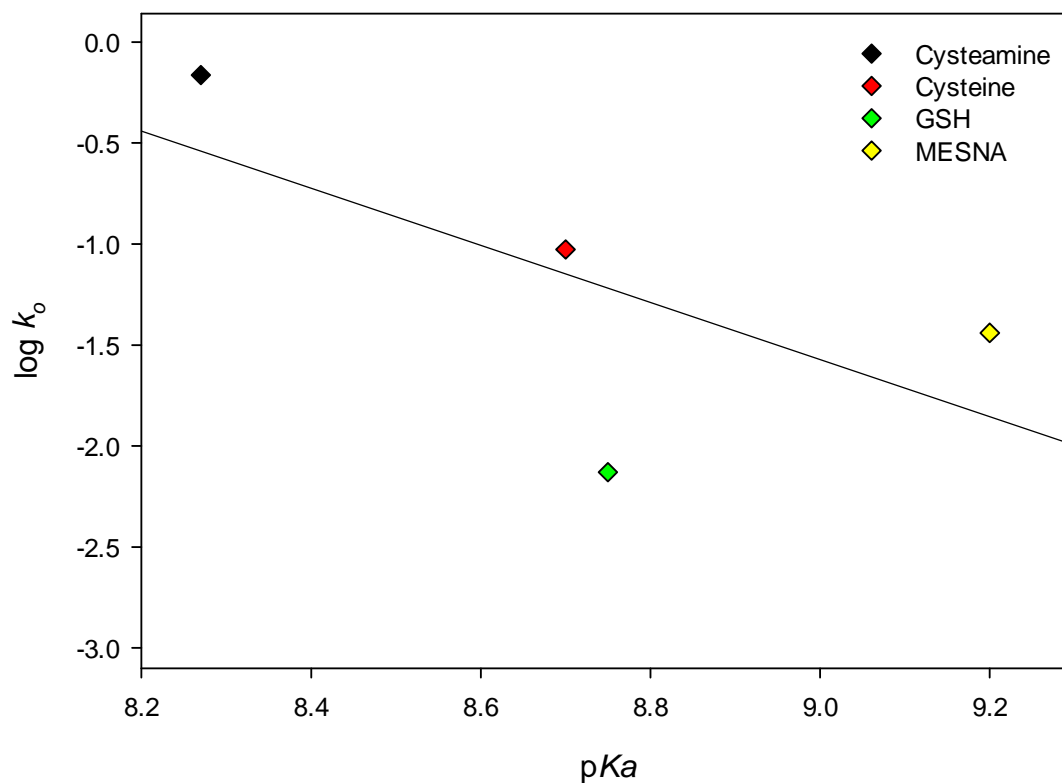
Figure 7-1: *Brønsted relationship for the reactivities of thiols towards NAMI-A. Linearity of this plot demonstrates significance of thiolate species in the reactions.*

All the reactions studied show positive temperature dependence. Positive low enthalpy of activation and distinctly negative entropy of activation (see Table 7-2)

determined in all of the reactions are indicative of organized transition state prior to product formation.

Thiol	$\Delta S^{\neq} / JK^{-1}mol^{-1}$	$\Delta H^{\neq} / kJmol^{-1}$	$\Delta G^{\neq} / kJmol^{-1}$
Cysteamine	-117	+41	+76
Cysteine	-200	+19	+79
MESNA	-175	+21	+73
GSH	-100	+55	+85

Table 7-2: *Activation parameters (at 25 ^{o}C) deduced from Arrhenius plot of Ln k_o against 1/T for thiols studied.*

Order of increasing free energy of activation of NAMI-A reaction with thiols in this study is MESNA < cysteamine < cysteine < GSH. This might explain the low rate constant obtained for GSH reaction. Higher than expected k_o, of 3.63 ± 0.3 x 10^{-2} s^{-1} obtained for the MESNA reaction (refer to Table 7-1) in comparison to others might be due to occupation of a lower energy space by its transition state complex.

Our results could help to understand the mechanism of interaction of NAMI-A with cellular thiols, proteins and enzymes containing cysteine residues in their active sites and thiol containing chemoprotectants. Antimetastatic effects of NAMI-A appear independent of route of administration but dependent on amount administered.[287] Mode of drug administration determines possible first contact. Intravenous NAMI-A

administration suggests interactions with biomolecules (especially in the plasma) might occur before interaction with DNA or other cellular targets yet to be identified and may proceed through similar mechanisms as those derived in this study. The use of MESNA should be particularly advantageous as interactions which precede ligand substitution should produce a more effective chemoprotectant, dimeric MESNA. The GSH-NAMI-A reaction is relatively slow compared to other thiols studied which might suggest minimal impact on cellular GSH especially in the presence of other cancer drugs which deplete GSH.

Reports attest to preferential binding of HSA to reduced NAMI-A,[288] and reduced antimetastatic activity of NAMI-A upon binding to albumin and transferrin.[93] Table 7-2 features results in literature of experimental and theoretical calculations for physiologically relevant interactions of NAMI-A.

	k_o/s^{-1}	$\Delta H^{\neq}$ / kJmol^{-1}	$\Delta G^{\neq}$ / kJmol^{-1}	Ref.
Aquation	$2.56 \times 10^{-4*a}$	-	-	281
	$5.17 \times 10^{-4*b}$	-	-	289
1st	$3.96 \times 10^{-6\#}$	$+101.5^{\#}$	$+103.7^{\#}$	279
2nd	-	$+118.7^{\#}$	$+125.0^{\#}$	279
Transferrin	$1.07 \times 10^{-3*b}$	-	-	289
Albumin	$2.77 \times 10^{-3*b}$	-	-	289

Table 7-3: *Observed rate constants and activation parameters reported by others for first/second aquation processes, transferrin and albumin binding constants. * Phosphate buffer pH 7.4, ^{a} at 25 ^{o}C, ^{b} at 37 ^{o}C, $^{\#}$ from density functional theory calculations.*

Results reported in this dissertation demonstrate that interactions of NAMI-A with biologically-active thiols are kinetically and thermodynamically favored and therefore might play significant roles in *in vivo* metabolism of NAMI-A.

CHAPTER EIGHT: SUPPLEMENTARY RESULTS

8.0 Kinetics and Mechanism of One-electron Oxidation of L-Cysteine by Tris(1,10-phenanthroline)iron(III) complex

8.1 Introduction: L-cysteine is the only sulfur contributor and the rate-limiting substrate in the biosynthesis of GSH.[290] 1,10-Phenanthroline ligand disturbs the proper functioning of a wide range of biological systems. In its metal-free state, it has been shown to have high inhibitory activity against *candida albicaans* and induced apoptosis in a yeast and mammalian cell line obtained from poorly differentiated carcinoma when complexed with metals.[291;292]Metal complexes are used to model biomolecules[293;294] and iron complexes in particular, have been used to model iron-porphyrin proteins[295;296] and active site of ribonucleotide reductase.[297] Some metal complexes of substituted 1,10-phenathroline have also shown antineoplastic activity with up to 50% growth inhibition of human cancer cells at concentrations of 10 to 100 times lower than cisplatin.[298] Structure-activity relationships have been established for metal complexes with anticancer activities.[289] In this study, tris(1,10-phenanthroline)iron(III) (see structure shown in Figure 8-1) is used as a model that offers a familiar metal to the physiological system and the octahedral structure of the antimetastatic prodrug of interest in an effort to establish mechanisms of interactions of the prodrug with biologically-active thiols.
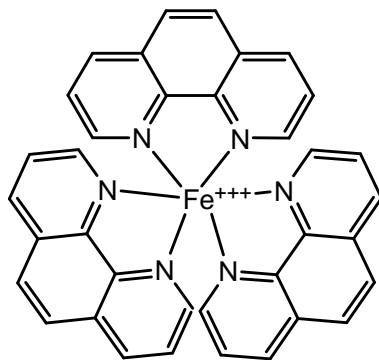
Figure 8-1 : *Tris(1,10-phenanthroline)iron(III)*

8.2   Materials

L-cysteine, sodium perchlorate ($NaClO_4$) and 1,10-phenanthroline monohydrate all with 99+% assays were purchased from Acros. Chlorine gas (Aldrich), sulfuric acid, perchloric acid (Fisher) and ferrous ammonium sulfate ($Fe(NH_4)_2(SO_4)_2$ (GFS) were all used without further purification. Solutions were prepared in distilled deionized water obtained from a Barnstead Corporation Nanopure water system.

Tris(1,10-phenanthroline)iron(III) perchlorate was prepared according to a published method.[299] A solution containing 0.3 g of $Fe(NH_4)_2(SO_4)_2.6H_2O$ (0.76 mmol), 0.6 g of 1,10-phenanthroline monohydrate and 0.2 mL of concentrated H_2SO_4 in 100 mL of water affords tris(1,10-phenathroline)iron(II) perchlorate. The iron(III) complex was prepared by oxidation of the iron(II) complex with chlorine gas. Chlorine gas was bubbled into this solution until the color changed from deep red to blue. 30% $NaClO_4$ was added to the mixture and then cooled in ice bath. Blue crystalline $Fe(phen)_3(ClO_4)_3$ was isolated by filtration and washed 3x with cold water. It was then dried in a desiccator. The blue iron(III) complex was recrystallized from aqueous

119

perchlorate solution and characterized spectrophotometrically. Stock solutions of the iron(III) complexes were freshly made in 2.0 M H_2SO_4.

8.3 Results and discussion

8.3.1 Stoichiometry and product identification

The stoichiometry of the reaction was found to be 1:1 with one mole of cysteine reacting with one mole of tris(1,10-phenanthroline)iron(III), $Fe(phen)_3^{3+}$, to form cystine (disulfide of cysteine) and tris(1,10-phenanthroline)iron(II), $Fe(phen)_3^{2+}$, as shown in stoichiometric reaction R1:

$$2RSH \ + \ 2Fe(phen)_3^{3+} \longrightarrow \quad RSSR \ + \ 2Fe(phen)_3^{2+} \ + \ 2H^+ \quad R1$$

Figure 3.3 shows the spectral changes observed from a solution of cysteine and $Fe(phen)_3^{3+}$ scanned at 30 second intervals. The absorbance at 350 nm (λ_{max} for $Fe(phen)_3^{3+}$) decreased as the reaction progressed showing conversion of $Fe(phen)_3^{3+}$ to $Fe(phen)_3^{2+}$. The absorption at 510 nm increases as the reaction progressed to a final absorbance at completion of reaction. The absorbance at 510 nm corresponds to $Fe(phen)_3^{2+}$ produced. The characteristic absorption at 510 nm of $Fe(phen)_3^{2+}$ as shown in Figure 8-2 gives spectrophotometric evidence for our product. The observation of an isobestic point suggests there are no intermediates of kinetic significance during this oxidation and the only absorbing species in this region are $Fe(phen)_3^{2+}$ and $Fe(phen)_3^{2+}$.
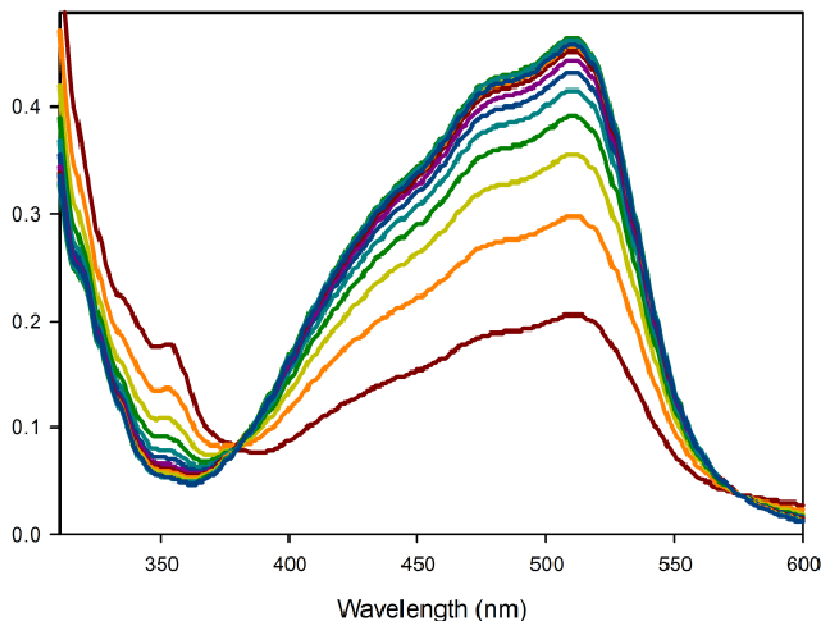
Figure 8-2: *Rapid spectral scan of solution of cysteine and Fe(phen)$_3^{3+}$ taken at 30 s interval. [Cysteine]$_o$ = 2.0 x 10^{-5} M; [Fe(phen)$_3^{3+}$]$_o$ = 5.0 x 10^{-5} M; [H$^+$]$_o$ = 0.5 M*

A full electro-spray ionization mass spectrum of stoichiometric solution was taken in the positive mode (Figure 8-3), showing m/z 241 and 298 for cysteine and Fe(phen)$_3^{2+}$ respectively. The observed peak for Fe(phen)$_3^{2+}$ is [M+H]$^+$, taking into account the molecular weight of 596.27 g/mol and the +2 charge.
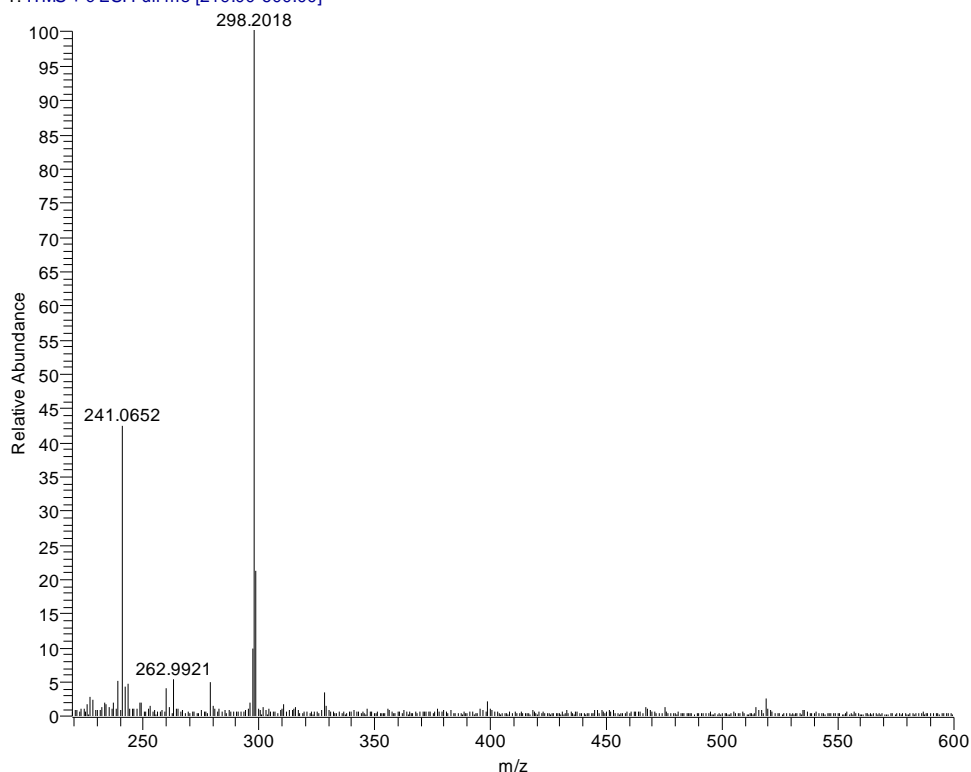
Figure 8-3: *Positive ESI-MS spectrum of the reaction products of a stoichiometric solution of cysteine and Fe(phen)$_3^{3+}$ in 50/50 methanol-water.*

8.3.2 Effect of [Fe(phen)$_3^{3+}$] on rate of reaction

Kinetics of reaction were carried out under pseudo-first order conditions of excess cysteine. At constant temperature, ionic strength and concentration of cysteine as well as initial acid concentrations, effect of Fe(phen)$_3^{3+}$ on rate of reaction was isolated at its wavelength of maximum absorption, 350 nm (see Figure 8-4a.). The rate of consumption of Fe(phen)$_3^{3+}$ increases with increasing initial Fe(phen)$_3^{3+}$ concentrations. The plot of initial rate against initial Fe(phen)$_3^{3+}$ concentrations is linear, Figure 8-4b; clearly suggesting a first-order dependence in Fe(phen)$_3^{3+}$.

122
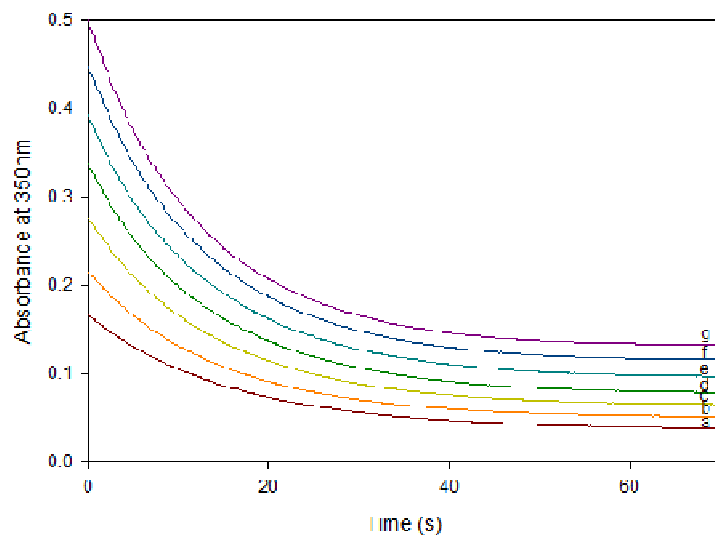
Figure 8-4a: *Kinetic traces showing the on $Fe(phen)_3^{3+}$ at its λ_{max}. [Cysteine]$_o$ = 2.0 x 10^{-3}M; [H$^+$]$_o$ = 0.5 M; [Fe(phen)$_3^{3+}$]$_o$ = (a) 3.0 x 10^{-5} M (b) 4.0 x 10^{-5} M (c) 5.0 x 10^{-5} M (d) 6.0 x 10^{-5} M (e) 7.0 x 10^{-5} M (f) 8.0 x 10^{-5} M (g) 9.0 x 10^{-5} M*

$Fe(phen)_3^{2+}$ has maximum absorption at 510 nm, and the effect of varying initial concentrations of $Fe(phen)_3^{2+}$ on the reaction was also examined at this wavelength (Figure 8-4c). The rate of formation of $Fe(phen)_3^{2+}$ increased with increasing initial $Fe(phen)_3^{3+}$ concentrations. The plot of initial rates against initial $Fe(phen)_3^{3+}$ concentration gave a straight line with intercept kinetically indistinguishable from zero. This affirms the results obtained at 350 nm observation wavelength. A pseudo-first-order rate constant of 1.43 x 10^{-2} s^{-1} was deduced.
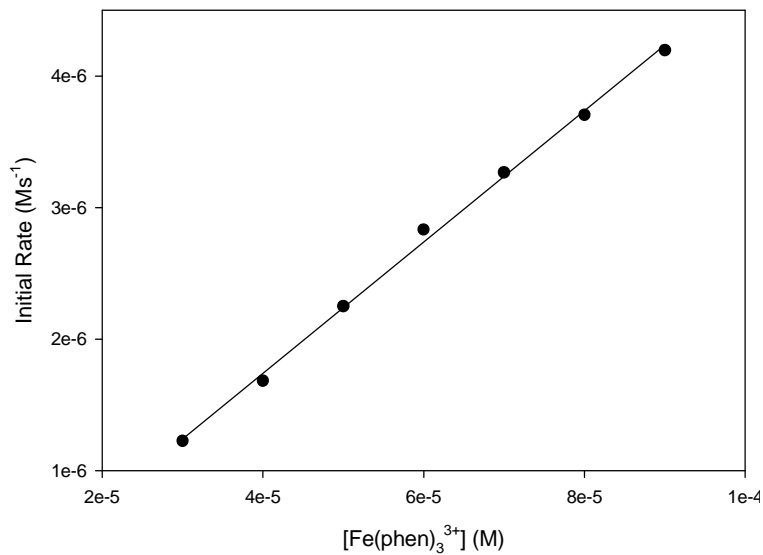
Figure 8-4b: *Initial rate plot derived from Figure 8-4a, showing linear dependence on* Fe(phen)$_3$$^{3+}$.

Figure 8-4c: *Effect of [Fe(phen)$_3$ $^{3+}$] variation on the formation of Fe(phen)$_3$ $^{2+}$ at 510 nm. [Cysteine]$_o$ = 2.0 x 10^{-3} M; [H$^+$]$_o$ = 0.5 M; [Fe(phen)$_3$ $^{3+}$]$_o$ = (a) 1.0 x 10^{-5} M through (h) 8.0 x 10^{-5} M*

124

8.3.3 Effect of cysteine on reaction rate: The effect of cysteine on its oxidation by Fe(phen)$_3$ $^{3+}$ was monitored at 350 nm and 510 nm Figure 8-5, summarizes this effect. The rate of consumption of Fe(phen)$_3$ $^{3+}$ (dashed lines) increased with increased concentrations of cysteine. The same trend was observed when monitoring the rate of formation of Fe(phen)$_3^{2+}$ at 510 nm (solid lines). Initial rate plots deduced from Figure S-5 show linear-order dependence but with saturation.

Figure 8-5: *The dashed lines show consumption of the oxidant, Fe(phen)$_3$ $^{3+}$ at 350 nm and the solid lines show formation of Fe(phen)$_3^{2+}$ at 510 nm. In both cases rate was increased with cysteine.*

8.3.4 Effect of acid on reaction rate: While other reaction conditions were kept constant, the dependence of reaction on initial acid concentrations was evaluated. Figure 8-6 summarizes the effect of acid variation on both the rate of consumption of

oxidant at 350 nm and the rate of formation of the reduced complex at 510 nm. The range of possible variations with respect to initial acid concentrations is limited since the stock $Fe(phen)_3{}^{3+}$ solution was made in 2.0 M acid. This was to prevent the aquation of $Fe(phen)_3{}^{3+}$ into the undetermined khaki colored polymeric hydroxo complexes.[300] The observation is that acid has an inhibitory effect on the reaction as the rate of product formation decreases with increase in acid concentrations. Both initial rates show inverse acid dependence.

Figure 8-6: *Evaluation of effect of initial acid concentrations. An inverse acid dependence observed on the rate of formation $Fe(phen)_3{}^{2+}$ (510 nm) and consumption of $Fe(phen)_3{}^{3+}$ (350)nm. $[Fe(phen)_3{}^{3+}]_o = 5.0 \times 10^{-3}$ M; $[Cysteine]_o = 5.0 \times 10^{-3}$ M; $[H^+]_o =$ (a) 0.30 M; (b) 0.40 M; (c) 0.50 M; (d) 0.60 M.*

8.3.5 Effect of ionic strength: The response of the present reaction to changes in concentration of an inert salt, at constant temperature and reactants concentrations, was examined (Figure 8-7). Increasing ionic strength decreased the rate of reaction. This might suggest that the rate determining step(s) contain species of different charges.

Figure 8-7: *Evaluation of effect of ionic strength. $[Cysteine]_o = 2.0 \times 10^{-3}M$; $[Fe(phen)_3{}^{3+}]_o = 5.0 \times 10^{-5} M$; $[H^+]_o = 0.5 M$; $[\mu]_{NaClO4} = (a) 0.4 M (b) 0.6 M (c) 0.8 M (d) 1.0 M (e) 1.2 M (f) 1.4 M (g) 1.6 M (h) 1.8 M (i) 2.0 M.*

8.3.6 Thermodynamic and activation parameters: At constant ionic strength, acid and concentrations of oxidant and substrate, the effect of temperature on the reaction was evaluated. Reaction rate increased proportionally with increasing temperatures as expected (see Figure 8-8a). The obtained kinetics data were used to construct an Arrhenius plot (see Figure 8-8b).

127

Figure 8-8a: *Temperature dependence of cysteine-ferriin reaction. Increase in rate observed with temperature increase. $[Cysteine]_o = 2.0 \times 10^{-3}M$; $[Fe(phen)_3{}^{3+}]_o = 5.0 \times 10^{-5}M$; $[H^+]_o = 0.5\ M$; Temperature in increament of 5 ^oC from 10 through 30 ^oC.*

Figure 8-8b: *Arrhenius plot extracted from study of effect of temperature variation on the reaction for determination of activation parameters.*

The Arrhenius plot afforded these activation parameters: entropy of activation, $\Delta S^{\neq} = -217.02 \pm 0.03$ J K^{-1} mol^{-1}, enthalpy of activation, $\Delta H^{\neq} = 35.85 \pm 0.38$ kJ mol^{-1} and free energy of activation as $\Delta G^{\neq} = 100.52$ kJ mol^{-1}. The distinctly negative entropy of activation suggests some degree of molecular ordering in the rate determining step. This is indicative of an associative mechanism.

8.3.7 Mechanism

The results obtained have allowed us to propose stepwise reactions involved in the oxidation of L-cysteine by $Fe(phen)_3^{3+}$. Reactions were carried out in acidic medium, therefore, cysteine (RSH) exists mostly in the protonated form as shown in R2.

$$RSH \quad + \quad H^+ \quad \rightleftharpoons \quad RSH_2^+ \qquad K_b \qquad R2$$

Unprotonated cysteine also exists but to a lesser extent in the reaction. Both protonated and unprotonated cysteine can react with $Fe(phen)_3^{3+}$ to associative complex (R3 and R4). This is supported by the thermodynamic parameters obtained from Figures 8-8a and b. The activated complexes formed in R3 and R4 then proceed to form products as shown in R5. Contribution from intermediate complex formed by R4 would be minimal since unprotonated cysteine concentrations are negligible

$$RSH \quad + \quad Fe(phen)_3^{3+} \quad \rightleftharpoons \quad (Fe(phen)_3^{3+}.RSH) \qquad k_1, k_{-1} \qquad R3$$

$$RSH_2^+ \quad + \quad Fe(phen)_3^{3+} \quad \rightleftharpoons \quad (Fe(phen)_3^{3+}.RSH_2^+) \quad k_1, k_{-1} \qquad R4$$

$(Fe(phen)_3^{3+}.RSH)$

$$RSSR \quad + \quad 2Fe(phen)_3^{2+} \quad + \quad 2H^+ \quad R5$$

$(Fe(phen)_3^{3+}.RSH_2^+)$

Following the disappearance of $Fe(phen)_3^{3+}$ the rate of reaction can be written as:

$$\frac{-d[Fe(phen)_3^{3+}]}{dt} \quad = \quad k_1[Fe(phen)_3^{3+}][RSH] \quad + \quad k_2[Fe(phen)_3^{3+}][RSH_2^+]$$

From R2, the concentration of protonated cysteine can be written as

$$[RSH_2^+] \quad = \quad K_b[RSH][H^+]$$

The concentrations of all cysteine species are derived from initial cysteine concentration, therefore,

$$[RSH]_o \quad = \quad [RSH] \quad + \quad [RSH_2^+]$$

Substituting for $[RSH_2^+]$ in equation

$$[RSH] \quad = \quad \frac{[RSH]_o}{1 + K_b[H^+]}$$

The rate then becomes:

$$\text{Rate} = \frac{k_1 + K_b k_2 [H^+]}{1 + K_b [H^+]} \{[RSH]_o [Fe(phen)_3^{3+}]\}$$

There is a first-order dependence on $Fe(phen)_3^{3+}$ and cysteine as demonstrated by Figures 8-4a – c and Figure 8-5 respectively. This rate shows a complex dependence on acid concentration. Figure 8-6 demonstrates inhibitory effect of acid on the reaction. At low acid concentrations, rate would be first-order in acid but in high acid concentrations, however, the reaction saturates as observed in Figure 8-6. An explanation for retardation by acid is that high acid concentration increasingly stabilizes $Fe(phen)_3^{3+}$, making it react more slowly. The rate law can then be simplified to

$$\text{Rate} = k_o [RSH]_o [Fe(phen)_3^{3+}]$$

where

$$k_o = \frac{k_1 + K_b k_2 [H^+]}{1 + K_b [H^+]}$$
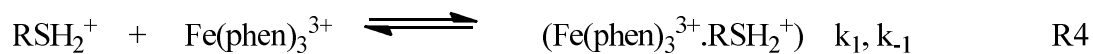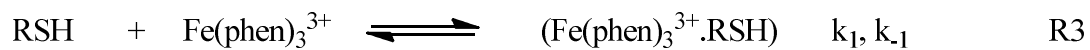
The bimolecular rate constant for the reaction was 7.15 $M^{-1}s^{-1}$. The thermodynamic parameters obtained indicate formation of associative intermediate prior to product formation. Saturation in cysteine dependence can may be due to sequestering

of cysteine by $Fe(phen)_3^{3+}$ to form an initial complex which does not contribute significantly to the product.

REFERENCES

1. Lehninger, A. L. *Physiological Reviews* **1950**, *30*, 393.

2. Lao, T. T.; Ho, L. F. *Diabetes Care* **2004**, *27*, 650-656.

3. Mackenzie, G. G.; Zago, M. P.; Aimo, L.; Oteiza, P. I. *Iubmb Life* **2007**, *59*, 299-307.

4. Olin, K.; Oteiza, P. I.; Keen, C. L. *Faseb Journal* **1994**, *8*, A716.

5. Oteiza, P. I. *Free Radical Research* **2006**, *40*, S41.

6. Pietrangelo, A. *American Journal of Physiology- Gastrointestinal and Liver Physiology* **2002**, *282*, 403-414.

7. Manunza, B.; Deiana, S.; Pintore, M.; Solinas, V.; Gessa, C. *Journal of Molecular Structure: THEOCHEM* **1997**, *419*, 33-36.

8. Lee, W. T.; Leung, S. S.; Leung, D. M.; Cheng, J. C. *American Journal of Clinical Nutrition* **1996**, *64*, 71-77.

9. Lloyd, R. V.; Hanna, P. M.; Mason, R. P. *Free Radical Biology and Medicine* **1997**, *22*, 885-888.

10. Crichton, R. R.; Ward, R. J. *Biochemistry* **1992**, *31*, 11255-11264.

11. Smith, M. A.; Harris, P. L. R.; Sayre, L. M.; Perry, G. *Proceedings of the National Academy of Sciences of the United States of America* **1997**, *94*, 9866-9868.

12. Weinberg, E. D. *Oxidative Medicine and Cellular Longevity* **2009**, *2*, 107-109.

13. Ryan, T. P.; Aust, S. D. *Critical Reviews in Toxicology* **1992**, *22*, 119-141.

14. Fraga, C. G.; Oteiza, P. I. *Toxicology* **2002**, *180*, 23-32.

15. Berg, D.; Gerlach, M.; Youdim, M. B. H.; Double, K. L.; Zecca, L.; Riederer, P.; Becker, G. *Journal of Neurochemistry* **2001**, *79*, 225-236.

16. Ho, E. *The Journal of nutritional biochemistry* **2004**, *15*, 572-578.

17. Pearson, M. A.; Michel, L. O.; Hausinger, R. P.; Karplus, P. A. *Biochemistry* **1997**, *36*, 8164-8172.

18. Koehntop, K. D.; Emerson, J. P.; Que, L. *Journal of Biological Inorganic Chemistry* **2005**, *10*, 87-93.

19. David, S. S.; Meggers, E. *Current Opinion in Chemical Biology* **2008**, *12*, 194.

20. Moore, S. A.; Anderson, B. F.; Groom, C. R.; Haridas, M.; Baker, E. N. *Journal of Molecular Biology* **1997**, *274*, 222-236.

21. Rozenfeld, R.; Iturrioz, X.; Okada, M.; Maigret, B.; Llorens-Cortes, C. *Biochemistry* **2003**, *42*, 14785-14793.

22. Jackson, M. S.; Lee, J. C. *Inorganic Chemistry* **2009**, *48*, 9303-9307.

23. Yaman, M.; Atici, D.; Bakirdere, S.; Akdeniz, I. *Journal of Medicinal Chemistry* **2005**, *48*, 630-634.

24. Hannon, M. J. *Pure and Applied Chemistry* **2007**, *79*, 2243-2262.

25. American Cancer Society. Cancer Basics. American Cancer Society . 7-18-2011. 1-22-2009.

Ref Type: Online Source

26. Heron, M.; Hoyert, D. L.; Murphy, S. L.; Xu, J.; Kochanek, K. D.; Tejada-Vera, B. *National vital statistics reports: from the Centers for Disease Control and Prevention, National Center for Health Statistics* **2009**, *57*, 1.

27. Heron, M.; Sutton, P. D.; Xu, J. Q.; Ventura, S. J.; Strobino, D. M.; Guyer, B. *Pediatrics* **2010**, *125*, 4-15.

28. Jemal, A.; Siegel, R.; Ward, E.; Hao, Y. P.; Xu, J. Q.; Thun, M. J. *Ca-A Cancer Journal for Clinicians* **2009**, *59*, 225-249.

29. Siegel, R.; Naishadham, D.; Jemal, A. *CA: A Cancer Journal for Clinicians* **2012**.

30. Rosenberg, B. *In Cisplatin: Chemistry and Biochemistry of a Leading Anticancer Drug*, 1999; 3-27.

31. BernersPrice, S. J.; Sadler, P. J. *Coordination Chemistry Reviews* **1996**, *151*, 1-40.

32. Jones, R. H.; Vasey, P. A. *Lancet Oncology* **2003**, *4*, 730-737.

33. Reisner, E.; Arion, V. B.; Keppler, B. K.; Pombeiro, A. J. L. *Inorganica Chimica Acta* **2008**, *361*, 1569-1583.

34. Jones, R. H.; Vasey, P. A. *Lancet Oncology* **2003**, *4*, 738-747.

35. Einhorn, L. H.; Donohue, J. *Annals of internal medicine* **1977**, *87*, 293.

36. Dobyan, D. C.; Levi, J.; Jacobs, C.; Kosek, J.; Weiner, M. W. *Journal of Pharmacology and Experimental Therapeutics* **1980**, *213*, 551-556.

37. Kelland, L. *Nature Reviews Cancer* **2007**, *7*, 573-584.

38. Desoize, B. *Anticancer Research* **2004**, *24*, 1529-1544.

39. Desoize, B.; Madoulet, C. *Critical Reviews in Oncology Hematology* **2002**, *42*, 317-325.

40. Yabroff, K. R.; Bradley, C. J.; Mariotto, A. B.; Brown, M. L.; Feuer, E. J. *JNCI Journal of the National Cancer Institute* **2008**, *100*, 1755.

41. Lezoche, E.; Baldarelli, M.; De Sanctis, A.; Lezoche, G.; Guerrieri, M. *Digestive Diseases* **2007**, *25*, 76-79.

42. Perez, R. P. *European Journal of Cancer* **1998**, *34*, 1535-1542.

43. Jemal, A.; Siegel, R.; Ward, E.; Hao, Y.; Xu, J.; Murray, T.; Thun, M. J. *CA: a cancer journal for clinicians* **2008**, *58*, 71.

44. Knight, K. R. G.; Kraemer, D. F.; Neuwelt, E. A. *Journal of Clinical Oncology* **2005**, *23*, 8588-8596.

45. Rybak, L. P.; Mukherjea, D.; Jajoo, S.; Ramkumar, V. *Tohoku Journal of Experimental Medicine* **2009**, *219*, 177-186.

46. Weiss, L. *Cancer metastasis reviews* **2000**, *19*, 193-383.

47. Jemal, A.; Clegg, L. X.; Ward, E.; Ries, L. A. G.; Wu, X. C.; Jamison, P. M.; Wingo, P. A.; Howe, H. L.; Anderson, R. N.; Edwards, B. K. *Cancer* **2004**, *101*, 3-27.

48. Arlt, F.; Stein, U. *The International Journal of Biochemistry & Cell Biology* **2009**, *41*, 2356-2359.

49. O'Connell, J. B.; Maggard, M. A.; Ko, C. Y. *Journal of the National Cancer Institute* **2004**, *96*, 1420-1425.

50. Gupta, G. P.; Massaguθ, J. *Cell* **2006**, *127*, 679-695.

51. Weiss, L.; Ward, P. M. *Cancer and Metastasis Reviews* **1983**, *2*, 111-127.

52. Mehlen, P.; Puisieux, A. *Nature Reviews Cancer* **2006**, *6*, 449-458.

53. Gupta, G. P.; Massague, J. *Cell* **2006**, *127*, 679-695.

54. Aslakson, C. J.; Miller, F. R. *Cancer Research* **1992**, *52*, 1399-1405.

55. Leibovici, J.; Klorin, G.; Huszar, M.; Hoenig, S.; Michowitz, M. *International Journal of Experimental Pathology* **1991**, *72*, 139-150.

56. Kuramochi, H.; Hayashi, K.; Uchida, K.; Miyakura, S.; Shimizu, D.; Vallbohmer, D.; Park, S.; Danenberg, K. D.; Takasaki, K.; Danenberg, P. V. *International Journal of Cancer* **2006**, *119*, 522-526.

57. Schmalfeldt, B.; Kuhn, W.; Reuning, U.; Pache, L.; Dettmar, P.; Schmitt, M.; Janicke, F.; Hofler, H.; Graeff, H. *Cancer Research* **1995**, *55*, 3958-3963.

58. Sava, G.; Bergamo, A. *Anticancer Research* **1999**, *19*, 1117-1124.

59. Testa, B. *Current Opinion in Chemical Biology* **2009**, *13*, 338-344.

60. Mura, P.; Casini, A.; Marcon, G.; Messori, L. *Inorganica Chimica Acta* **2001**, *312*, 74-80.

61. Mestroni, G.; Alessio, E.; Santi, A. S.; Geremia, S.; Bergamo, A.; Sava, G.; Boccarelli, A.; Schettino, A.; Coluccia, M. *Inorganica Chimica Acta* **1998**, *273*, 62-71.

62. Sava, G.; Capozzi, I.; Clerici, K.; Gagliardi, G.; Alessio, E.; Mestroni, G. *Clinical & Experimental Metastasis* **1998**, *16*, 371-379.

63. Iengo, E.; Mestroni, G.; Geremia, S.; Calligaris, M.; Alessio, E. *Journal of the Chemical Society-Dalton Transactions* **1999**, 3361-3371.

64. Heffeter, P.; Jakupec, M. A.; Korner, W.; Chiba, P.; Pirker, C.; Dornetshuber, R.; Elbling, L.; Sutterluty, H.; Micksche, M.; Keppler, B. K.; Berger, W. *Biochemical Pharmacology* **2007**, *73*, 1873-1886.

65. Sava, G.; Pacor, S.; Mestroni, G.; Alessio, E. *Clinical & Experimental Metastasis* **1992**, *10*, 273-280.

66. Galanski, M.; Arion, V. B.; Jakupec, M. A.; Keppler, B. K. *Current Pharmaceutical Design* **2003**, *9*, 2078-2089.

67. Bergamo, A.; Masi, A.; Jakupec, M. A.; Keppler, B. K.; Sava, G. *Metal-Based Drugs* **2009**, *2009*, 1-9.

68. Hartinger, C. G.; Zorbas-Seifried, S.; Jakupec, M. A.; Kynast, B.; Zorbas, H.; Keppler, B. K. *Journal of Inorganic Biochemistry* **2006**, *100*, 891-904.

69. Bergamo, A.; Cocchietto, M.; Capozzi, I.; Mestroni, G.; Alessio, E.; Sava, G. *Anti-Cancer Drugs* **1996**, *7*, 697-702.

70. Mestroni, G., Alessio, E., and Sava, G. Salts of anionic complexes of RU (III), as antimetastatic and antineoplastic agents. Sigea S.r.l, Trieste IT. 09/214,254[US 6,221,905 B1]. 1998.

Ref Type: Patent

71. Sava, G.; Gagliardi, R.; Bergamo, A.; Alessio, E.; Mestroni, G. *Anticancer Research* **1999**, *19*, 969-972.

72. Bergamo, A.; Gagliardi, R.; Scarcia, V.; Furlani, A.; Alessio, E.; Mestroni, G.; Sava, G. *Journal of Pharmacology and Experimental Therapeutics* **1999**, *289*, 559-564.

73. Rademaker-Lakhai, J. M.; van den Bongard, D.; Pluim, D.; Beijnen, J. H.; Schellens, J. H. M. *Clinical Cancer Research* **2004**, *10*, 3717-3727.

74. Sava, G.; Zorzet, S.; Turrin, C.; Vita, F.; Soranzo, M.; Zabucchi, G.; Cocchietto, M.; Bergamo, A.; DiGiovine, S.; Pezzoni, G.; Sartor, L.; Garbisa, S. *Clinical Cancer Research* **2003**, *9*, 1898-1905.

75. Gava, B.; Zorzet, S.; Spessotto, P.; Cocchietto, M.; Sava, G. *Journal of Pharmacology and Experimental Therapeutics* **2006**, *317*, 284-291.

76. Bergamo, A.; Gaiddon, C.; Schellens, J. H. M.; Beijnen, J. H.; Sava, G. *Journal of Inorganic Biochemistry* **2012**, *106*, 90-99.

77. Frausin, F.; Scarcia, V.; Cocchietto, M.; Furlani, A.; Serli, B.; Alessio, E.; Sava, G. *Journal of Pharmacology and Experimental Therapeutics* **2005**, *313*, 227-233.

78. Sava, G.; Frausin, F.; Cocchietto, M.; Vita, F.; Podda, E.; Spessotto, P.; Furlani, A.; Scarcia, V.; Zabucchi, G. *European Journal of Cancer* **2004**, *40*, 1383-1396.

79. Bergamo, A.; Sava, G. *Dalton Transactions* **2007**, 1267-1272.

80. Collins, V. P.; Loeffler, R. K.; Tivey, H. *American Journal of Roentgenology Radium Therapy and Nuclear Medicine* **1956**, *76*, 988-1000.

81. Sundararajan, S.; Tohno, E.; Kamma, H.; Ueno, E.; Minami, M. *Clinical Radiology* **2007**, *62*, 252-261.

82. Ravera, M.; Baracco, S.; Cassino, C.; Zanello, P.; Osella, D. *Dalton Trans.* **2004**, 2347-2351.

83. Bouma, M.; Nuijen, B.; Jansen, M. T.; Sava, G.; Bult, A.; Beijnen, J. H. *Journal of Pharmaceutical and Biomedical Analysis* **2002**, *30*, 1287-1296.

84. Sava, G.; Bergamo, A.; Zorzet, S.; Gava, B.; Casarsa, C.; Cocchietto, M.; Furlani, A.; Scarcia, V.; Serli, B.; Iengo, E.; Alessio, E.; Mestroni, G. *European Journal of Cancer* **2002**, *38*, 427-435.

85. Groessl, M.; Hartinger, C. G.; Polec-Pawlak, K.; Jarosz, M.; Dyson, P. J.; Keppler, B. K. *Chemistry & Biodiversity* **2008**, *5*, 1609-1614.

86. Cocchietto, M.; Zorzet, S.; Sorc, A.; Sava, G. *Investigational new drugs* **2003**, *21*, 55-62.

87. Clarke, M. J.; Bitler, S.; Rennert, D.; Buchbinder, M.; Kelman, A. D. *Journal of Inorganic Biochemistry* **1980**, *12*, 79-87.

88. Laliberte, F.; Sun, I. L.; Crane, F. L.; Clarke, M. J. *Journal of Bioenergetics and Biomembranes* **1987**, *19*, 69-81.

89. Mestroni, G.; Alessio, E.; Sava, G.; Pacor, S.; Coluccia, M.; Boccarelli, A. *Metal-Based Drugs* **1994**, *1*, 41-63.

90. Tannock, I. F.; Rotin, D. *Cancer Research* **1989**, *49*, 4373-4384.

91. Sava, G.; Pacor, S.; Bregant, F.; Ceschia, V.; Mestroni, G. *Anti-Cancer Drugs* **1990**, *1*, 99-108.

92. Allardyce, C. S.; Dyson, P. J. *Platinum Metals Review* **2001**, *45*, 62-69.

93. Bergamo, A.; Messori, L.; Piccioli, F.; Cocchietto, M.; Sava, G. *Investigational new drugs* **2003**, *21*, 401-411.

94. Brindell, M.; Stawoska, I.; Supel, J.; Skoczowski, A.; Stochel, G.; van Eldik, R. *Journal of Biological Inorganic Chemistry* **2008**, *13*, 909-918.

95. Griffith, O. W. *Free Radical Biology and Medicine* **1999**, *27*, 922-935.

96. Jones, D. P.; Carlson, J. L.; Mody, V. C.; Cai, J. Y.; Lynn, M. J.; Sternberg, P. *Free Radical Biology and Medicine* **2000**, *28*, 625-635.

97. Jonas, C. R.; Ziegler, T. R.; Gu, L. H.; Jones, D. P. *Free Radical Biology and Medicine* **2002**, *33*, 1499-1506.

98. Nkabyo, Y. S.; Ziegler, T. R.; Gu, L. H.; Watson, W. H.; Jones, D. P. *American Journal of Physiology-Gastrointestinal and Liver Physiology* **2002**, *283*, G1352-G1359.

99. Nkabyo, Y. S.; Gu, L. H.; Jones, D. P.; Ziegler, T. R. *Journal of Nutrition* **2006**, *136*, 1242-1248.

100. Jones, D. P. *Protein Sensors and Reactive Oxygen Species, Pt B, Thiol Enzymes and Proteins* **2002**, *348*, 93-112.

101. Schafer, F. Q.; Buettner, G. R. *Free Radical Biology and Medicine* **2001**, *30*, 1191-1212.

102. Maher, P. *Antioxidants & Redox Signaling* **2006**, *8*, 1941-1970.

103. Jonas, C. R.; Puckett, A. B.; Jones, D. P.; Griffith, D. P.; Szeszycki, E. E.; Bergman, G. F.; Furr, C. E.; Tyre, C.; Carlson, J. L.; Galloway, J. R.; Blumberg, J. B.; Ziegler, T. R. *American Journal of Clinical Nutrition* **2000**, *72*, 181-189.

104. De Flora, S.; Agostini, F. D.; Masiello, L.; Giunciuglio, D.; Albini, A. *International Journal of Cancer* **1998**, *67*, 842-848.

105. Shaw, I. C.; Graham, M. I. *Cancer Treatment Reviews* **1987**, *14*, 67-86.

106. Kabasakal, L.; Sehirli, A. O.; Cetinel, S.; Cikler, E.; Gedik, N.; Sener, G. *Life Sciences* **2004**, *75*, 2329-2340.

107. Yurkow, E. J. and Mermelstein, F. H. Method for treating cancer. 10/522092[PCT/US03/23867]. 7-30-2003. Google Patents. 7-30-2003.

Ref Type: Patent

108. Ypsilantis, P.; Tentes, I.; Lambropoulou, M.; Anagnostopoulos, K.; Papadopoulos, N.; Kortsaris, A.; Simopoulos, C. *Journal of Gastroenterology and Hepatology* **2008**, *23*, 328-335.

109. Weissman, I., Kristal, B., Sela, S., and Shahsa, S. Therapeutic uses for sodium 2-mercaptoethanesulphonate (mesna). 1997.

Ref Type: Patent

110. Yue, J.; Dong, G.; He, C.; Chen, J.; Liu, Y.; Peng, R. *Toxicology* **2009**, *264*, 185-191.

111. Zhang, J. G.; Lindup, W. E. *Toxicology and Applied Pharmacology* **1996**, *141*, 425-433.

112. Koide, T.; Yamagushi, S.; Utsonomiya, M.; Yoshioka, T. "A new therapeutic agent for cystinuria".

Ref Type: Conference Proceeding

113. Hercelin, B.; Leroy, P.; Nicolas, A.; Gavriloff, C.; Chassard, D.; Thebault, J. J.; Reveillaud, M. T.; Salles, M. F.; Netter, P. *European Journal of Clinical Pharmacology* **1992**, *43*, 93-95.

114. Kroning, R.; Lichtenstein, A. K.; Nagami, G. T. *Cancer Chemotherapy and Pharmacology* **2000**, *45*, 43-49.

115. Davis, D. A.; Dorsey, K.; Wingfield, P. T.; Stahl, S. J.; Kaufman, J.; Fales, H. M.; Levine, R. L. *Biochemistry* **1996**, *35*, 2482-2488.

116. Ambroz, H. B.; Kornacka, E. M.; Przybytniak, G. K. *Radiation Physics and Chemistry* **2004**, *70*, 677-686.

117. Moran, L. K.; Quinlan, G. J. *Current medicinal chemistry* **2001**, *8*, 763-772.

118. Stocker, R.; Huang, A.; Jeranian, E.; Hou, J. Y.; Wu, T. T.; Thomas, S. R.; Keaney, J. F. *Arteriosclerosis Thrombosis and Vascular Biology* **2004**, *24*, 2028-2033.

119. Fu, X. Y.; Mueller, D. M.; Heinecke, J. W. *Biochemistry* **2002**, *41*, 1293-1301.

120. Raftery, M. J.; Yang, Z.; Valenzuela, S. M.; Geczy, C. L. *Journal of Biological Chemistry* **2001**, *276*, 33393-33401.

121. Luo, D. Y.; Anderson, B. D. *Pharmaceutical Research* **2006**, *23*, 2239-2253.

122. Read, J. F.; Bewick, S. A.; Graves, C. R.; MacPherson, J. M.; Salah, J. C.; Theriault, A.; Wyand, A. E. H. *Inorganica Chimica Acta* **2000**, *303*, 244-255.

123. Read, J. F.; Graves, C. R.; Jackson, E. *Inorganica Chimica Acta* **2003**, *348*, 41-49.

124. El-Ayaan, U.; Linert, W. *Journal of Coordination Chemistry* **2002**, *55*, 1309-1314.

125. Nagy, P.; Jameson, G. N. L.; Winterbourn, C. C. *Chemical research in toxicology* **2009**, 113-139.

126. Darkwa, J.; Mundoma, C.; Simoyi, R. H. *Journal of the Chemical Society-Faraday Transactions* **1998**, *94*, 1971-1978.

127. Darkwa, J.; Olojo, R.; Chikwana, E.; Simoyi, R. H. *Journal of Physical Chemistry A* **2004**, *108*, 5576-5587.

128. Chigwada, T. R.; Simoyi, R. H. *Journal of Physical Chemistry A* **2005**, *109*, 1094-1104.

129. Chigwada, T. R.; Chikwana, E.; Simoyi, R. H. *Journal of Physical Chemistry A* **2005**, *109*, 1081-1093.

130. Martincigh, B. S.; Mundoma, C.; Simoji, R. H. *Journal of Physical Chemistry A* **1998**, *102*, 9838-9846.

131. Harman, L. S.; Mottley, C.; Mason, R. P. *Journal of Biological Chemistry* **1984**, *259*, 5606-5611.

132. Svensson, E.; Gräslund, A.; Moldeus, P. *Free Radical Biology and Medicine* **1993**, *14*, 167-175.

133. DeGray J. A.; Mason, R. P. *Biothiols in Health and Disease*; Marcel Dekker, Inc.: New York, 1995; Chapter 4, pp. 65-81.

134. Wang, X.; Stanbury, D. M. *Inorg.Chem* **2008**, *47*, 1224-1236.

135. Oae S.; Doi, J. T. *Organic sulfur chemistry: structure and mechanism*; CRC Press Inc.: Boca Raton, Florida, 1991; Chapter 6, pp. 203-291.

136. Harman, L. S.; Mottley, C.; Mason, R. P. *Journal of Biological Chemistry* **1984**, *259*, 5606-5611.

137. Filho, J. R.; Silva, W. C.; Pereira, J. C.; Franco, D. W. *Inorganica Chimica Acta* **2006**, *359*, 2888-2895.

138. Wang, F.; Chen, H.; Parkinson, J. A.; Murdoch, P. S.; Sadler, P. J. *Inorganic Chemistry* **2002**, *41*, 4509.

139. Lee, Y.; Choi, S.; Cho, M.; im, Y. *Bull.Korean Chem.Soc* **1990**, *11*, 281-286.

140. Crichton, R. R.; Dexter, D. T.; Ward, R. J. *Monatshefte fur Chemie* **2011**, *142*, 341-355.

141. Durand, F.; Bernuau, J.; Giostra, E.; Mentha, G.; Shouval, D.; Degott, C.; Benhamou, J. P.; Valla, D. *Gut* **2001**, *48*, 849-852.

142. Brewer, G. J. *Current Treatment Options in Neurology* **2000**, *2*, 193-203.

143. Tummino, P. J.; Scholten, J. D.; Harvey, P. J.; Holler, T. P.; Maloney, L.; Gogliotti, R.; Domagala, J.; Hupe, D. *Proceedings of the National Academy of Sciences of the United States of America* **1996**, *93*, 969-973.

144. Loo, J. A.; Holler, T. P.; Sanchez, J.; Gogliotti, R.; Maloney, L.; Reily, M. D. *J.Med.Chem* **1996**, *39*, 4313-4320.

145. Tummino, P. J.; Harvey, P. J.; McQuade, T.; Domagala, J.; Gogliotti, R.; Sanchez, J.; Song, Y.; Hupe, D. *Antimicrobial agents and chemotherapy* **1997**, *41*, 394.

146. Aposhian, H. V.; Aposhian, M. M. *Annual Review of Pharmacology and Toxicology* **1990**, *30*, 279-306.

147. Aposhian, H. V.; Maiorino, R. M.; Gonzalez-Ramirez, D.; Zuniga-Charles, M.; Xu, Z.; Hurlbut, K. M.; Junco-Munoz, P.; Dart, R. C.; Aposhian, M. *Toxicology* **1995**, *97*, 23-38.

148. Domingo, J. L. *Reproductive Toxicology* **2003**, *9*, 105-113.

149. Andersen, O. *Chem.Rev* **1999**, *99*, 2683-2710.

150. Graziano, J. H.; Lolacono, N. J.; Moulton, T.; Mitchell, M. E.; Slavkovich, V.; Zarate, C. *Journal of Pediatrics* **1992**, *120*, 133-139.

151. Giles, N. M.; Watts, A. B.; Giles, G. I.; Fry, F. H.; Littlechild, J. A.; Jacob, C. *Chemistry & Biology* **2003**, *10*, 677-693.

152. Tognella, S. *Cancer Treatment Reviews* **1990**, *17*, 139-142.

153. Wang, X.; Guo, Z. *Anti-Cancer Agents in Medicinal Chemistry (Formerly Current Medicinal Chemistry* **2007**, *7*, 19-34.

154. Johnson, S. W.; Ferry, K. V.; Hamilton, T. C. *Drug Resistance Updates* **1998**, *1*, 243-254.

155. Kartalou, M.; Essigmann, J. M. *Mutation Research-Fundamental and Molecular Mechanisms of Mutagenesis* **2001**, *478*, 23-43.

156. Oprea, A.; Bazzazi, H.; Kangarloo, B.; Wolff, J. E. A. *Anticancer Research* **2001**, *21*, 1225-1229.

157. Stewart, D. J. *Critical Reviews in Oncology/Hematology* **2007**, *63*, 12-31.

158. Bose, R. N.; Ghosh, S. K.; Moghaddas, S. *Journal of Inorganic Biochemistry* **1997**, *65*, 199-205.

159. Brindell, M.; Piotrowska, D.; Shoukry, A. A.; Stochel, G.; van Eldik, R. *Journal of Biological Inorganic Chemistry* **2007**, *12*, 809-818.

160. Bacac, M.; Hotze, A. C. G.; van der Schilden, K.; Haasnoot, J. G.; Pacor, S.; Alessio, E.; Sava, G.; Reedijk, J. *Journal of Inorganic Biochemistry* **2004**, *98*, 402-412.

161. Chatlas, J.; Vaneldik, R.; Keppler, B. K. *Inorganica Chimica Acta* **1995**, *233*, 59-63.

162. Pluim, D.; van Waardenburg, R. C. A. M.; Beijnen, J. H.; Schellens, J. H. M. *Cancer Chemotherapy and Pharmacology* **2004**, *54*, 71-78.

163. Ravera, M.; Baracco, S.; Cassino, C.; Colangelo, D.; Bagni, G.; Sava, G.; Osella, D. *Journal of Inorganic Biochemistry* **2004**, *98*, 984-990.

164. Gallori, E.; Vettori, C.; Alessio, E.; Vilchez, F. G.; Vilaplana, R.; Orioli, P.; Casini, A.; Messori, L. *Archives of Biochemistry and Biophysics* **2000**, *376*, 156-162.

165. Malina, J.; Novakova, O.; Keppler, B. K.; Alessio, E.; Brabec, V. *Journal of Biological Inorganic Chemistry* **2001**, *6*, 435-445.

166. Gibson, D. *Dalton Trans.* **2009**, 10681-10689.

167. Perkin Elmer *UV WinLab Software User's Guide*, Perkin Elmer Inc: United Kingdom, 2000.

168. Smith, R. D.; Loo, J. A.; Edmonds, C. G.; Barinaga, C. J.; Udseth, H. R. *Analytical Chemistry* **1990**, *62*, 882-899.

169. Fenn, J. B.; Mann, M.; Meng, C. K.; Wong, S. F.; Whitehouse, C. M. *Science* **1989**, *246*, 64-71.

170. Gates, P. Mass Spectrometry Resource: Electrospray Ionization. The University of Bristol, School of Chemistry . 2004. 2-4-2012.

Ref Type: Online Source

171. Makarov, A.; Denisov, E.; Lange, O.; Horning, S. *Journal of the American Society for Mass Spectrometry* **2006**, *17*, 977-982.

172. Makarov, A.; Denisov, E.; Kholomeev, A.; Baischun, W.; Lange, O.; Strupat, K.; Horning, S. *Analytical Chemistry* **2006**, *78*, 2113-2120.

173. Ewing, G. W. *Analytical Instrumentation Handbook*, 2nd ed.; Dekker, Inc.: New York Marcel, 1997.

174. Marder, K.; Stosser, R.; Borchert, H. H. *Free Radical Biology and Medicine* **1993**, *14*, 339-342.

175. Velasco, J.; Andersen, M. L.; Skibsted, L. H. *Food Chemistry* **2004**, *85*, 623-632.

176. Sibrian-Vazquez, M.; Escobedo, J. O.; Lim, S.; Samoei, G. K.; Strongin, R. M. *Proceedings of the National Academy of Sciences of the United States of America* **2010**, *107*, 551-554.

177. Mestroni, G., Alessio, E., and Sava, G. Salts of Anionic Complexes of Ru(III), as Antimetastatic and Antineoplastic Agents. Sigea S.r.l., Trieste IT. WO/1998/000431[US]. 1998. 6-30-1997.

Ref Type: Patent

178. Messori, L.; Orioli, P.; Vullo, D.; Alessio, E.; Iengo, E. *European Journal of Biochemistry* **2000**, *267*, 1206-1213.

179. Bouma, M.; Nuijen, B.; Jansen, M. T.; Sava, G.; Bult, A.; Beijnen, J. H. *Journal of Pharmaceutical and Biomedical Analysis* **2002**, *30*, 1287-1296.

180. Schluga, P.; Hartinger, C. G.; Egger, A.; Reisner, E.; Galanski, M.; Jakupec, M. A.; Keppler, B. K. *Dalton Trans.* **2006**, 1796-1802.

181. Rademaker-Lakhai, J. M.; van den Bongard, D.; Pluim, D.; Beijnen, J. H.; Schellens, J. H. M. *Clinical Cancer Research* **2004**, *10*, 3717-3727.

182. National cancer Institute. Types of Treatment. National Institute of Health . 2012. 5-10-2009.

Ref Type: Online Source

183. al-Mefty, O.; Kersh, J. E.; Routh, A.; Smith, R. R. *J Neurosurg* **1990**, *73*, 502-512.

184. Choi, Y. W.; Munden, R. F.; Erasmus, J. J.; Joo Park, K.; Chung, W. K.; Jeon, S. C.; Park, C. K. *Radiographics* **2004**, *24*, 985-997.

185. de Jonge, M. J. A.; Verweij, J. *Seminars in Oncology* **2006**, *33*, 68-73.

186. Kintzel, P. E. *Drug Safety* **2001**, *24*, 19-38.

187. Ahles, T.; Saykin, A. *Cancer Investigation* **2001**, *19*, 812.

188. Sahni, V.; Choudhury, D.; Ahmed, Z. *Nature Reviews Nephrology* **2009**, *5*, 450-462.

189. Jennifer, J. *Leukemia Research* **1998**, *22, Supplement 1*, S27-S33.

190. Antonadou, D.; Throuvalas, N.; Petridis, A.; Bolanos, N.; Sagriotis, A.; Synodinou, M. *International Journal of Radiation Oncology*Biology*Physics* **2003**, *57*, 402-408.

191. Tannehill, S. P.; Mehta, M. P.; Larson, M.; Storer, B.; Pellet, J.; Kinsella, T. J.; Schiller, J. H. *Journal of Clinical Oncology* **1997**, *15*, 2850-2857.

192. William, P. *Seminars in Oncology Nursing* **2007**, *23*, 213-224.

193. Hosseinimehr, S. J.; Karami, M. *Archives of Toxicology* **2005**, *79*, 482-486.

194. Culy, C. R.; Spencer, C. M. *Drugs* **2001**, *61*.

195. Santini, V. *Expert Opin.Pharmacother.* **2001**, *2*, 479-489.

196. Sweeney, T. R. "A survey of compounds from the antiradiation drug development program of the US Army Medical Research and Development Command," 1979.

197. Vujaskovic, Z.; Feng, Q. F.; Rabbani, Z. N.; Samulski, T. V.; Anscher, M. S.; Brizel, D. M. *Experimental Lung Research* **2002**, *28*, 577-590.

198. Hospers, G. A. P.; Eisenhauer, E. A.; Vries, E. G. E. *British Journal of Cancer* **1999**, *80*, 629.

199. Majsterek, I.; Gloc, E.; Blasiak, J.; Reiter, R. J. *Journal of Pineal Research* **2005**, *38*, 254-263.

200. Aydemir, N.; Sevim, N.; Celikler, S.; Vatan, O.; Bilaloglu, R. *Mutation Research/Genetic Toxicology and Environmental Mutagenesis* **2009**, *679*, 1-5.

201. Brizel, D. M.; Wasserman, T. H.; Henke, M.; Strnad, V.; Rudat, V.; Monnier, A.; Eschwege, F.; Zhang, J.; Russell, L.; Oster, W.; Sauer, R. *Journal of Clinical Oncology* **2000**, *18*, 3339-3345.

202. Calabro-Jones, P. M.; Aguilera, J. A.; Ward, J. F.; Smoluk, G. D.; Fahey, R. C. *Cancer Research* **1988**, *48*, 3634-3640.

203. Shaw, L. M.; Glover, D.; Turrisi, A.; Brown, D. Q.; Bonner, H. S.; Norfleet, A. L.; Weiler, C.; Glick, J. H.; Kligerman, M. M. *Pharmacology & Therapeutics* **1988**, *39*, 195-201.

204. Block, K. I.; Block, P. B.; Gyllenhaal, C.; Nathan, D.; de la Torre, M. *Journal of Clinical Oncology* **2005**, *23*, 798S.

205. Djurhuus, R.; Svardal, A. M.; Ueland, P. M. *Molecular Pharmacology* **1990**, *38*, 327-332.

206. Vitvitsky, V.; Garg, S. K.; Banerjee, R. *Journal of Biological Chemistry* **2011**, *286*, 32002-32010.

207. Dominy, J. E., Jr.; Simmons, C. R.; Hirschberger, L. L.; Hwang, J.; Coloso, R. M.; Stipanuk, M. H. *J.Biol.Chem.* **2007**, *282*, 25189-25198.

208. Cavallini, D.; Scandurra, R.; De Marco, C. *Journal of Biological Chemistry* **1963**, *238*, 2999-3005.

209. Stipanuk, M.; Simmons, C.; Andrew Karplus, P.; Dominy, J. *Amino Acids* **2011**, *41*, 91-102.

210. Gahl, W. A.; Tietze, F.; Butler, J. D.; Schulman, J. D. *Biochemical Journal* **1985**, *228*, 545.

211. Gahl, W. A.; Balog, J. Z.; Kleta, R. *Ann.Intern.Med.* **2007**, *147*, 242-250.

212. Kleta, R.; Gahl, W. A. *Expert Opin.Pharmacother.* **2004**, *5*, 2255.

213. Min-Oo, G.; Ayi, K.; Bongfen, S. E.; Tam, M.; Radovanovic, I.; Gauthier, S.; Santiago, H.; Rothfuchs, A. G.; Roff+¬, E.; Sher, A.; Mullick, A.; Fortin, A.; Stevenson, M. M.; Kain, K. C.; Gros, P. *Experimental Parasitology* **2010**, *125*, 315-324.

214. Min-Oo, G.; Fortin, A.; Poulin, J. F.; Gros, P. *Antimicrob.Agents Chemother.* **2010**, *54*, 3262-3270.

215. Min-Oo, G.; Gros, P. *Mamm.Genome* **2011**, *22*, 486-494.

216. Ozcan, A. G. *Cancer Chemother.Pharmacol.* **2005**, *56*, 221-229.

217. Santos-Mello, R.; Deimling, L. I.; Lauer J+¦nior, C.; Carvalho, T. R. *Genetics and Molecular Biology* **2005**, *28*, 156-160.

218. Hoffmann, G. R.; Shorter, R. A.; Quaranta, J. L.; McMaster, P. D. *Toxicol.In Vitro* **1999**, *13*, 1-9.

219. Purdie, J. W. *Radiation research* **1979**, *77*, 303.

220. Shrieve, D. C.; Harris, J. W. *International Journal of Radiation Oncology*Biology*Physics* **2003**, *8*, 585-588.

221. Lide, D. R. *CRC handbook of chemistry and physics: a ready-reference book of chemical and physical data*, CRC Pr I Llc: 2004.

222. Webb, M. I.; Walsby, C. J. *Dalton Trans.* **2011**, *40*, 1322-1331.

223. Tredan, O.; Galmarini, C. M.; Patel, K.; Tannock, I. F. *Journal of the National Cancer Institute* **2007**, *99*, 1441-1454.

224. Tannock, I. F. *Cancer and Metastasis Reviews* **2001**, *20*, 123-132.

225. Braun, S.; Hepp, F.; Sommer, H. L.; Pantel, K. *Int.J.Cancer* **1999**, *84*, 1-5.

226. Chu, E.; Devita, V. T. *Physicians' Cancer Chemotherapy Drug Manual*, 10th ed.; Jones and Bartlett Publishers: Sudbury, MA, 2010.

227. Sava, G.; Capozzi, I.; Clerici, K.; Gagliardi, G.; Alessio, E.; Mestroni, G. *Clinical & Experimental Metastasis* **1998**, *16*, 371-379.

228. Bergamo, A.; Sava, G. *Dalton Trans.* **2007**, 1267-1272.

229. Bergamo, A.; agliardi, R.; carcia, V.; urlani, A.; Alessio, E.; estroni, G.; ava, G. *Journal of Pharmacology and Experimental Therapeutics* **1999**, *289*, 559-564.

230. Dyson, P. J.; Sava, G. *Dalton Trans.* **2006**, 1929-1933.

231. Kaye, S. B. *British Journal of Cancer* **1998**, *78*, 1.

232. Grady, W. M.; Ulrich, C. M. *Gut* **2007**, *56*, 318.

233. Hausheer, F. H.; Kochat, H.; Parker, A. R.; Ding, D.; Yao, S.; Hamilton, S. E.; Petluru, P. N.; Leverett, B. D.; Bain, S. H.; Saxe, J. D. *Cancer Chemotherapy and Pharmacology* **2003**, *52*, 3-15.

234. Schuchter, L. M.; Hensley, M. L.; Meropol, N. J.; Winer, E. P. *Journal of Clinical Oncology* **2002**, *20*, 2895-2903.

235. Links, M.; Lewis, C. *Drugs* **1999**, *57*, 293-308.

236. Hensley, M. L.; Hagerty, K. L.; Kewalramani, T.; Green, D. M.; Meropol, N. J.; Wasserman, T. H.; Cohen, G. I.; Emami, B.; Gradishar, W. J.; Mitchell, R. B.;

Thigpen, J. T.; Trotti, A.; von Hoff, D.; Schuchter, L. M. *Journal of Clinical Oncology* **2009**, *27*, 127-145.

237. Brock, N.; Hilgard, P.; Pohl, J.; Ormstad, K.; Orrenius, S. *Journal of Cancer Research and Clinical Oncology* **1984**, *108*, 87-97.

238. Brock, N.; Pohl, J.; Stekar, J.; Scheef, W. *European Journal of Cancer & Clinical Oncology* **1982**, *18*, 1377-1387.

239. Hausheer, F. H.; Shanmugarajah, D.; Leverett, B. D.; Chen, X. H.; Huang, Q. L.; Kochat, H.; Petluru, P. N.; Parker, A. R. *Cancer Chemotherapy and Pharmacology* **2010**, *65*, 941-951.

240. Verschraagen, M.; Boven, E.; Torun, E.; Erkelens, C. A. M.; Hausheer, F. H.; van der Vijgh, W. J. F. *British Journal of Cancer* **2004**, *90*, 1654-1659.

241. Parker, A. R.; Petluru, P. N.; Wu, M.; Zhao, M.; Kochat, H.; Hausheer, F. H. *Molecular Cancer Therapeutics* **2010**, *9*, 2558-2567.

242. Khalaila, I.; Bergamo, A.; Bussy, F.; Sava, G.; Dyson, P. J. *International Journal of Oncology* **2006**, *29*, 261-268.

243. Masuda, N.; Negoro, S.; Hausheer, F.; Nakagawa, K.; Matsui, K.; Kudoh, S.; Takeda, K.; Yamamoto, N.; Yoshimura, N.; Ohashi, Y.; Fukuoka, M. *Cancer Chemotherapy and Pharmacology* **2011**, *67*, 533-542.

244. Verschraagen, M.; Boven, E.; Ruijter, R.; van der Born, K.; Berkhof, J.; Hausheer, F. H.; van der Vijgh, W. J. F. *Clinical Pharmacology & Therapeutics* **2003**, *74*, 157-169.

245. Bouma, M.; Nuijen, B.; Jansen, M. T.; Sava, G.; Flaibani, A.; Bult, A.; Beijnen, J. H. *International Journal of Pharmaceutics* **2002**, *248*, 239-246.

246. Valko, M.; Leibfritz, D.; Moncol, J.; Cronin, M. T. D.; Mazur, M.; Telser, J. *International Journal of Biochemistry & Cell Biology* **2007**, *39*, 44-84.

247. Jones, D. P. *Protein Sensors and Reactive Oxygen Species, Pt B, Thiol Enzymes and Proteins* **2002**, *348*, 93-112.

248. Wu, G.; Fang, Y. Z.; Yang, S.; Lupton, J. R.; Turner, N. D. *The Journal of nutrition* **2004**, *134*, 489-492.

249. Fang, Y. Z.; Yang, S.; Wu, G. *Nutrition* **2002**, *18*, 872-879.

250. Dalton, T. P.; Chen, Y.; Schneider, S. N.; Nebert, D. W.; Shertzer, H. G. *Free Radical Biology and Medicine* **2004**, *37*, 1511-1526.

251. Townsend, D. M.; Tew, K. D.; Tapiero, H. *Biomedicine & Pharmacotherapy* **2003**, *57*, 145-155.

252. Helmut, S. *Free Radical Biology and Medicine* **1999**, *27*, 916-921.

253. Filomeni, G.; Rotilio, G.; Ciriolo, M. R. *Biochemical Pharmacology* **2002**, *64*, 1057-1064.

254. Circu, M. L.; Yee Aw, T. *Free Radic Res* **2008**, *42*, 689-706.

255. Mitchell, J. B.; Russo, A. *The British journal of cancer.Supplement* **1987**, *8*, 96.

256. Ortega, A. L.; Mena, S.; Estrela, J. M. *Cancers* **2011**, *3*, 1285-1310.

257. Perez, R. P. *European Journal of Cancer* **1998**, *34*, 1535-1542.

258. Komiya, S.; Gebhardt, M. C.; Mangham, D. C.; Inoue, A. *Journal of Orthopaedic Research* **1998**, *16*, 15-22.

259. Burg, D.; Mulder, G. J. *Drug Metabolism Reviews* **2002**, *34*, 821-863.

260. Russo, A.; Carmichael, J.; Friedman, N.; Degraff, W.; Tochner, Z.; Glatstein, E.; Mitchell, J. B. *International Journal of Radiation Oncology Biology Physics* **1986**, *12*, 1347-1354.

261. Joncourt, F.; Buser, K.; Altermatt, H.; Bacchi, M.; Oberli, A.; Cerny, T. *Gynecologic Oncology* **1998**, *70*, 176-182.

262. Balendiran, G. K.; Dabur, R.; Fraser, D. *Cell Biochemistry and Function* **2004**, *22*, 343-352.

263. Chaudhary, S.; Van Horn, J. D. *Mutation Research-Genetic Toxicology and Environmental Mutagenesis* **2006**, *610*, 56-65.

264. Deleve, L. D.; Kaplowitz, N. *Pharmacology & Therapeutics* **1991**, *52*, 287-305.

265. Duh, P. D.; Wu, S. C.; Chang, L. W.; Chu, H. L.; Yen, W. J.; Wang, B. S. *Food Chemistry* **2009**, *114*, 87-92.

266. Giles, N. M.; Giles, G. I.; Jacob, C. *Biochemical and Biophysical Research Communications* **2003**, *300*, 1-4.

267. Aldini, G.; Vistoli, G.; Regazzoni, L.; Gamberoni, L.; Facino, R. M.; Yamaguchi, S.; Uchida, K.; Carini, M. *Chemical Research in Toxicology* **2008**, *21*, 824-835.

268. Roche, M.; Rondeau, P.; Singh, N. R.; Tarnus, E.; Bourdon, E. *FEBS Letters* **2008**, *582*, 1783-1787.

269. Quinlan, G. J.; Martin, G. S.; Evans, T. W. *Hepatology* **2005**, *41*, 1211-1219.

270. Sarasin, A.; Giglia-Mari, G. *Experimental Dermatology* **2002**, *11*, 44-47.

271. Osborne, R. J.; Merlo, G. R.; Mitsudomi, T.; Venesio, T.; Liscia, D. S.; Cappa, A. P. M.; Chiba, I.; Takahashi, T.; Nau, M. M.; Callahan, R.; Minna, J. D. *Cancer Research* **1991**, *51*, 6194-6198.

272. Hollstein, M.; Sidransky, D.; Vogelstein, B.; Harris, C. C. *Science* **1991**, *253*, 49-53.

273. Harris, C. C. *Journal of the National Cancer Institute* **1996**, *88*, 1442-1455.

274. Kim, D. H.; Kundu, J. K.; Surh, Y. J. *Mol.Carcinog.* **2011**, *50*, 222-234.

275. Buzek, J.; Latonen, L.; Kurki, S.; Peltonen, K.; Laiho, M. *Nucleic Acids Research* **2002**, *30*, 2340-2348.

276. Scotcher, J.; Clarke, D.; Weidt, S.; Mackay, C.; Hupp, T.; Sadler, P.; Langridge-Smith, P. *Journal of the American Society for Mass Spectrometry* **2011**, *22*, 888-897.

277. Rainwater, R.; Parks, D.; Anderson, M. E.; Tegtmeyer, P.; Mann, K. *Molecular and Cellular Biology* **1995**, *15*, 3892-3903.

278. Jung, H.; Seong, H. A.; Ha, H. *Journal of Biological Chemistry* **2008**, *283*, 20383-20396.

279. Besker, N.; Coletti, C.; Marrone, A.; Re, N. *Journal of Physical Chemistry B* **2008**, *112*, 3871-3875.

280. Vargiu, A. V.; Robertazzi, A.; Magistrato, A.; Ruggerone, P.; Carloni, P. *Journal of Physical Chemistry B* **2008**, *112*, 4401-4409.

281. Bouma, M.; Nuijen, B.; Jansen, M. T.; Sava, G.; Bult, A.; Beijnen, J. H. *Journal of Pharmaceutical and Biomedical Analysis* **2002**, *30*, 1287-1296.

282. Chen, J.; Chen, L.; Liao, S.; Zheng, K.; Ji, L. *J Phys Chem B* **2007**, *111*, 7862-7869.

283. Souid, A. K.; Fahey, R. C.; Aktas, M. K.; Sayin, O. A.; Karjoo, S.; Newton, G. L.; Sadowitz, P. D.; Dubowy, R. L.; Bernstein, M. L. *Drug Metabolism and Disposition* **2001**, *29*, 1460-1466.

284. Whitesides, G. M.; Lilburn, J. E.; Szajewski, R. P. *Journal of Organic Chemistry* **1977**, *42*, 332-338.

285. Tacka, K. A.; Dabrowiak, J. C.; Goodisman, J.; Souid, A. K. *Drug Metabolism and Disposition* **2002**, *30*, 875-882.

286. Hu, T. M.; Ho, S. C. *J Med Sci* **2011**, *31*, 109-115.

287. Cocchietto, M.; Zorzet, S.; Sorc, A.; Sava, G. *Investigational new drugs* **2003**, *21*, 55-62.

288. Brindell, M.; Stawoska, I.; Supel, J.; Skoczowski, A.; Stochel, G.; van Eldik, R. *Journal of Biological Inorganic Chemistry* **2008**, *13*, 909-918.

289. Groessl, M.; Reisner, E.; Hartinger, C. G.; Eichinger, R.; Semenova, O.; Timerbaev, A. R.; Jakupec, M. A.; Arion, V. B.; Keppler, B. K. *Journal of Medicinal Chemistry* **2007**, *50*, 2185-2193.

290. Owen, W. *Free Radical Biology and Medicine* **1999**, *27*, 922-935.

291. Coyle, B.; Kavanagh, K.; McCann, M.; Devereux, M.; Geraghty, M. *Biometals* **2003**, *16*, 321-329.

292. Coyle, B.; Kinsella, P.; McCann, M.; Devereux, M.; O'Connor, R.; Clynes, M.; Kavanagh, K. *Toxicology in Vitro* **2004**, *18*, 63-70.

293. Doonan, C. J.; Nielsen, D. J.; Smith, P. D.; White, J. M.; George, G. N.; Young, C. G. *Journal of the American Chemical Society* **2006**, *128*, 305-316.

294. Hoffmeyer, R. E.; Singh, S. P.; Doonan, C. J.; Ross, A. R. S.; Hughes, R. J.; Pickering, I. J.; George, G. N. *Chemical Research in Toxicology* **2006**, *19*, 753-759.

295. Munro, O. Q.; Marques, H. M. *Inorganic Chemistry* **1996**, *35*, 3768-3779.

296. James, B. R.; Lyons, J. R.; Williams, R. J. P. *Biochemistry* **1962**, *1*, 379-+.

297. Goldberg, D. P.; Caneschi, A.; Delfs, C. D.; Sessoli, R.; Lippard, S. J. *Journal of the American Chemical Society* **1995**, *117*, 5789-5800.

298. Gracia-Mora, I.; Ruiz-Ramírez, L.; Gómez-Ruiz, C.; Tinoco-Méndez, M.; Márquez-Quiñones, A.; Romero-De Lira, L.; Marín-Hernández, A.; Macías-Rosales, L.; Bravo-Gómez, M. *Metal-Based Drugs* **2001**, *8*, 19-28.

299. Schilt, A. A.; Taylor, R. C. *Journal of Inorganic & Nuclear Chemistry* **1959**, *9*, 211-221.

300. SAUD, M.; FARRUKH, M. A.; NAQVI, I. I. *Nucleus* **2003**, *40*, 107-114.